INFORMATION TO USERS

This material was produced from a microfilm copy of the original document. While the most advanced technological means to photograph and reproduce this document have been used, the quality is heavily dependent upon the quality of the original submitted.

The following explanation of techniques is provided to help you understand markings or patterns which may appear on this reproduction.

1. The sign or "target" for pages apparently lacking from the document photographed is "Missing Page(s)". If it was possible to obtain the missing page(s) or section, they are spliced into the film along with adjacent pages. This may have necessitated cutting thru an image and duplicating adjacent pages to insure you complete continuity.

2. When an image on the film is obliterated with a large round black mark, it is an indication that the photographer suspected that the copy may have moved during exposure and thus cause a blurred image. You will find a good image of the page in the adjacent frame.

3. When a map, drawing or chart, etc., was part of the material being photographed the photographer followed a definite method in "sectioning" the material. It is customary to begin photoing at the upper left hand corner of a large sheet and to continue photoing from left to right in equal sections with a small overlap. If necessary, sectioning is continued again – beginning below the first row and continuing on until complete.

4. The majority of users indicate that the textual content is of greatest value, however, a somewhat higher quality reproduction could be made from "photographs" if essential to the understanding of the dissertation. Silver prints of "photographs" may be ordered at additional charge by writing the Order Department, giving the catalog number, title, author and specific pages you wish reproduced.

5. PLEASE NOTE: Some pages may have indistinct print. Filmed as received.

University Microfilms International
300 North Zeeb Road
Ann Arbor, Michigan 48106 USA
St. John's Road, Tyler's Green
High Wycombe, Bucks, England HP10 8HR

SPECIFIC HEAT OF SUBMONOLAYER HELIUM FILMS ADSORBED ON ARGON COATED GRAFOIL

by

CHRISTOS N. KOUTSOGEORGIS

A dissertation submitted to the Graduate Faculty in Physics in partial fulfilment of the requirements for the degree of Doctor of Philosophy, The City University of New York.

1978

This manuscript has been read and accepted for the Graduate Faculty in Physics in satisfaction of the dissertation requirement for the degree of Doctor of Philosophy.

10/26/77
date

William Miller
Chairman of Examining Committee

11/9/77
date

Myriam P. Sarachik
Executive Officer

John C. Garland

Stuart A. Rice

Peter Lindenfeld

George Stamkos
Supervisory Committee

The City University of New York

ABSTRACT

Specific Heat of Submonolayer Helium Films Adsorbed on Argon Coated Grafoil

by

Christos N. Koutsogeorgis

Advisor: Professor William Miller

Measurements have been made of the specific heat of submonolayer ^3He and ^4He films, adsorbed on Grafoil pre-coated with a monolayer of Argon. The ^4He measurements were made in the temperature range of 0.4 to 4.2 K for areal densities D equal to 0.008, 0.015, 0.022, 0.029, 0.035, 0.040 and 0.043 $\AA^{-2}$. The ^3He measurements were made in the temperature range of 0.8 to 6.0 K. The densities studied were 0.012, 0.024, 0.035, 0.045 and 0.056 $\AA^{-2}$ on an Argon coating of 1% less than the Argon monolayer (as determined at 77.3 K), and 0.023, 0.045, 0.073 $\AA^{-2}$ on an Argon coating of 5% more than the monolayer. The resulting ^4He curves, with the exception of D equal to 0.008 $\AA^{-2}$, showed marked peaks, reaching values of reduced specific heat C/Nk of 2.5 to 3.6 in the temperature range of 1.95 to 2.55 K. The temperature of the peaks increased with density. At temperatures below those of the peaks, the data fitted an interpolation formula $C/Nk=aT^n$, with n approximately 3.

Above 3.5 K, C/Nk falls to approximately temperature independent values between 0.85 and 1.0, suggesting a 2D interacting gas behaviour, but not accounted for by the Siddon and Schick model (ref. 69). The resulting curves for ^{3}He showed maxima at about 3.5 K, with the maximum value of C/Nk decreasing with density. Above 3.5 K, C/Nk seemed to fall to temperature independent values for the low density films. The results of the high density films, i.e: D=0.045 and 0.073 $\mathring{A}^{-2}$, on the 1.05 layer Argon coating, were masked by desorption effects. A comparison with previous specific heat data of Helium on bare Grafoil and with theoretical models is given, together with a discussion.

ACKNOWLEDGEMENTS

I would like to express my deepest gratitude to Professor William Miller for suggesting this work and for his constant encouragement, and to Professor John G. Daunt, Stevens Institute of Technology, for making available the facilities of the Cryogenics Center, for his constant guidance and for his patience with my shortcomings.

I am greatly indebted to Dr. Richard Roberts for his excellent introduction to the techniques of low temperature Physics as well as his assistance during the long hours of data taking, and to his wife, Moira Roberts, for her pleasant way of introducing us to a new life-style.

I am grateful to Dr. Suryanaryan Hegde, Dr. Donald Husa and Mr. Ed Ezell for the close attention given to my work and their constructive criticism.

I thank Mr. Pim Van Iperen for his assistance in the construction of the experimental set-up and during long runs. I thank Mr. George Kleiner and Mr. John Mager for their help in creating special computer programs.

Most of all, from the deepest of my heart, I thank

my constant inspiration, my wife Georgia, without whose endless patience and unrelenting encouragement, a long and arduous career as a graduate student could not have been brought to a succesful conclusion.

To my father Nikolaos,

and my brother Gregory

TABLE OF CONTENTS

LIST OF TABLES

LIST OF FIGURES

CHAPTER 1: INTRODUCTION

1.1. Two Dimensional Systems

Theoretical interest in the properties of the two dimensional (2D) systems has been active for over 40 years. As early as 1936 R.E. Peierls[1] tried to describe the properties of a 2D magnet, based on an Ising model. Later, important as well as peculiar results were found that can be summarized as follows: no long range order exists, i.e: no superfluidity[2], superconductivity or ferromagnetism should occur in 2D systems. However, experimental work revealed that Helium formed superfluid films[3]. As further theoretical investigations were undertaken it was realized that the results of the calculations often drastically depended upon the initial assumptions, casting doubt on the established theories to the point where extensive experimental investigations were warranted.

Meaningful comparison of theoretical and experimental results required the realization of a 2D system. Adsorption is a phenomenon assumed to result in a nearly 2D system[4][5]. It occurs whenever two phases are in contact and deals with the boundary of the common surface, i.e: with those molecules

which have not penetrated the interatomic field of the other phase. Of all the possible combinations, let us restrict ourselves to the case of physisorption, where physical forces characterized as weak Van der Waals forces are involved, one phase being a solid (the adsorbent) and the other phase a gas (the adsorbate). It should be made clear that adsorption of a gas by a solid is energetically favourable. It is accompanied by a decrease in the free energy of the gas-solid system and, therefore, it occurs spontaneously[4]. In fact, due to the reduction of the number of degrees of freedom of the gas phase the entropy is also reduced, i.e: it is an exothermic process.

The conditions for weak physical interaction are satisfied for rare gases being the adsorbate. They are inert, monatomic and spherical, avoiding thus complications of chemisorption and molecular rotation. Particularly attractive seems to be the case of Helium. It gives the choice of two isotopes obeying different statistics. Its interaction is the weakest. One then hopes that the solid adsorbent will not interfere with the properties of the adsorbate which, in turn, will behave as a true 2D system governed by the adatom-adatom interaction.

The mobility and the phase diagram of such an

adsorbate-adsorbent system would then tell us under what conditions, if any, the adsorbate behaves as a solid. A physical quantity very sensitive to phase changes is the specific heat. Measurements of the specific heat of Helium films were made as early as 1949[6] but the phase diagram of a 2D system is far from being complete. There is a number of reasons for this incompleteness. The most important is the interaction of the adsorbate with the adsorbent. The latter does not necessarily play the role of an inert substrate.

The problems appear as one tries to measure the properties of thinner and thinner films. In order to distinguish the properties of the adsorbate from those of the adsorbent it is necessary to use materials with high surface to volume ratio. These have traditionally been powders, sintered metals and glasses. Powders and glasses have very poor thermal conductivity making almost impossible any work at low temperatures. In any case, none provides a smooth, uniform and homogeneous surface from the adsorption point of view, and the results are often non reproducible. Substrates that have been recently studied include Vycor glass[7], Copper[8] and Copper coated with a single layer of an inert gas[9]. The results and interpretations of those measurements can often be considered as contradictory if the interaction with the substrate is neglected, in other words

if the surface is assumed uniform and homogeneous. Actually, it is this hope of achieving a more uniform substrate which prompted the experiments with an intervening layer of an inert gas, i.e: to smooth out nonuniformities thus getting a true 2D substrate lattice.

Nevertheless, some agreement exists. For coverages (amounts of adsorbate) close to one layer a specific heat proportional to the square of the temperature was seen. This was interpreted as an evidence of a 2D solid. But neither a gas phase was clearly seen nor a phase transition of any kind[10].

1.2. Grafoil

In the meantime interest in the properties of surfaces, per se, has increased. New techniques were developed for their studies. In 1967, one of them, the low energy electron diffraction (LEED)[11] revealed a multitude of phases for different gases weakly chemisorbed on graphite single crystals, and only near the monolayer coverage could Xenon, for instance, be seen forming a solid, what is now commonly referred to as lattice gas, with a characteristic long range order. In 1970[12], for the first time traditional adsorption work showed that exfoliated graphite as substrate

could be identified as an adsorbent with very uniform and homogeneous surface. Rare gases as adsorbates clearly show phase transitions.

Graphite proved to be an excellent substrate. It is unreactive under the usual conditions for adsorption work. It has a relatively high surface to volume ratio. Its thermal conductivity is much larger than that of glasses. It can be cleaned easily by heating under vacuum and it could be prepared easily. Soon exfoliated graphite became available commercially under the name Grafoil[13].

Measurements of the specific heat followed using Helium as the adsorbate. Transitions were clearly seen and a phase diagram for both of the Helium isotopes was presented[14]. The substrate, however, was still responsible for most of the structure[15]. It is only the behaviour of multilayer adsorbed films that suggests the possibility of every layer retaining its individuality, eventually independent of the substrate and, therefore, with a 2D character (before it starts behaving as a bulk liquid).

1.3. Argon On Grafoil

Motivated by the work of the group at the University

of Washington[14], and encouraged by the results of the group of this laboratory[16] (Cryogenics Center, Stevens Institute of Technology) we decided to measure the specific heat at constant coverage of both Helium isotopes, adsorbed on Grafoil precoated with one layer of Argon. Study of the adsorption properties of this system, specifically the analysis of the isosteric heat[16], revealed a more homogeneous surface compared to the surface of (bare) Grafoil. In adition the coating provides a different symmetry and a weaker binding for the Helium adatoms[17] most likely due to the short range of the Van der Waals forces, that is, the Helium atoms no longer see the underlying carbon lattice.

1.4. This Work

This dissertation is basically presented in three parts. Chapter 2 describes the equipment, method and procedures used in this study. Chapter 3 is a short review of the current theory closely related with our experiment. Chapter 4 gives a detailed account of our results, comparisons and interpretations in accord with the theory developed in the previous chapter. Finally some suggestions for further work will be given that could provide more definitive answers to questions raised by this work.

CHAPTER 2: EXPERIMENTAL SET-UP

2.1. Introduction

The heat capacity C was calculated from the measurements of the heat Q dissipated in the sample heater and the resultant temperature change ΔT:

$$C = Q/\Delta T$$

The time t the heater power was on was directly measured together with the voltages V_H across the heater and V_{SH} across a known resistance R_{SH} in series with the heater. Then, assuming an infinite input impedance for the voltmeter the heat is given by:

$$Q = V_{SH} \cdot V_H \cdot t/R_{SH}$$

In the appendix A, a corrected formula is derived to take into account the finite input impedance of the voltmeter as well as other sources of systematic errors.

The heating periods were selectable over a range of 28 to 56 sec. and followed by drift periods of 210 sec. Discrete temperature readings were taken every 7 sec. and the 12 last ones were least square fitted to a straight line (in time). These temperature vs time fits were then extrapolated to the half integral point[18] and the

temperature increase was thus determined (see figure 24).

2.2. Thermometry

There were three thermometers mounted on the sample holder. A 220 Ω Carbon 1/2 W Speer resistor was used as a monitor. Its resistance was measured by a (2-lead) A.C. Wheatstone bridge as shown in figure 1. A signal generator provided a standard frequency of 100 Hz with an accuracy of 0.001%. To avoid self heating the output voltage of the generator was attenuated so thatbridge input voltages from 90 μV to 2800 μV could be selected. The power dissipated in the thermometer was never more than 10^{-10} W. The off balance voltage was transformer coupled to a preamplifier followed by a two-phase lock-in amplifier, the output of which was recorded as a function of time. A typical output of the chart recorder is shown in figure 2. For completeness sake and comparison with the other thermometers figure 3 is included showing the resistance vs temperature of the Carbon thermometer (the monitor), as calibrated by the other two thermometers.

Sample temperature was measured by Germanium thermometers because of their excellent reproducibility after repeated cycling to 300 K. We found no thermometer with

acceptable performance for the temperature range of 0.2 K up to 5.0 K. A set of two thermometers was therefore chosen. One was used for low temperatures (below 1.5 K) and the other for the higher temperature range (up to 6.0 K).

The ^{4}He data was taken using Cryo-Cal[19] thermometers. A CR250-^{3}He, hereafter called Ge2, covered the high temperatures and a CR50-^{3}He, hereafter called Ge1, covered the low temperatures. Both were calibrated against ^{3}He and ^{4}He vapor pressure for temperatures above 0.70 K and Ge1 by the susceptibility of Cerium Magnesium Nitrate (CMN) for temperatures down to 0.14 K. Appendix B describes the calibration procedure in some detail. There an estimate of the (random) errors is also included whereas the systematic errors are discussed in Appendix A, being related to our electronic equipment. The effect of the latter error is obvious in the Ge1 resistance vs temperature curve, shown in figure 4, together with the Ge2 curve.

The low temperature ^{3}He data was taken using a Solitron thermometer[20], hereafter called Ge3 due to accidental destruction of Ge1. It was calibrated against CMN as described in Appendix B[21]. In order to extend our measurements beyond the limit of Ge2, i.e: 4.20 K, the high temperature range for the ^{3}He data was covered by a Cryo-Cal

FIGURE 1

A. C. Resistance Bridge

Frequency Standard: American Time Products, model 2002

Lock-in Amplifier : Princeton Applied Research, model JB-6

Chart Recorder : Varian, model G-14A-1

Preamplifier : Keithley, model 103R

Transformer : Thordarson Interstage, GEO-84

R_a, R_b = 2 KΩ

R_t = 270 KΩ

R_c = 1 KΩ

C = 850 pF

L = 1500 pH

R_v = 0 - 111,111 Ω, a DB62 Dekabox (ref. 57)

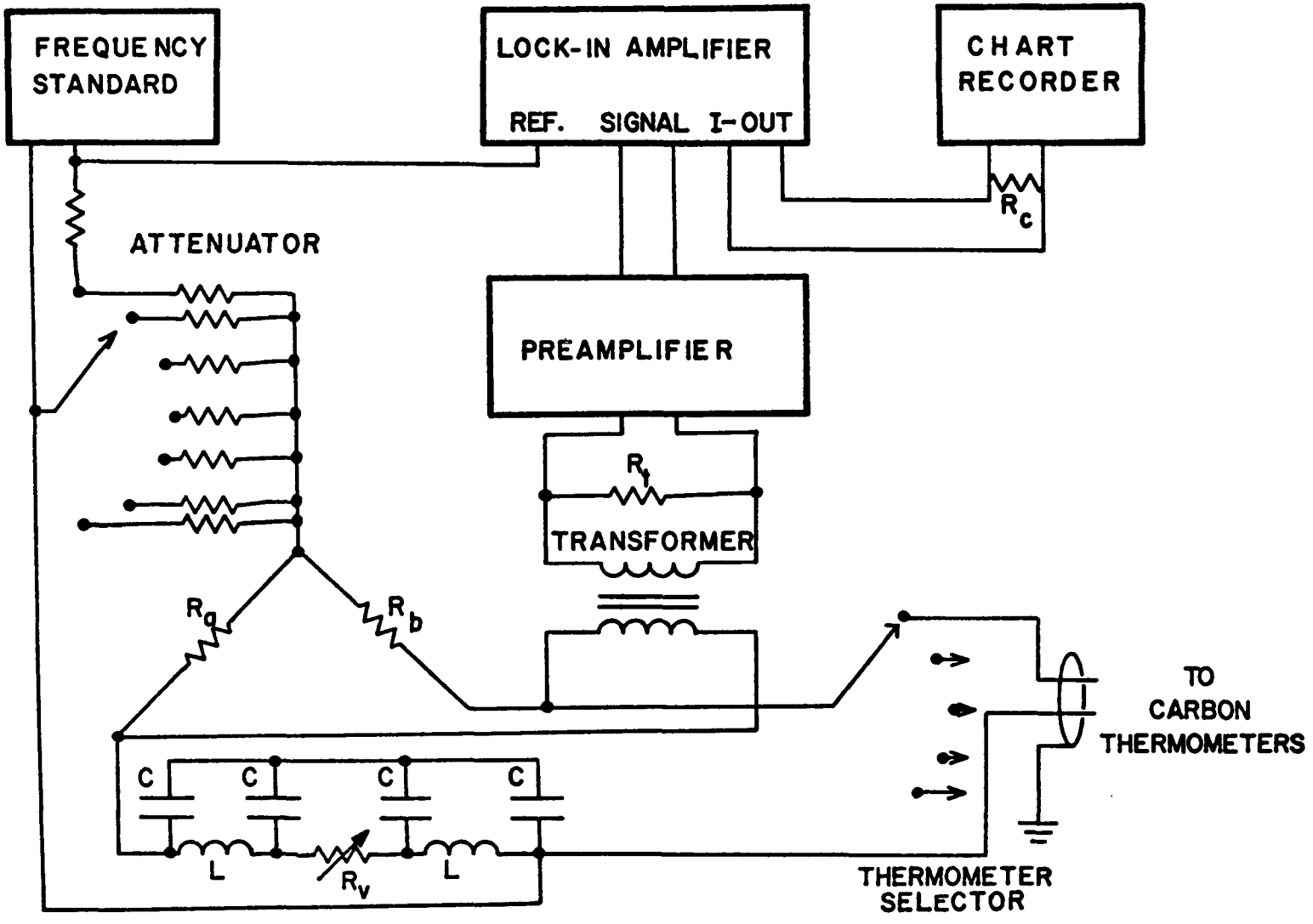
FREQUENCY STANDARD
LOCK-IN AMPLIFIER
REF. SIGNAL I-OUT
CHART RECORDER
R_c
ATTENUATOR
PREAMPLIFIER
R_t
TRANSFORMER
R_a
R_b
C
C
C
C
L
R_v
L
TO CARBON THERMOMETERS
THERMOMETER SELECTOR

FIGURE 2

Chart Recorder Output

This is a typical chart recorder trace of the sample carbon thermometer (the monitor), during a heat capacity run. The value of the Dekabox setting (1022 Ω in this case) is the resistance of the thermometer when the off-balance output is zero, which corresponds to division 50 on the paper.Smaller resistance values (higher temperatures) are to the right (divisions 50 to 100). The sensitivity, in divisions/mK was also recorded.

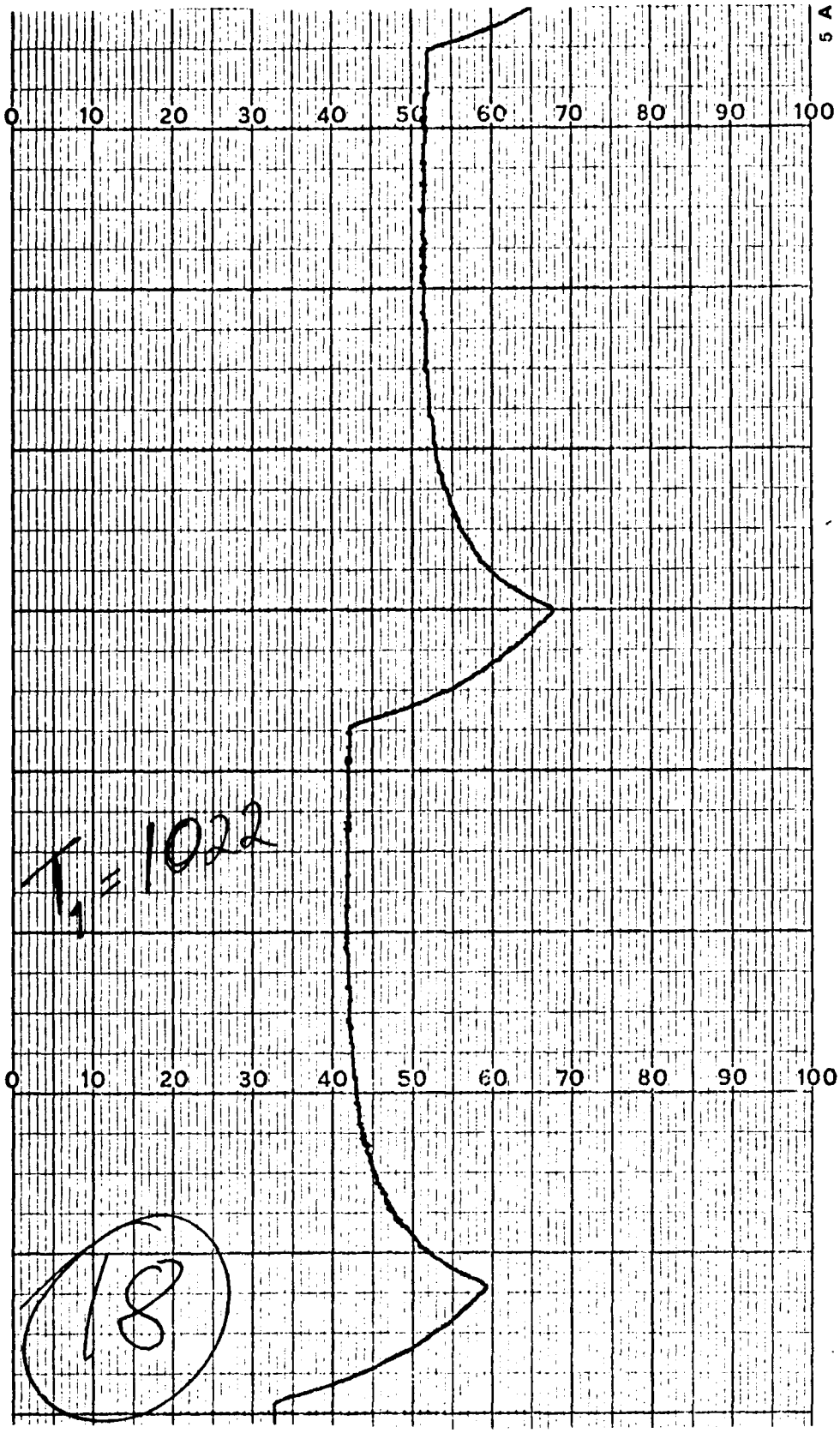
5 A
0 10 20 30 40 50 60 70 80 90 100
$T_1 = 1022$
0 10 20 30 40 50 60 70 80 90 100
18

FIGURE 3

Resistance vs Temperature for the Monitor

. Total resistance, evanohm wiring included
+ Total resistance minus room temperature value
By subtracting the room temperature value of the carbon thermometers, which included the wiring resistance, we found that temperature reproducibility was better than 0.2% during the course of this work, and indepedent of changes in the wiring.

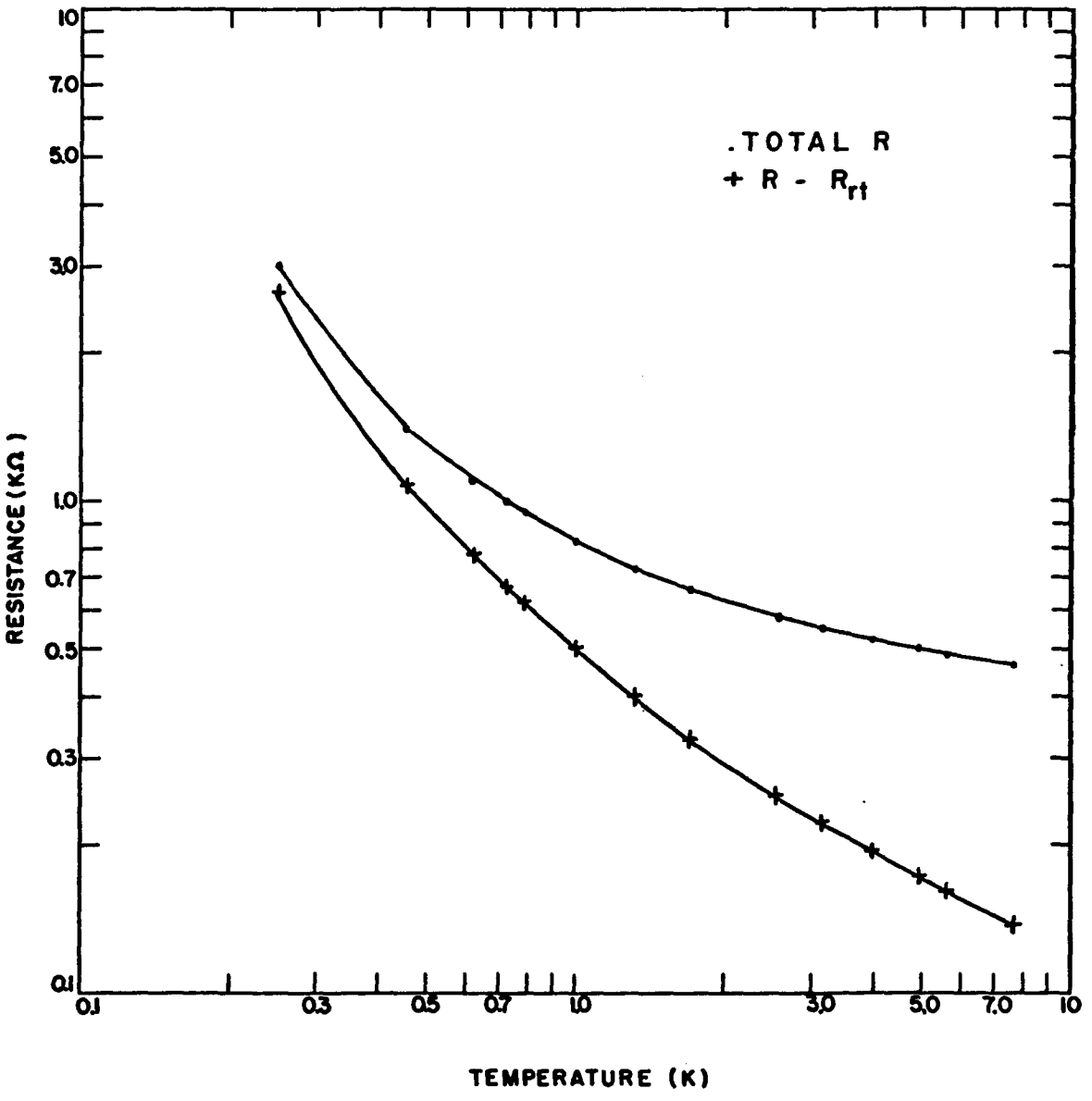
.TOTAL R
+ R - R_{rt}
RESISTANCE (KΩ)
10
7.0
5.0
3.0
1.0
0.7
0.5
0.3
0.1
0.1
0.3
0.5
0.7
1.0
3.0
5.0
7.0
10
TEMPERATURE (K)

FIGURE 4

Resistance vs Temperature for Ge1 and Ge2

Least square fitted curves for Ge1, Ge2. The anomaly seen at 0.3 K for Ge1 is due to a systematic error introduced by the thermometer current reversal. No heat capacity data were taken below 0.4 K.

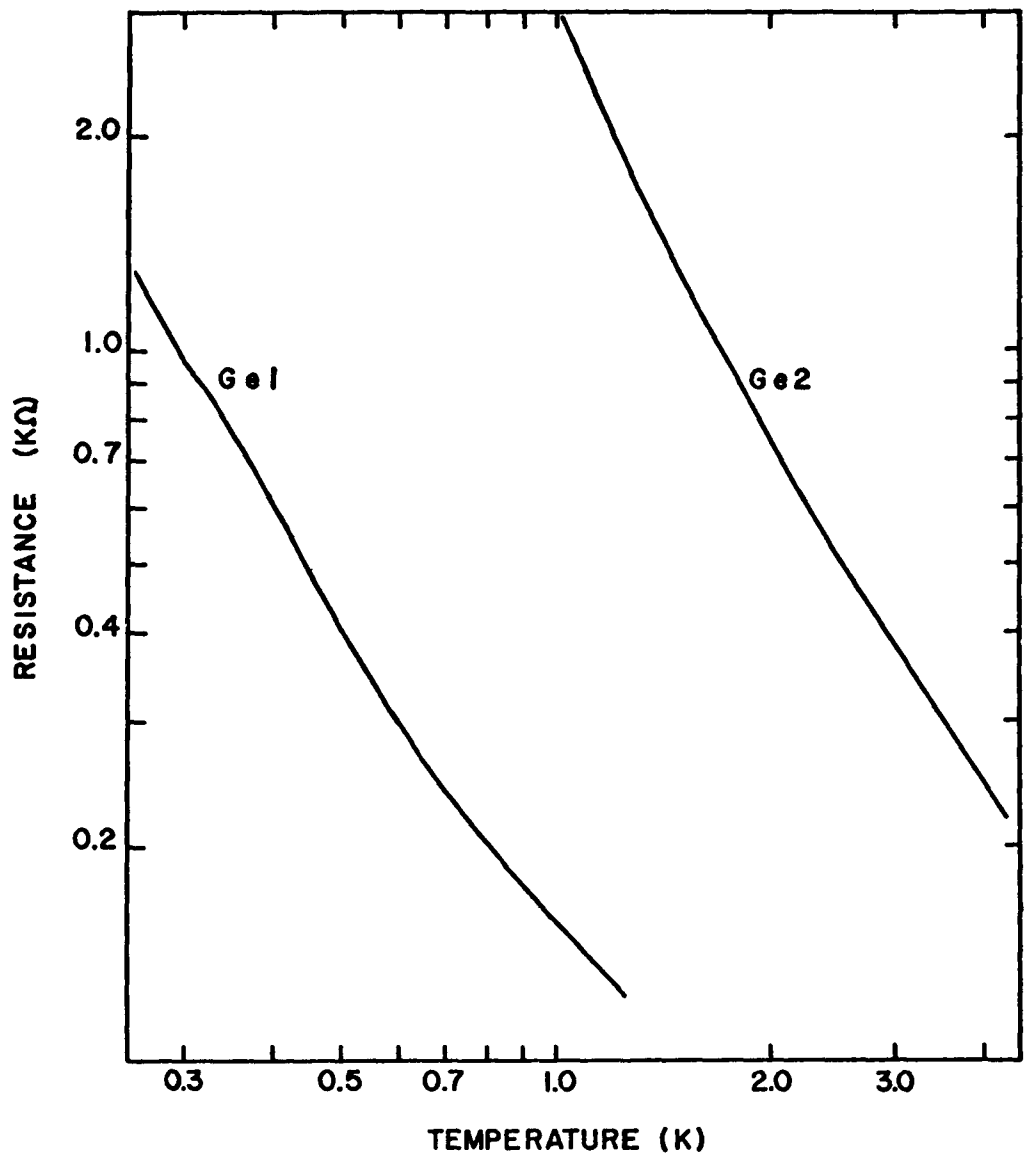
2.0
1.0
0.7
0.4
0.2
RESISTANCE (KΩ)
Ge1
Ge2
0.3
0.5
0.7
1.0
2.0
3.0
TEMPERATURE (K)

CR1000 thermometer calibrated by N.B.S. from 1.50 K up to 100.0 K[22]. Figure 5 shows the resistance vs temperature curve for Ge3 and Ge4 (the CR1000 Germanium resistor).

For Ge1, Ge2 and Ge4 eigth order least square polynomials, fitting the log of the resistance to the log of the temperature, were found to give the best agreement with the experimental calibration points, and were used for the temperature calculations in the heat capacity computations. For Ge3 a fourth order polynomial of the inverse temperature as a function of the square root of the log of the resistance was used instead[21].

2.3. Calorimeter

The calorimeter was made of Oxygen Free High Conductivity (OFHC) Copper in the form of a right circular cylinder with a center post. It is shown in figure 6, as part of the cryostat. The sample-substrate, in the form of a tape, was wound around the center post as tight as possible by hand. To improve thermal contact with the calorimeter body copper wires were silver epoxied[23] to the sample every 4" and connected to the top of the post. The latter also served as the housing of the heater.

The heater consisted of 0.230 m of #40 AWG Evanohm[24] wire wound bifilarly and varnished[25] in a single layer around a properly threaded OFHC Copper rod which fitted tightly inside the center post. Its room temperature resistance was 1110 Ω

Thermometer holders were silver soldered to the top of the calorimeter. These were OFHC Copper cylinders with a cut so that they could be squeezed to assure good thermal contact with the thermometers. To minimize thermal contact resistance Cryo-Con[26] grease was used inside these holders. Cryo-Con grease was also used on all threaded connections. We found that an excellent contact is achieved when both parts are covered by this low temperature high conductivity grease , and then screwed together tight enough to make the grease flow out the thread.

Finally a brass bushing was provided for connecting the fill tube, made of thin wall 0.050" O.D. cupro-nickel. All wires from the three thermometers and the heater were thermally anchored to the calorimeter body to reduce stray thermal effects. They were soft soldered to approximately 3 m of #36 AWG Copper wire wrapped around the calorimeter in pairs and varnished on to it for mechanical support and electrical insulation.

FIGURE 5

Resistance vs Temperature for Ge3 and Ge4

Least square fitted curves for Ge3, Ge4 as supplied to us.

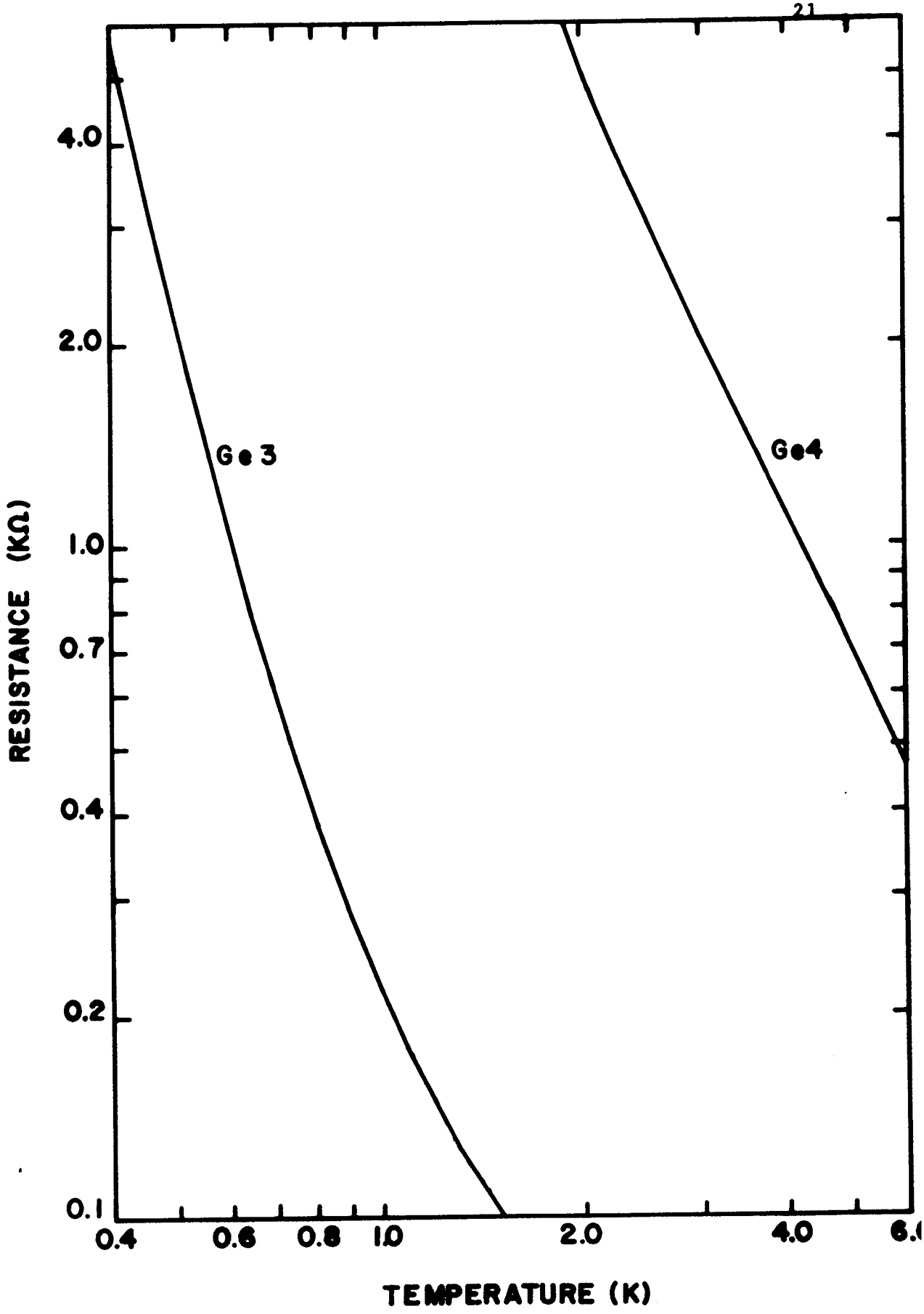
4.0
2.0
1.0
0.7
0.4
0.2
0.1
RESISTANCE (KΩ)
Ge 3
Ge4
0.4
0.6
0.8
1.0
2.0
4.0
TEMPERATURE (K)

Table A shows the materials composing the calorimeter and their weights.

2.4. Sample

For the reasons mentioned in section 1.2, the adsorbent chosen for this work was Grafoil[13]. This is made by exfoliation of natural Madagascar graphite particles in oxidizing medium. Then, after rapid heating they are compressed to form sheets. These sheets have about half the density of the original graphite with a large surface to volume ratio, of the order of 20 m^2/gm. Neutron rocking curve[27] measurements established that the graphite forms crystallites of average size about 100 Å and an average thickness of 110 Å. The crystallites are oriented in the sheets with their c-axis distribution peaked normal to the macroscopic sheet plane. The full width at half maximum of the c-axis distribution is about 30° [28].

Sheets of 0.010" thickness, $1\frac{37}{64}$" wide and about 15" long were cut and heated to 900°C in vacuum[29] for eight hours. Then Copper was vacuum deposited[30] on one side to approximately 0.5 μm. Before they were placed in the calorimeter they were heated to 150°C for four hours in a Hydrogen atmosphere. Finally, 57.82 gm were selected, sealed in the

TABLE A

Materials Composing the Calorimeter

Material	Use	Weight gm
OFHC copper	heater rod	5.4
OFHC copper	calorimeter body	213.4
copper	thermal anchorage,sample	1.00
copper	thermal anchorage,wiring	-
copper,germanium	thermometers	1.0
grafoil	adsorbent (substrate)	57.82
soft solder	connect parts	3.1
silver epoxy	connect thermal anchorage	1.25
varnish	insulation, support	7
evanohm	heater wire	-
cotton	spacer	-

calorimeter where they stayed in vacuum for one week at 120°C before any measurements were taken.

The void volume of the calorimeter with the sample was 52.50 cm^3. This volume is indicated in figure 8 as V_c, and it will be referred as such from here on. It was found by comparison to a geometrically known volume, the standard volume V_s of figure 8, using Helium as the test gas. The total volume V_{cr} the sample gas could occupy in the cryostat was, of course, larger as it included the volume of the fill tube. V_{cr} was found to be 55.30 cm^3. The fill tube terminated at a toggle valve (TVS in figure 8) with an estimated volume of 1.0 cm^3. Therefore the fill tube had a volume of 1.8 cm^3. The amount of the gas sample in this volume was always negligible compared to that in V_c. This was rather fortunate, as it eliminated the necessity for complicated formulas estimating the gas amount in the fill tube, i.e: the temperature gradient region, which is a requirement for precision adsorption work. We shall return to the subject of the errors related with the amount of the adsorbed phase in section 2.7, the gas handling system.

2.5. Heat Switch

Cooling and subsequent thermal isolation of the calori-

meter was achieved through a superconducting heat switch. It consisted of Lead wire[31] soft soldered[32] at threaded Copper pieces (see figure 6) placed in a solenoid capable of producing a magnetic field strong enough to drive the Lead normal.

For pure metals the ratio of the thermal conductivities K_n/K_s, normal over superconducting state, has the following temperature dependence for low temperatures[33]:

$$K_n/K_s = C/T^2$$

The switch performs the better the lower the temperature. The critical temperature of lead is about 7 K. For both states, however, conductivity increases for a while as temperature decreases, then it decreases rapidly[34]. This makes the switch very effective at the temperature range below 1.5 K and moderate up to 3.0 K. For higher temperatures the sample is practically connected with the refrigerator, but data were taken because it was felt that if the conditions of the refrigerator were always identical the 'background' specific heat would be reproducible and, therefore, measurements of the specific heat of a sample meaningful. This will be seen in chapter 4, where the data are presented and analyzed.

The solenoid was made of Nb-Zr alloy, commercially

available[35]. It was $2\frac{1}{4}$" long, wound in 15 layers with a total of 1450 turns. At a current of 3.0 A it produced a field of about 1 KGauss. No persistent mode of operation was provided, since it would be energized for short periods of time only. A Kepco D.C. power supply[36], resistance programmed, manually operated was used as the power source.

2.6. Refrigerator

The temperatures required for this work were produced by two methods of refrigeration: pumping on liquid ^{4}He and diluting a ^{3}He-^{4}He mixture.

The ^{4}He sub-bath consisted of a Copper cylinder of approximately 300 cm^3 capacity, a cupro-nickel $\frac{5}{8}$" O.D. pumping line and a fill needle valve communicating with the main ^{4}He bath. It would either precool and liquify the ^{3}He-^{4}He mixture or cool the sample down to 1.5 K to take the high temperature data. A Stokes[37] mechanical pump, model Microvac 149H-10, was used for pumping. According to the manufacturer it has a pumping speed of 500 lit/min at 0.1 mmHg pressure. It was located in another room to avoid mechanical vibrations. A 470 Ω 1/2 W Speer carbon resistor was used to monitor the temperature. All wires were thermally anchored to the sub-bath body, as described already in

available[35]. It was $2\frac{1}{4}$" long, wound in 15 layers with a total of 1450 turns. At a current of 3.0 A it produced a field of about 1 KGauss. No persistent mode of operation was provided, since it would be energized for short periods of time only. A Kepco D.C. power supply[36], resistance programmed, manually operated was used as the power source.

2.6. Refrigerator

The temperatures required for this work were produced by two methods of refrigeration: pumping on liquid ^{4}He and diluting a ^{3}He-^{4}He mixture.

The ^{4}He sub-bath consisted of a Copper cylinder of approximately 300 cm^3 capacity, a cupro-nickel $\frac{5}{8}$" O.D. pumping line and a fill needle valve communicating with the main ^{4}He bath. It would either precool and liquify the ^{3}He-^{4}He mixture or cool the sample down to 1.5 K to take the high temperature data. A Stokes[37] mechanical pump, model Microvac 149H-10, was used for pumping. According to the manufacturer it has a pumping speed of 500 lit/min at 0.1 mmHg pressure. It was located in another room to avoid mechanical vibrations. A 470 Ω 1/2 W Speer carbon resistor was used to monitor the temperature. All wires were thermally anchored to the sub-bath body, as described already in

section 2.3, by connecting each to 3.0 m Copper wire #36 AWG. The sample fill tube was also thermally anchored to the sub-bath by soldering it to a Copper piece threaded on to the sub-bath body.

A radiation shield, made of Copper, was also threaded on the sub-bath. This covered the rest of the cryostat in the vacuum can. The schematic cross section of the ^{4}He refrigerator is shown in figure 6. Cotton padding was used as a spacer between the shield and the calorimeter.

The dilution refrigerator was designed[38] to be similar to the one described in a paper by A.C.Anderson[39], and a detailed description of the construction and theory of operation will not be given here as there are excellent papers on the subject[40]. We shall only give some dimensions and comment on the performance. The still and mixing chamber are identical, OFHC Copper $1\frac{5}{8}$" O.D., $\frac{1}{2}$" height. Half the volume of the mixing chamber was filled with sintered Copper to reduce the thermal resistance. A 340 Ω and a 220 Ω 1/2 W Speer carbon resistors were used to monitor the temperature of the still and the mixing chamber respectively. All carbon thermometers were measured by the A.C. bridge. A continuous heat excanger was employed consisting of concentric cupro-nickel tubes. The mixture was 0.4 gmol with 20% ^{3}He.

The refrigerator would cool down to 100 mK with no load and about 250 mK with the calorimeter. Of course, turning the Lead switch off to isolate the calorimeter would create eddy currents that usually warmed the sample up to 450 mK. We feel that exchangegas in the vacuum can was the main reason for heat leaks although oscillations around the support rod (that actually houses the thermal switch) might have contributed. In any case, no tests were made to identify heat leaks and estimate their contributions.

The schematic cross sectional diagram of the dilution refrigerator is shown in figure 6.

2.7. Gas Handling System

It should be clarified that two systems were actually in use, because the operation of the dilution refrigerator required handling of a ^{3}He-^{4}He mixture. Figure 7 is a schematic representetion of the mixture handling system. It provided for the circulation, recovery and storage of the necessary amount to run the refrigerator as well as for making new mixture, in case of an accidental loss. The following procedure was adopted for running the dilution refrigerator:

While the cryostat was at room temperature all the lines of the handling system, and the cryostat, were subjected to a high vacuum (10^{-6} Torr) for at least 48 hours. Then the cryostat valves (not shown in figure 7) were closed and precooling started. To help the diffusion pump of the high vacuum system, and prevent any outgassing in case the high vacuum was needed for other purposes, the charcoal traps (T_1 and T_2 in figure 7) were held at 77 K at all times. When the ^{4}He sub-bath was cold, i.e: 2 K or less, the mixture was allowed to condense by opening valves TV14, NV1, cryostat valve to condenser. When enough mixture was liquified, about 350 mmHg of our 1000 cu. inch container (SM in figure 7), circulation would start by closing TV14 and opening cryostat still valve, BV2, BV11, TV12 and TV6. The diffusion pump DP was not turned on until input pressure was less than 1 mmHg.

To stop the refrigerator either exchangegas was allowed in the vacuum can or the still heater power was turned on at the maximum, 10 mW. The mixture was collected using the mechanical pump MP only (NV1 closed, TV10 and TV14 open).

The storage container SSM equipped with the pressure sensitive valve SV1 was employed as a protective device for the mechanical pump during recovery, in case trap T1 should

FIGURE 6

The Cryostat

Scale is approximately 1:1.6

A ^{4}He sub-bath pumping line

B Vacuum can pumping line

C Still pumping line

D Tube connecting sub-bath with fill valve (not shown)

E Vacuum can (of stainless steel)

F ^{4}He sub-bath

G The return line (mixture condenser)

H Mixture flow impedance

I Thermometer holder

J The still

K Heat exchanger

L Support (of nylon)

M Radiation shield (of copper)

N The mixing chamber

O Sample fill line (of cupro-nickel)

P The solenoid

Q Thermal switch housing and calorimeter support (of nylon)

R Thermal switch

S The calorimeter

T The heater

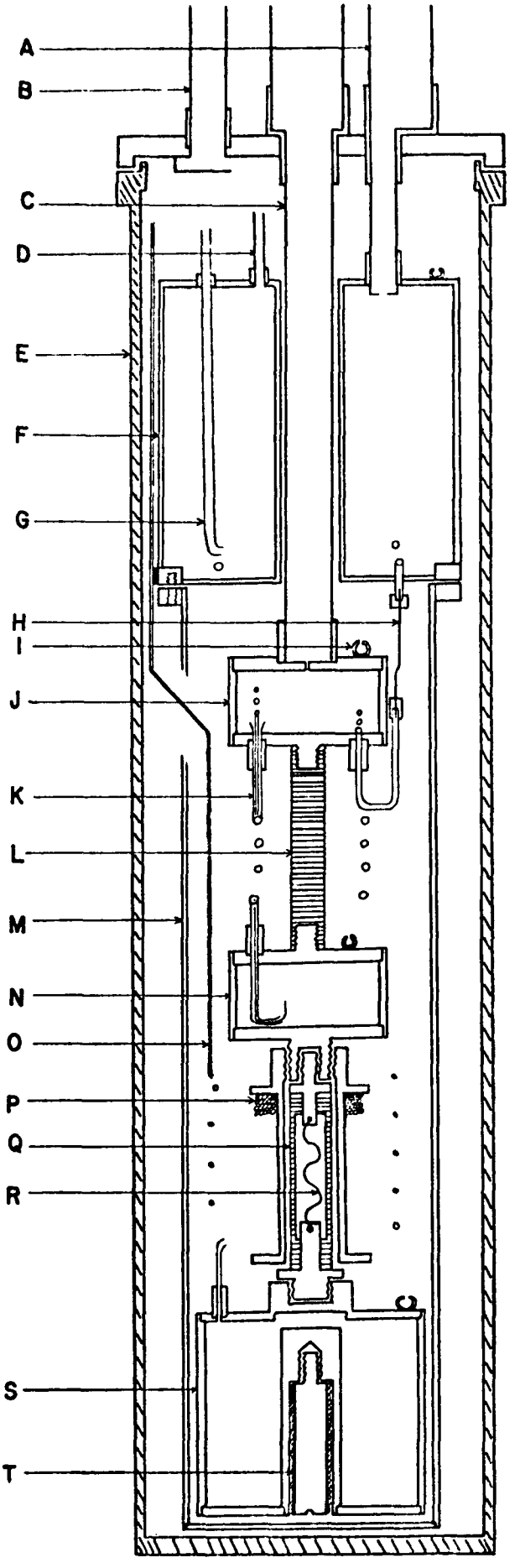
A
B
C
D
E
F
G
H
I
J
K
L
M
N
O
P
Q
R
S
T

FIGURE 7

Mixture Handling System

BV	Bellows valve
DP	Diffusion pump, NRC Booster type 126B (ref. 41)
G	800 mmHg absolute pressure gauge (ref. 42)
KF	Quick coupling connectors
MP	Sealed mechanical pump, Edwards Speedivac ED660(ref. 43)
NV	Needle valve
SM	(Normal) mixture storage. 1000 cu. inch
SSM	(Safety) mixture storage. 1000 cu. inch
SV1	Pressure sensitive valve, set to open at 1 Atm
^3He	Supply of pure ^3He
T	Traps. Cocoanut Charcoal, activated, mesh 6-14(ref. 44)
TC	Thermocouples (ref. 45)
TV	Toggle valve

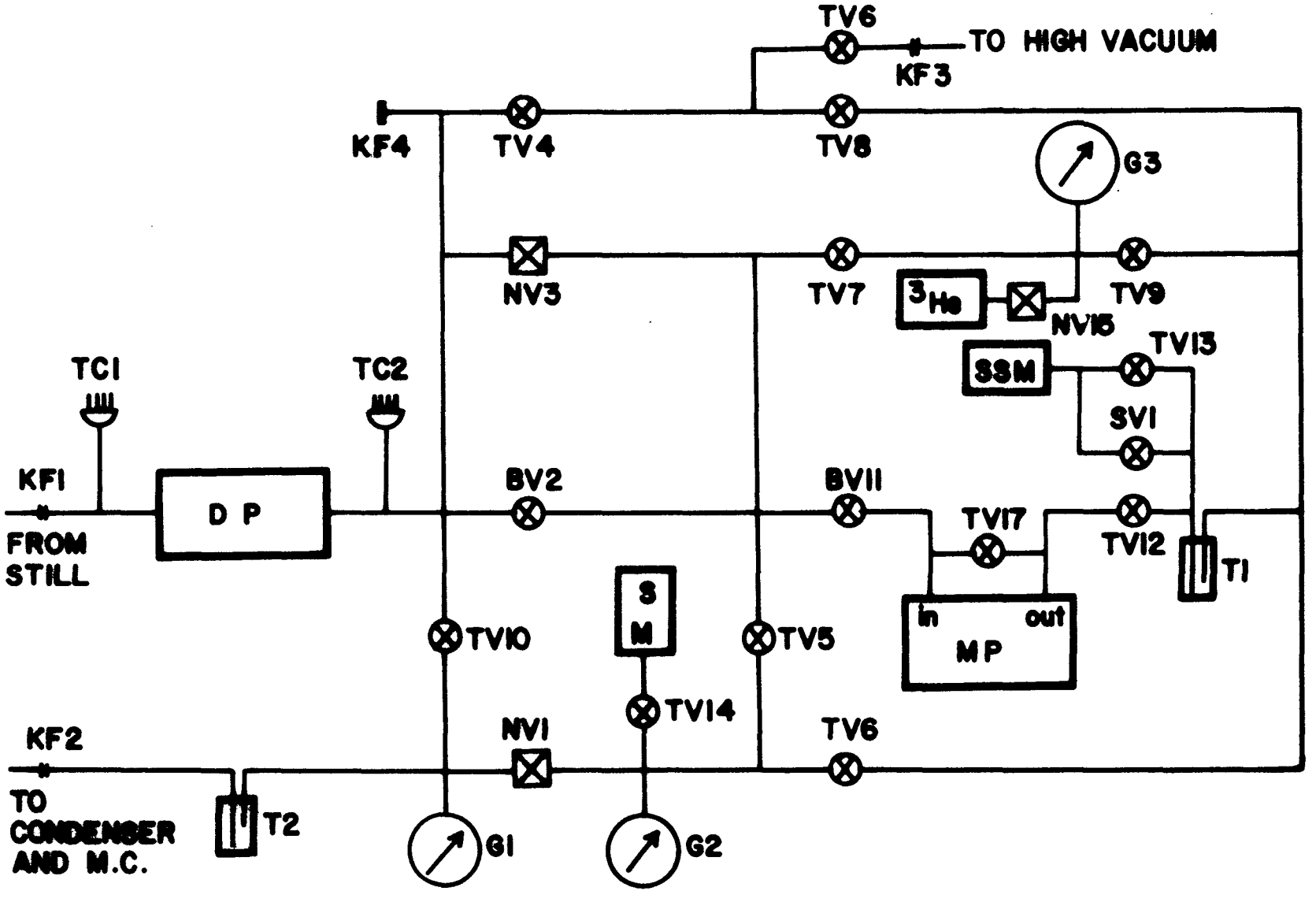
TV6
TO HIGH VACUUM
KF3
KF4
TV4
TV8
G3
NV3
TV7
^{3}He
TV9
NV15
TV13
SSM
SV1
TC1
TC2
KF1
D P
BV2
BV11
TV17
TV12
T1
FROM STILL
S M
TV10
TV5
in
out
MP
TV14
NV1
TV6
KF2
TO CONDENSER AND M.C.
T2
G1
G2

block and output pressure become too high. The extra KF4 connection was included for leak testing or mixture ratio monitoring.

Figure 8 is a schematic represantation of the sample gas handling system. It was composed of three parts, a ^{3}He supply and recovery system, actually built on a separate rack for easy transport and attachment to other experiments, an Argon and ^{4}He supply and a precision pressure gauge.

The ^{3}He supply was tested for ^{4}He impurities by measuring the ^{3}He-^{4}He ratio using a Veeco leak detector[46], model MS-90, which gave an estimated purity of 99.85%. Both Helium samples were assumed free of any other contaminants as they were always cleaned by the charcoal trap T1 held at 77 K. Argon was not tested for purity. When Argon samples were prepared, trap T1 was at dry ice temperature.

To make a sample the following procedure was adopted: For a few days all the lines would be subjected to a high vacuum and the zero of the Ruska[47] pressure counter was set. Next with the counter in measuring configuration a quantity of sample gas was allowed in the standard volume V_s. Room temperature and pressure was recorded. Then the cryostat sample valve TVS was opened and enough time was allowed for

the sample to be adsorbed at the desired temperature, usually overnight. The Helium samples were annealed at about 10 K to assure uniform adsorption. Annealing was not necessary for Argon.

The cryostat valve TVS was normally open for pressure monitoring. An exception was made when cooling to 4.2 K, after a monolayer of Argon was deposited at 77.3 K. The amount of the Argon in the room temperature volume V_1 (see figure 8) plus the amount in the void volume of the calorimeter V_c was enough to block the sample fill tube. Instead it was decided to isolate the cryostat volume (V_c) and transfer liquid Helium very slowly, in such a way as to cool the calorimeter together with the fill line. Obviously there was an uncertainty in our Argon coverage used as preplating. As it is shown in section 4.1 this was not more than 2%.

The uncertainty, however, of a typical incremental amount of gas entering the sample cell during either an adsorption isotherm or a plating for heat capacity measurements was less than 1%. This came mainly from the uncertainty of the standard volume V_s estimated to be about 1% (from its geometrical shape). Pressure could be measured with a resolution of 3 microns of Hg which typically yielded an error of 0.01%. Room temperature was read within 0.1 $^{\circ}$C,

FIGURE 8

Sample Handling System

C Compound gauge, 30-0-15

RUSKA GAUGE precision pressure counter, model XR-38(ref. 47)

MP Sealed mechanical pump, Duo-seal, model 1402 (ref. 48)

The rest symbols are identical to those of figure 7

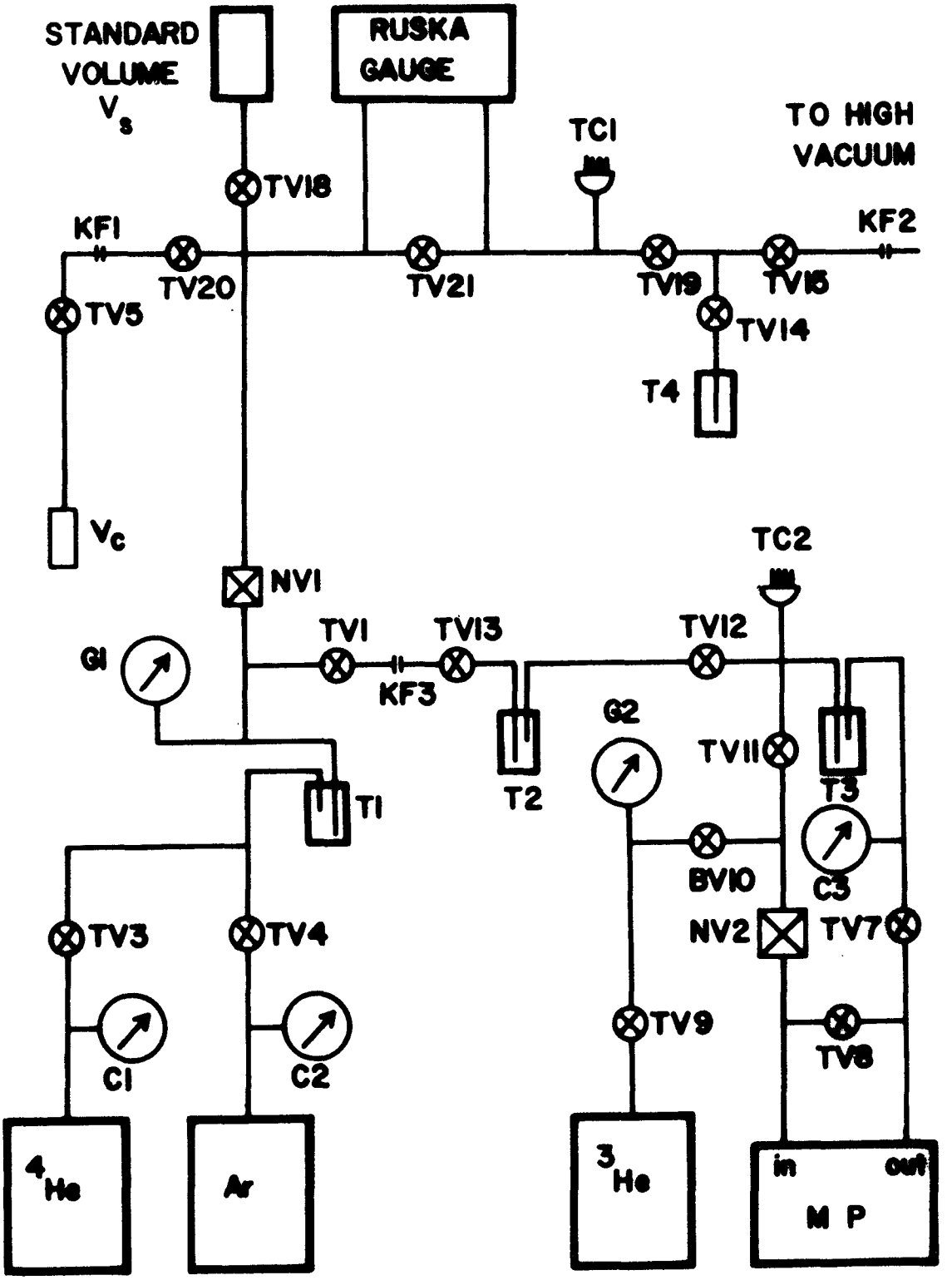
STANDARD VOLUME V_s
RUSKA GAUGE
TO HIGH VACUUM
TC1
TV18
KF1
KF2
TV20
TV21
TV19
TV15
TV5
TV14
T4
V_c
NV1
TC2
TV1
TV13
TV12
G1
KF3
G2
T2
TV11
T3
T1
BV10
C3
TV3
TV4
NV2
TV7
C1
C2
TV9
TV8
^{4}He
Ar
^{3}He
in
out
M P

i.e: within 0.03%. Therefore, the reproducibility of a certain coverage was better than 0.1%, since repeating a coverage was indepedent of the value of V_s.

For reference purposes we give in Table B the values of volumes we had to know for calculating the amount of the sample adsorbed. They were all estimated compared to V_s, and the recordeduncertainties do not include the V_s uncertainty. Void volume corrections were made following the procedure adopted by Daunt and Rosen[49]. Pressure corrections were made based on the Weber-Schmidt equation[50].

2.8. Data Acquisition System

Figure 9 is a block diagram of the electronics data collection system. The voltage across the Germanium thermometers was amplified by a Keithley 140 nV DC amplifier and measured by a Hewlett—Packard 3460A digital voltmeter which also measured the thermometer current, heater voltage and heater current. The heating period was measured by the Hewlett—Packard 5223L electronic counter (TIMER in the figure). These voltages and timings were recorded on magnetic tape via a Dymec[51] 2546A magnetic tape coupler and a Kennedy[52] 1406 magnetic tape transport. Redundandly the digital information was printed on paper via a Digitem[53]

TABLE B

Sample Gas Handling System Volumes

Description	Symbol (fig. 9)	Volume cm^3	Error %
Standard volume	V_s	1073.	-
Room temperature lines	V_l	81.3	0.8
Cryostat void volume	V_{cr}	55.3	0.9
Calorimeter void volume	V_c	52.5	2.
Sample fill tube	V_g	1.8	20.
TVS valve (half)	V_w	1.0	10.

FIGURE 9

Data Acquisition System. Block Diagram

Basically a 4-lead DC resistance measurement system.
Arrows indicate the 'flow' of information

Programmer	see text (ref. 55)
Controller	see text (ref. 55)
Power supply	5-40-170 VDC (ref. 55)
DC Amplifier	Keithley nV DC Amplifier, model 140
Digital Voltmeter	Hewlett—Packard, model 3460A
Timer	Hewlett —Packard Electronic Counter 5223L
Teletype	Teletype Corp., model 33(ref. 54)
Teletype Coupler	Digitem, model BAC (ref. 53)
Magnetic Tape Deck	Kennedy 1406 (ref. 52)
Magnetic Coupler	Dymec, model 2546A (ref. 51)

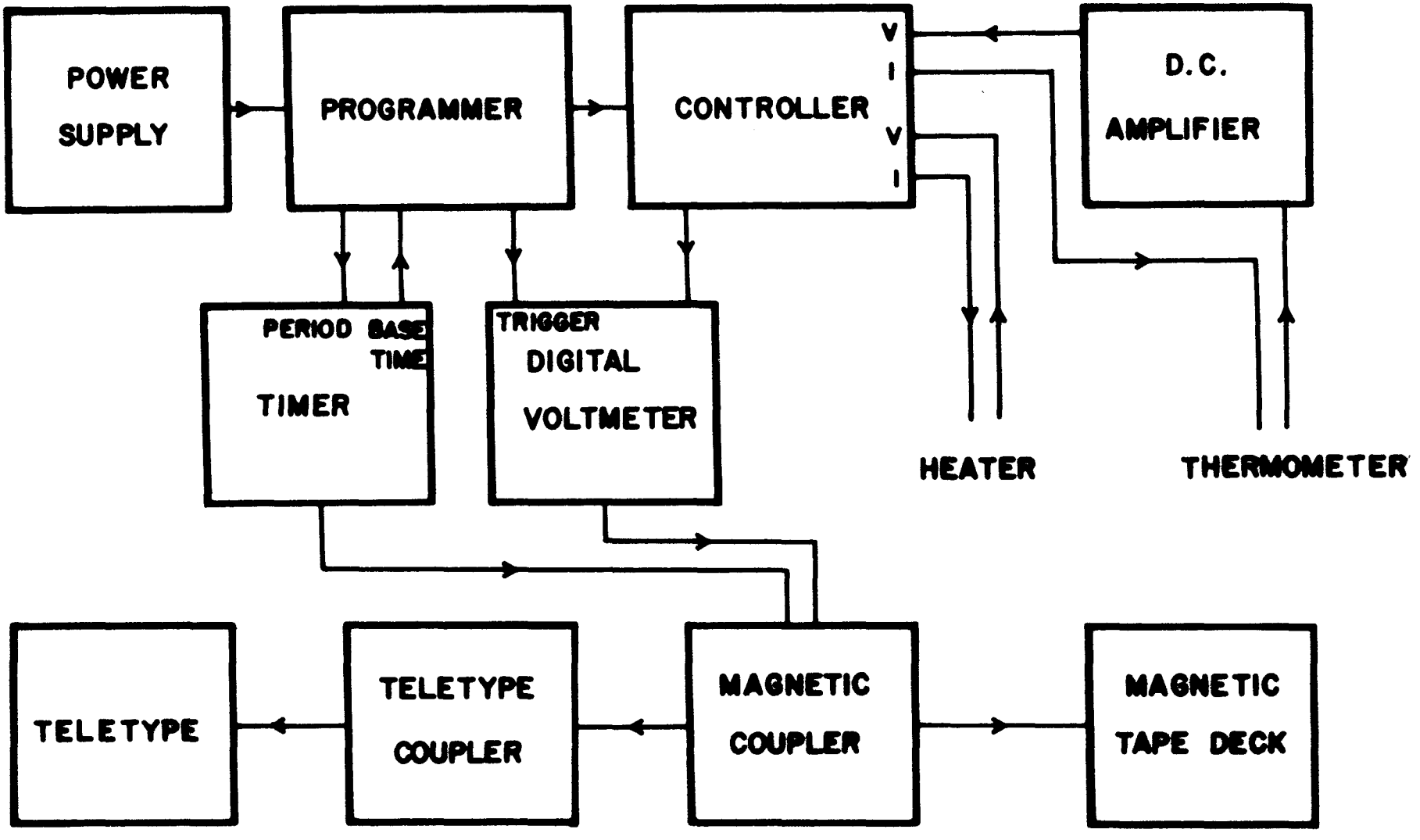
POWER SUPPLY
PROGRAMMER
CONTROLLER
V
I
V
I
D.C. AMPLIFIER
PERIOD BASE TIME
TIMER
TRIGGER
DIGITAL VOLTMETER
HEATER
THERMOMETER
TELETYPE
TELETYPE COUPLER
MAGNETIC COUPLER
MAGNETIC TAPE DECK

BAC coupler and a model 33 Teletype[54]. A FORTRAN program was written to read the magnetic tape and calculate the heat capacity. The teletype simply provided a hard copy of the data useful for on the spot preliminary calculations. The programmer generated the command pulses for selecting and reading the right voltage whereas the controller carried out these commands.

Figure 10 is the logic diagram of the programmer. The design employed DTL and TTL compatible integrated circuits (IC's). It was constructed[55] in a modular way. The idea was to automatically cycle and perform the necessary operations for measuring the heat capacity of a specimen. These operations were the following, in sequence:

Read thermometer current (i.e: voltage across R_{st}, fig. 13)
Read temperature (i.e: voltage across thermometer)
Turn on heater. Turn on timer
Read heater current (i.e: voltage across R_{SH}, fig. 13)
Read heater voltage
Turn off heater. Stop timer. Read timer.
Repeat...

It was basically a (binary) counter. At certain configurations of the counter gates would activate flip-flops, which in turn energized the relays of the controller. The 5223L HP electronic counter provided the timing pulses

we used as a base time. The period selected was 1.0 sec. accurate to 1 ppm. The base time pulses, after proper amplification and shaping, were fed into the clock input of the first counter, the waveform of which is shown in figure 12. The cycling period of this counter was called the unit time and was normally set at 7 sec. There was one DVM reading per unit time. When thermometer current reversal was desired, the unit time was chosen as the period of the reversal. The output of the last flip-flop was the clock pulse of the next counter and so on. The second and third counter determined the length of the drift and heating periods. Figure 11 shows the second counter in more detail omited from figure 10 due to space limitations. The outputs of the binary-to-decimal (BCD) decoders drove the inputs of the AND and NOR gates. It was found necessary to use capacitors because these outputs had many undesired fast pulses, due to the fact that we used asynchronous counters. We also needed voltage dividers because the decoder outputs are usually high voltage outputs in order to drive Nixie[56] tube displays. The dividers and relevant waveforms are shown in figure 12. The output of the gates controlled the state of the flip-flops and the reset of the counters. The output of the flip-flops did not provide enough power to activate the relays chosen (see figure 13), and thus transistors were used as the final stage.

FIGURE 10

The Programmer

R = 2 KΩ
R1 = 100 KΩ
R2 = 5 KΩ
R3 = 20 KΩ
R4 = 300KΩ
R5 = 6 KΩ
All capacitors .001 pF
All transistors RCA 2N2270
NOR gates are TI SN7402N
AND gates are TI SN74H11N
Diode any general use diode
Reset switch is single throw, double pole
Rotary switch 1 is ten throw, double pole
Rotary switch 2 and 3 are ten throw, single pole
PJ1 is 8-prong Amphenol plug
The dividers (following the capacitors) are shown in fig. 12
A typical counter of ten is shown in fig. 11

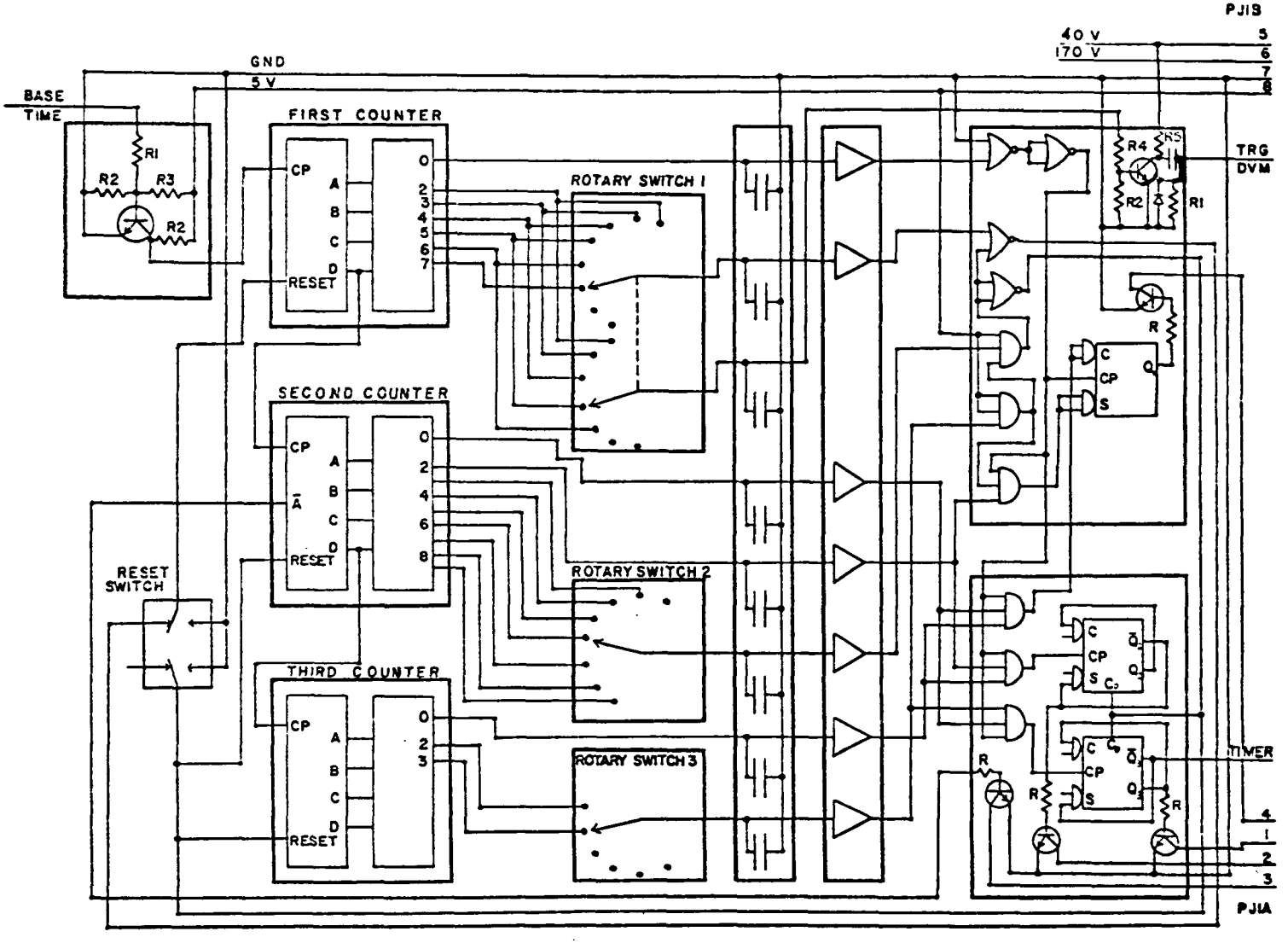
PJ1B
40 V
170 V
5
6
7
8
GND
5 V
BASE
TIME
R1
R2
R3
R2
FIRST COUNTER
CP
A
B
C
D
RESET
0
2
3
4
5
6
7
ROTARY SWITCH 1
R4
R5
R2
R1
TRG
DVM
R
C
CP
S
SECOND COUNTER
CP
Ā
A
B
C
D
RESET
0
2
4
6
8
RESET
SWITCH
ROTARY SWITCH 2
THIRD COUNTER
CP
A
B
C
D
RESET
0
2
3
ROTARY SWITCH 3
TIMER
4
1
2
3
PJ1A

FIGURE 11

Decade Counters

Flip-flops are Fairchild DTμL945
Binary to decimal decoders are TI SN7441N
Nixie is the numerical display, type 8421(B5092) (ref. 56)

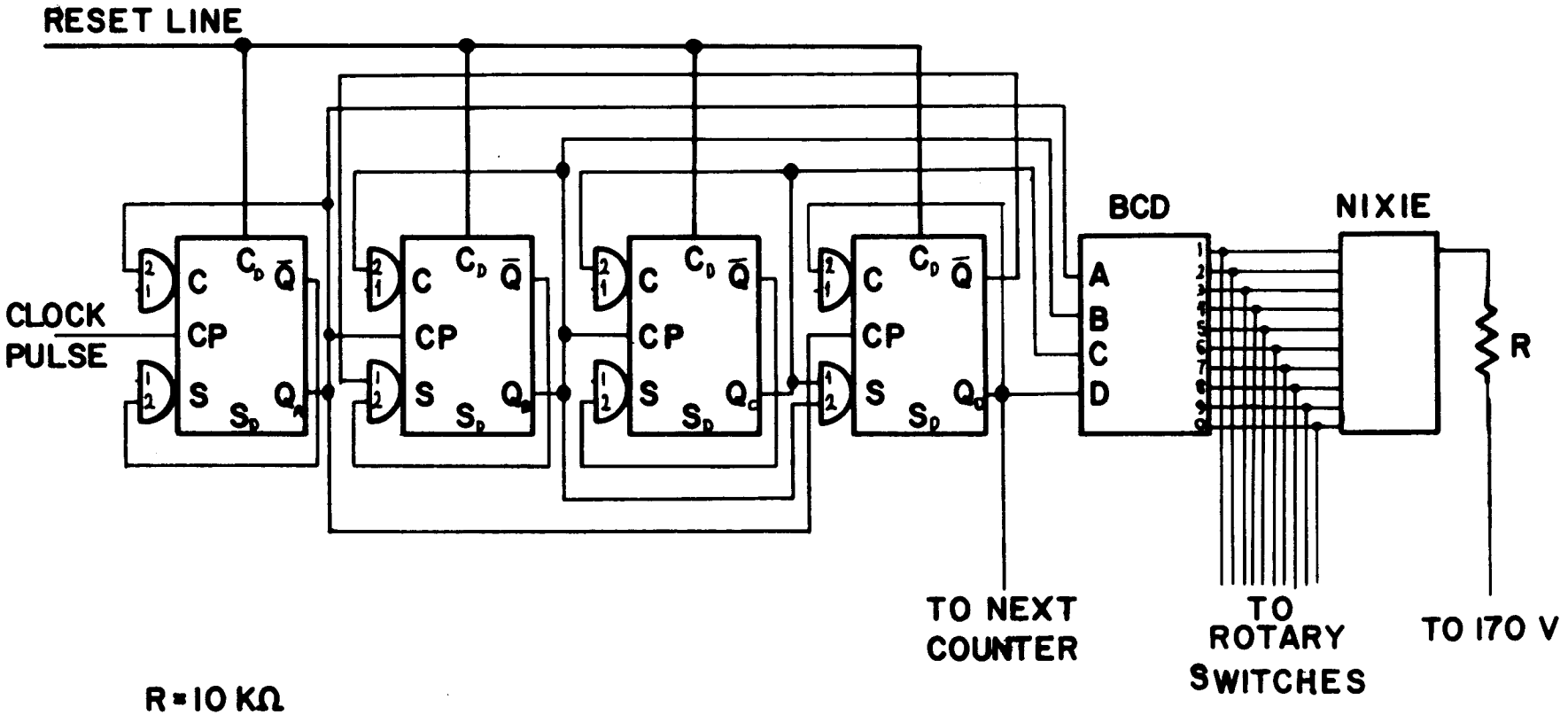
RESET LINE
CLOCK PULSE
C
CP
S
C_D
S_D
$\bar{Q}$
Q
BCD
A
B
C
D
NIXIE
R
TO NEXT COUNTER
TO ROTARY SWITCHES
TO 170 V
R = 10 KΩ

FIGURE 12

BCD Output Waveform Shaping

Without the capacitors (see figure 10) the negative going pulses at the collector, i.e: the output, could reach 0 Volts and upset the subsequent logic, as they would be accepted as the logical '0' level by the gates.

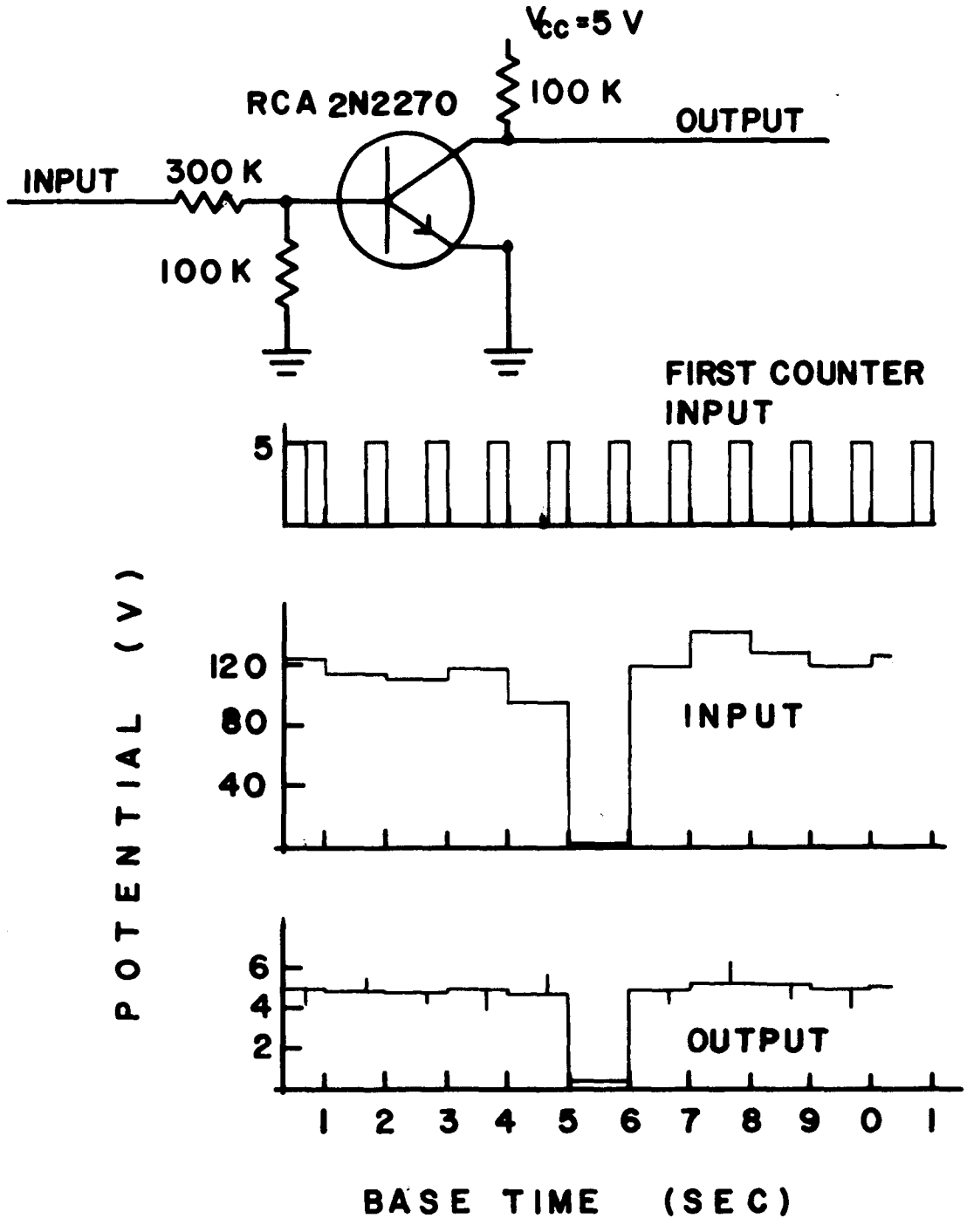
V_{cc}=5 V
100 K
RCA 2N2270
OUTPUT
INPUT
300 K
100 K
FIRST COUNTER INPUT
5
POTENTIAL (V)
120
80
40
INPUT
6
4
2
OUTPUT
1 2 3 4 5 6 7 8 9 0 1
BASE TIME (SEC)

FIGURE 13

The Controller

CR1, CR4	Potter and Brumfield mercury relays, type JM2-106-21
CR2, CR3, CR5	Potter and Brumfield mercury relays, type JM3-110-31
E1, E2	12.6 V mercury batteries, Mallory TR-169
N1 - N4	Neon voltage indicators
D1 - D5	Diodes, general use
M1	1.0 mA milliammeter
S1	Switch double throw, single pole
S2, S3	Rotary switches, ten throw, single pole
PJ1, PJ2	8-prong Amphenol plugs
R1, R2, R4	600 Ω, 2 W
R3	120 Ω, 2 W
R5	1150 Ω, the dummy heater
RT1 - RT9	1.5-2.2-3.3-3.0-5.6-6.8-5.6-22.0 MΩ
R_{st}	100 kΩ standard resistor, General Radio, type 1440
R_{SH}	10 kΩ standard resistor, General Radio, type 1440
RH1 - RH8	3.6-1.2-1.5-2.2-2.6-7.5-44.0-270 kΩ
	the RH8 could be bypassed by a jumper wire

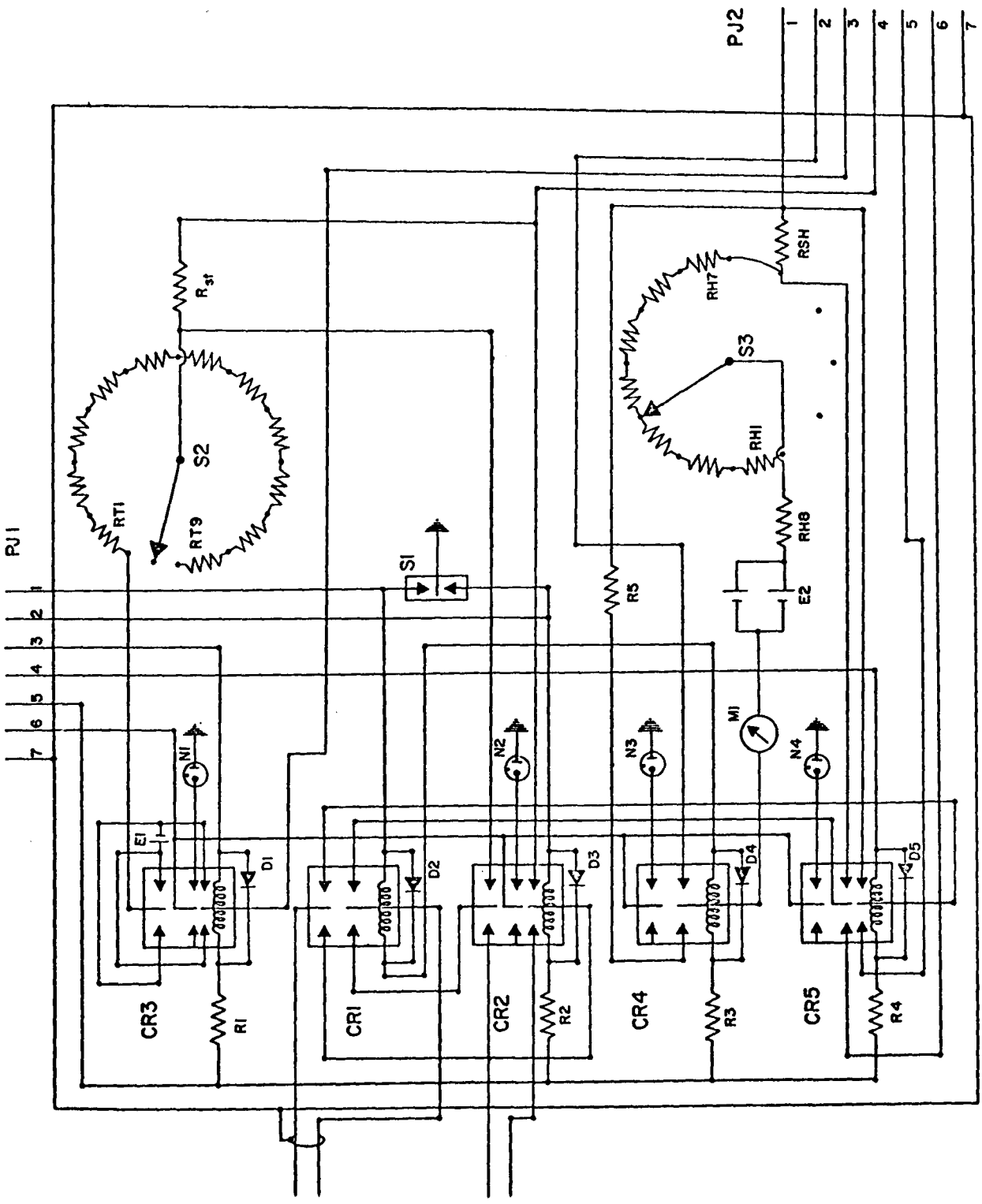
PJ1
PJ2
S1
S2
S3
RT1
RT9
R_{st}
RH7
RSH
RH1
RH8
R5
E2
M1
N1
N2
N3
N4
E1
D1
D2
D3
D4
D5
CR3
CR1
CR2
CR4
CR5
R1
R2
R3
R4

Figure 13 is the circuit diagram of the controller. Relays CR1, CR2 and CR5 connected the input of the digital voltmeter across the desired resistor or at the output of the DC nV amplifier. CR3 was reversing the thermometer current, selected by the switch S2. CR4 switched the heater power to a dummy heater when the sample heater was off, so that the battery would be continuously loaded. We found this improved the stability of the battery voltage, compared to a real switch on-off situation. Switch S3 selected the heater power. We also included a milliammeter (MA) for a gross reading and adjustment of the power. Switch S1 was used for testing the relays CR1 and CR2 by activating them independently of the logic state of the programmer.

CHAPTER 3: THEORY

3.1. Introduction

Before presenting our experimental results and attempting to interpret them, we feel it is appropriate to discuss the theory of adsorption and the thermodynamic properties of the adsorbate. No new theories will be presented here, but only a short account of well established concepts and ideas with their predictions, which we will find necessary as a background for the next chapter.

The basic references for this chapter are two books mentioned earlier[4],[5] and references to some original work which appears in great detail in these two books will not be repeated here.

3.2. Adsorption Isotherms. Monolayer

Experimental results of adsorption work are usually given in a form relating the amount V of the adsorbed phase, the temperature T of the system and the pressure P of the gas phase, under equilibrium conditions. Perhaps, because of the convenience of measuring V as a function of P, keeping

T constant the form

$$V = f(P)_T$$

i.e: an adsorption isotherm, is the most usual form found in the literature. Besides the convenience, the adsorption isotherm is important in determining the amount V_m of the first completed layer, the so called monolayer, which provides a measure of the adsorbent surface area. The definition of the monolayer is not truly independent of the geometry of the adsorbent surface, but, hopefully, the concept is a clear one.

Obviously an analytic expression for the isotherm containing V_m as a parameter would be extremely useful, reducing the problem to a mathematical fit with experimental points. It turns out, however, that for certain systems, such as Argon on Grafoil, the shape of the isotherm can yield quantitative information about the monolayer.

According to the classification introduced by Brunauer et al[58] the systems under investigation yield a type II isotherm, the typical shape of which is shown in figure 14. Brunauer and Emmett observed that this isotherm contains a linear portion and they argued that this must be due to the formation of the second layer. They considered several points associated with the straight line that could possibly

indicate the monolayer coverage. We show these points in figure 14. Experience has shown that the point 'B', the point where the straight line deviates from the isotherm, is the best choice yielding monolayers in agreement with other methods. In our analysis the point 'B' method will be used.

This method has an advantage over methods which estimate the monolayer based on a model. No assumptions regarding the structure and geometry of the system are necessary. In order to derive a simple and analytic isotherm all models use very restrictive, almost unrealistic, assumptions casting doubts on the validity of their predictions. The BET[59] isotherm, very succesful in estimating monolayers in the cases of physical multilayer adsorption (type II isotherms) fail for systems such as rare gases on graphite. These systems are known to excibit stepwise isotherms due to the uniformity of the substrate,[16] and the continuous BET equation is, in principle, inadequate. In the case of Helium no stepwise isotherms have been reported so far, but the BET monolayer is often as much as 300% in error[92].

In appendix C, a discussion of the BET isotherm shortcomings together with another isotherm due to Langmuir is given.

FIGURE 14

Type II Isotherm. Monolayer Determination

Brunauer and Emmett proposed the following points as possibilities for monolayer indication:

A: the intercept of the straight line with the vertical axis

B: the point where the isotherm deviates from the straight line at low pressures

C: half way of the common part of the isotherm and the straight line

D: the point where the isotherm deviates from the straight line at high pressures

E: the intercept of the straight line and an isobaric at the liquifaction (or solidification) pressure of the bulk gas, at the temperature of the isotherm

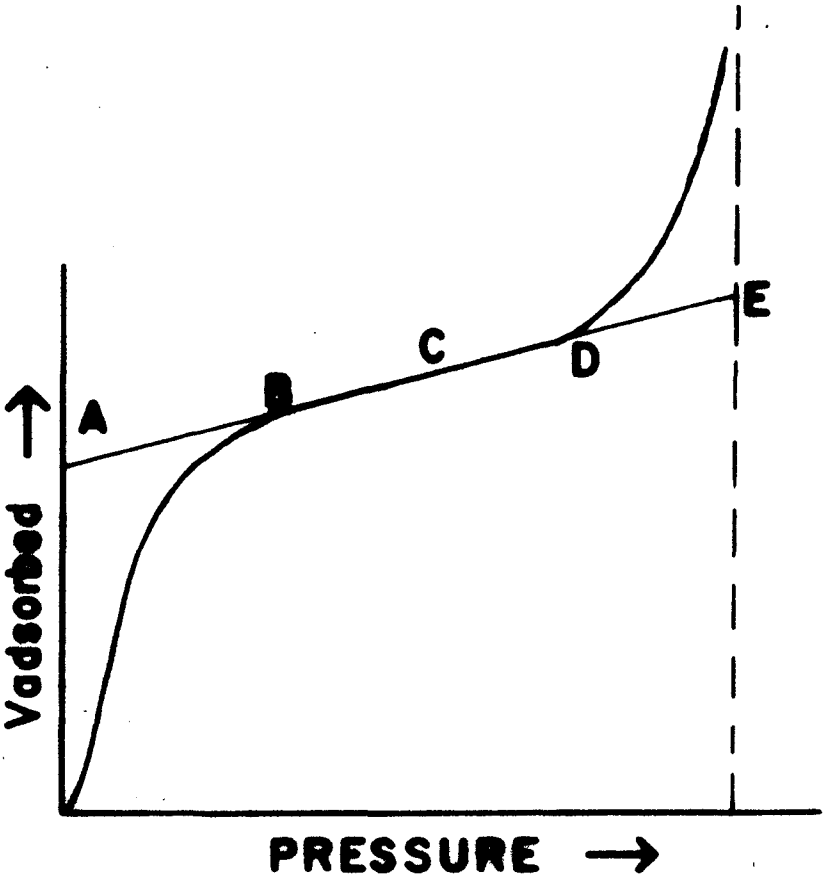
A
B
C
D
E
Vadsorbed
PRESSURE

3.3. Surface Area

Once the monolayer coverage is known, the surface area of the adsorbent can be found if the size and packing of the adatoms are known. Following the procedure adopted by Daunt and Lerner[60] it will be assumed that the Argon monolayer forms a close-packed array with a nearest-neighbour distance d of 3.83 Å, equal to that of solid Argon at 20 K[61]. This value is in excellent agreement with d values calculated or measured by others. Milford and Novaco[62] calculated d by minimizing a 2D sum of Lenard-Jones potentials, using appropriate parameters for the Argon-Argon interaction[63]. They found d=3.84 Å. From the density of the solid[64], we calculated a distance of 3.86 Å at 77 K. Kjems et al[27] measured d to be 3.88 Å at 5 K for almost monolayer coverage using (elastic) neutron diffraction.

Picturing the adatoms as hard spheres (see figure 15) with diameter equal to d, one can see that their molecular area σ will be that of a hard disc:

$$\sigma = \pi(d/2)^2 = 11.5 \text{ Å}^2$$

However, the area the adatoms occupy is larger than σ due to the packing, which leaves some void space. As is schematically shown in figure 15, the hexagonal symmetry requires that

every adatom actually occupies an hexagon with area a_m, or if we wish, the areal density D_m of the monolayer will be

$$D_m = 1/a_m$$

With the symbols as shown in the figure, the area a_m is:

$$a_m = \sigma(h/2)(d/2) = \sigma(4\cos 30/\pi) = 1.103\sigma$$

Now, if V_m is the monolayer measured in cm^3(STP) and σ in $\mathring{A}^2$, the area Σ of the adsorbent, in m^2, will be given by:

$$\Sigma = N_A V_m a_m / V_A = 0.296 V_m \sigma$$

where N_A is Avogadro's number and V_A the volume of one mole gas in cm^3(STP).

3.4. Thermodynamics In Two Dimensions

The description of the macroscopic properties of bulk (3D) systems is precise and clear through careful definition of the (familiar) thermodynamic physical quantities. Certain assumptions are, of course, unavoidable. When dealing with 2D systems extra care must be exercised, if the same thermodynamic quantities are to be used, as some of the assumptions may no longer be valid.

Let us concentrate on the additivity of the (extensive) thermodynamic quantities. For a 3D closed system, say with energy E, which can be imagined to be separated in subsystems

FIGURE 15

Monolayer of Argon on Grafoil

The Argon atoms are represented by the circles with diameter equal to their nearest-neighbor distance. They form a close-packed array. Due to the hexagonal symmetry the area occupied by an atom is that of the hexagon, as shown.

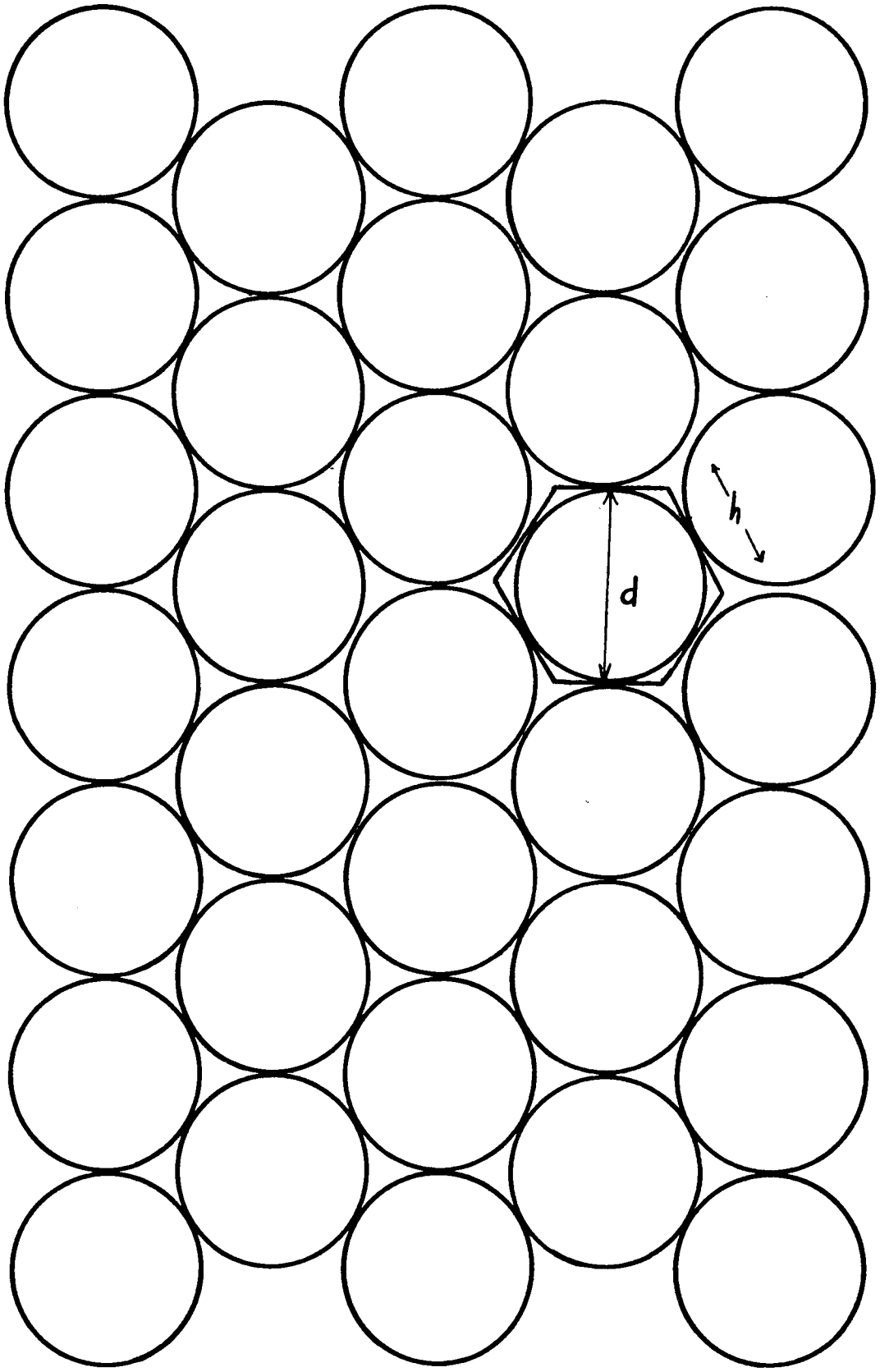
h
d

with energies E_1, E_2, ..., considered themselves macroscopic but much smaller than the whole system, one usually assumes that

$$E = E_1 + E_2 + \ldots$$

In other words, the energy of the interaction of the subsystems among themselves, is neglected, although this is the energy that holds the subsystems together. The reasoning is that the particles which take part in this interaction are those near the surface (of a subsystem), of the order of $N^{2/3}$ if N is the number of the particles in the subsystem. For N large, i.e: for macroscopic systems, the number of particles at the surface is much smaller than the total number of particles and, concequently, the energy of the interaction with the surrounding subsystems is much smaller than its (internal) energy.

In the case of adsorption, the number of particles on a certain surface is no longer small compared to that of any subsystem, and the indiscriminate application of the additivity is not permissible. Nevertheless, we need the thermodynamic quantities to be additive, because then an equation valid for a subsystem, can be integrated over the whole system.

To preserve the additivity, Gibbs proposed the use of

carefully taken dividing surfaces (see figure 16), i.e: not intersecting the surface under investigation, but arbitrarily close to it so that all pfysical quantities of the system have the same value on both sides, and one can still write down

$$E = E_1 + E_2 + E_a$$

where a refers to the part contained between the two (imaginary) surfaces, i.e: the adsorbed phase mainly, and 1, 2 refer to the rest (bulk) phases. In this sense, the properties of the adsorbed phase, or otherwise called: the film, are 'excess' properties. That is, if one wants to find, say, the energy of the film, then one must subtract the energies of the bulk phases from the total energy of the system.

In view of the system of our study, we now restrict our discussion to systems with the two bulk phases being a solid (usually called the adsorbent or substrate) and a gas (the adsorbate). This system is assumed contained in a closed vessel, so that the volume of the gas phase is constant and the total number of the adsorbate atoms, i.e: those in the gas phase plus those in the adsorbed phase (the adatoms), is also constant. From now on we shall use the letter V for the volume of the gas phase, and N for the number of atoms (N_g in the gas phase, N_a in the

FIGURE 16

Gibbs' Dividing Surfaces

// Phase 1 (bulk)

\\ Phase 2 (bulk)

FILM Adsorbed phase

One usually assumes the dividing surfaces can approach each other at zero distance and form one dividing surface, strictly 2D, with the properties of the adsorbed phase. Real configurations are, however, much more complicated, and the limit to zero distance is not always conceivable.

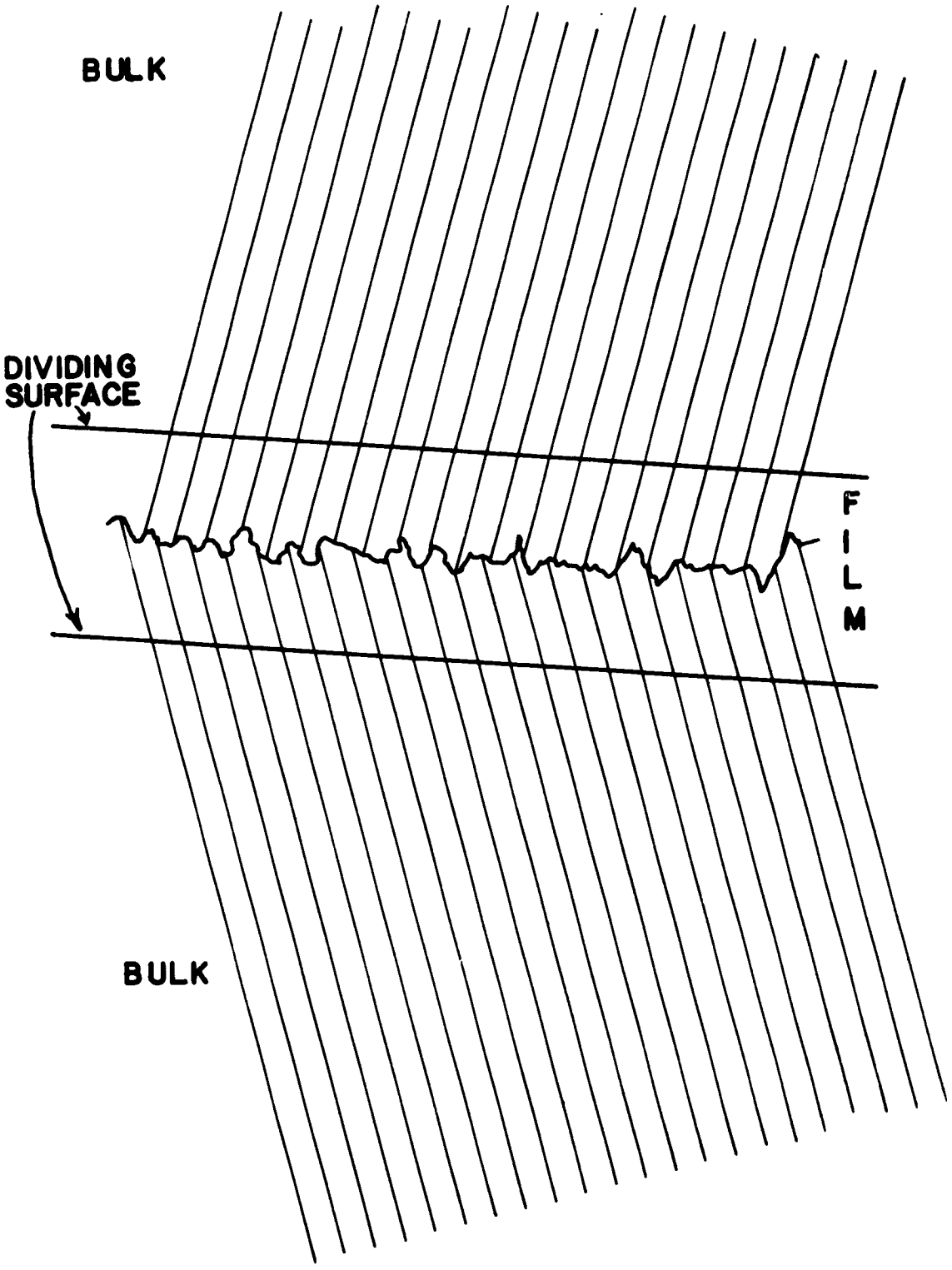
BULK
DIVIDING SURFACE
FILM
BULK

adsorbed phase). The solid provides a certain surface Σ for adsorption, assumed indepedent of any changes in the system. In short, the changes of our system are under constant N,V,Σ. Finally, due to the small pressures involved at the temperature range of interest, the gas will be assumed perfect.

In case of possible confusion, we shall use indices to distinguish between the phases as follows: s for the solid, g for the gas, a for the film. As an example we write down the entropy of the system:

$$S = S_s + S_g + S_a$$

3.5. Isosteric Heat

The isosteric heat q_{st} is the energy required to remove an adatom from the adsorbed phase and return it to the gas phase, under constant temperature and pressure (which implies constant coverage). In analogy with the evaporation, we could call the isosteric heat the 'latent heat' of desorption. Figure 17 shows the relation of the isosteric heat with other energies that one usually encounters in physical adsorption.

The isosteric heat depends on the gas-solid system,

but for a certain system it depends on the coverage very drastically. There are two reasons for this dependence. For a surface with adsorption sites characterized by different adatom-substrate potentials, i.e: for a heterogeneous surface, the isosteric heat decreases with coverage (see curve a in figure 18). The larger binding energy adsorption sites will be occupied first, because an adatom trapped there, will stay there much longer than what at another site with smaller binding energy. As more and more adatoms are adsorbed, the sites with larger energies will be exausted, and sites with smaller energies will start being occupied. All real surfaces show some heterogeneity and the isosteric heat always increases at smaller and smaller coverages. When all the sites are filled (the monolayer is completed) the isosteric heat will suddenly decrease, as the adatoms of the second layer are further away from the substrate and, therefore, their interaction with the substrate is much weaker.

Adatom-adatom interactions also cause the isosteric heat to depend on coverage. As coverage is increased, the number of neighbours is increased, and at the same time their interatomic distances are decreased, bringing the adatoms at distances where the attractive part of the inter-

FIGURE 17

Adsorbent-Adsorbate Potential

E_K Kinetic energy of gas phase
q_{st} Isosteric heat
E_b Binding energy (equal to $-E_0$)
E_1 Energy level of first excited state of the adsorbate
E_0 Energy of ground state of the adsorbate
E_m Minimum of the interaction potential

At low temperatures one can safely assume that all adatoms are at the ground state. However, strictly speaking, at any non zero temperature other excited states will be occupied, hence the two lines indicating q_{st}.

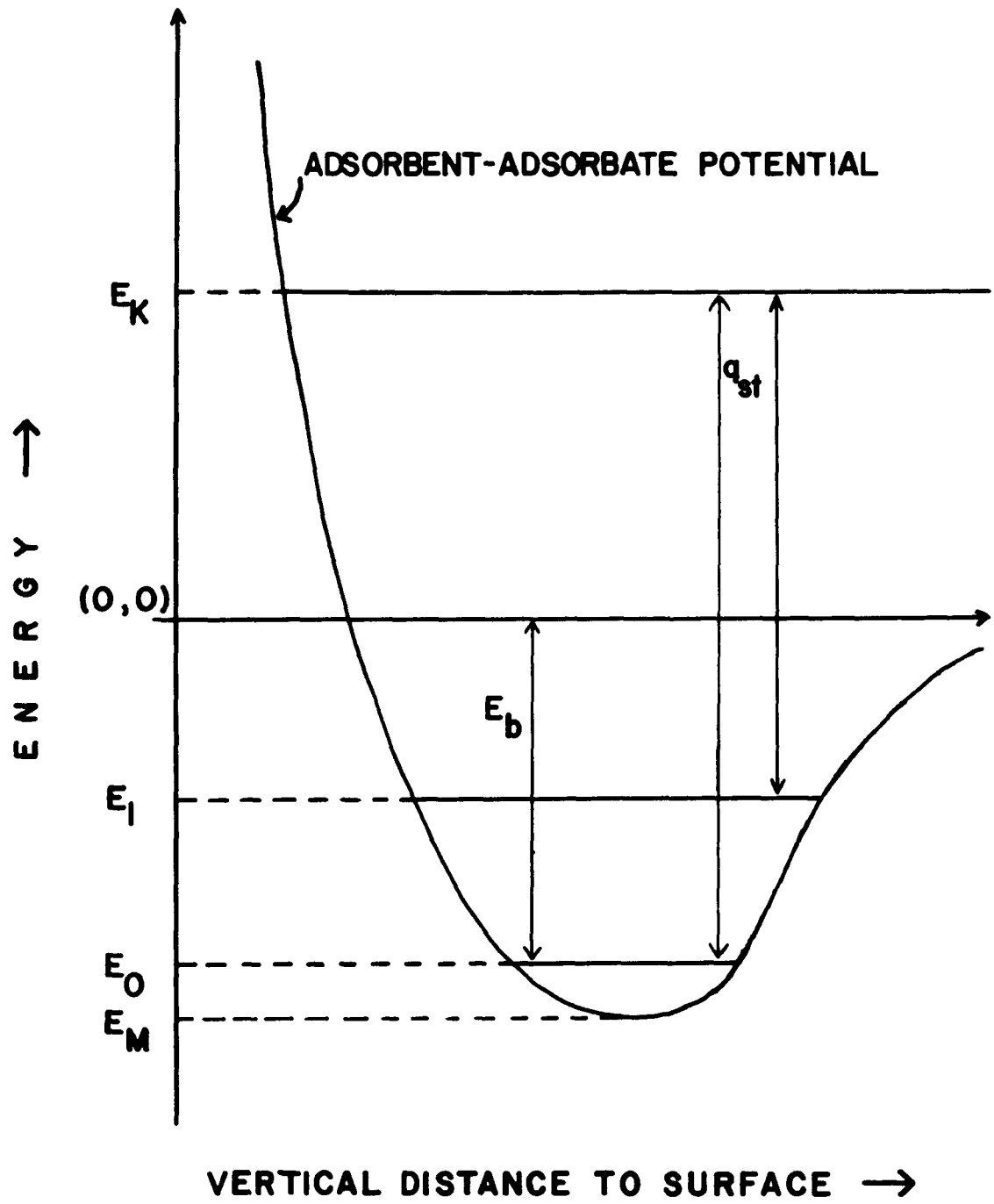
ADSORBENT-ADSORBATE POTENTIAL
E_K
q_{st}
ENERGY
(0,0)
E_b
E_1
E_0
E_M
VERTICAL DISTANCE TO SURFACE

FIGURE 18

Isosteric Heat vs Coverage

a Heterogeneous surface, adatom-adatom interaction negligible

b Homogeneous surface, with adatom-adatom interaction

c Heterogeneous surface with adatom-adatom interaction, or Homogeneous surface without adatom-adatom interaction

N_m Monolayer coverage

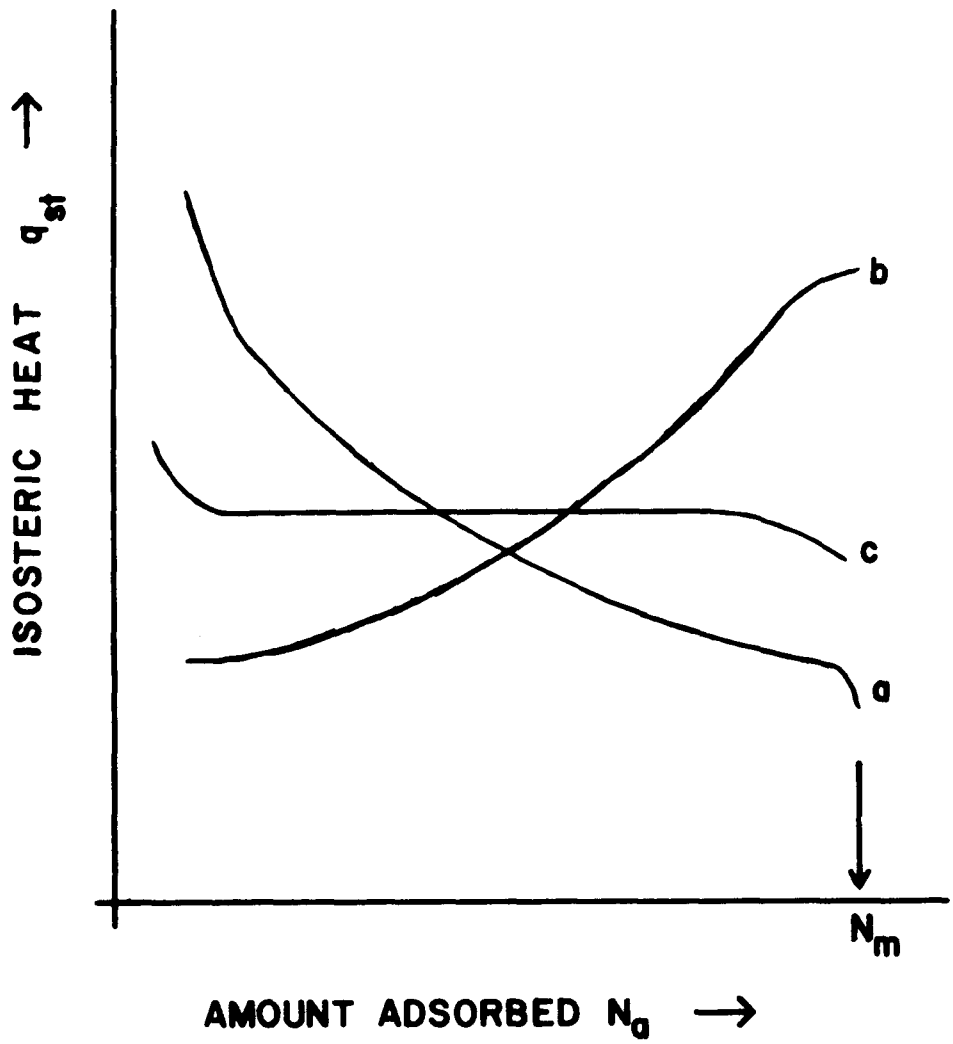
ISOSTERIC HEAT q_{st} →
b
c
a
N_m
AMOUNT ADSORBED N_a →

atomic potential becomes deeper and deeper. Therefore, the isosteric heat increases with coverage (see curve b in figure 18). This effect obviously stops when the adatoms are at distances equal to the distance of the minimum of the potential. Any further adition of adatoms will start the second layer.

It is then conceivable that for a certain gas-solid system, the isosteric heat to be indepedent of coverage (see curve c in figure 18), for submonolayer films. For a heterogeneous surface this would imply a strong adatom-adatom interaction, so that the result of summing curves a plus b (figure 18) would yield curve c. However, if one can neglect the adatom-adatom interaction, either because the interatomic distances are large (as in submonolayer films), or the interaction is weak compared to the gas-solid interaction, the independence of the isosteric heat on the coverage indicates a homogeneous surface. This is very important, as one can have an indication of the quality of the surface.

The isosteric heat can be measured either directly, using an adiabatic calorimeter, or calculated from adsorption isosteres, i.e: from equations of the form

$$P = f(T)_{N_a}$$

using a Clausius-Clapeyron type equation

$$\left(\frac{\partial \ln P}{\partial (1/T)}\right)_{N_a,\Sigma} = -\frac{q_{st}}{k}$$

where k is Boltzmann's constant. In section 4.4, the results of such measurements are shown and discussed.

3.6. Film Heat Capacity

The film heat capacity C_a is defined as

$$C_a = T\left(\frac{\partial S_a}{\partial T}\right)_{N_a,\Sigma}$$

i.e: under constant coverage. Experimentally, however, the convenient quantity to measure is the (total) heat capacity C of the system with N,V,Σ constant, i.e:

$$C = T\left(\frac{\partial S}{\partial T}\right)_{N,V,\Sigma} = T\left[\frac{\partial}{\partial T}\left(S_s+S_g+S_a \right)\right]_{N,V,\Sigma}$$

The first term $T(\partial S_s/\partial T)$ is nothing else than the heat capacity C_s of the solid adsorbent, and can be easily separated from the rest of the terms. It can be measured directly, as it is the heat capacity of the system with no adsorbate (N=0). Later, in section 4.5, this term is called the 'background' heat capacity, and includes the heat capacity of the calorimeter. The rest of the terms are not easy to recognize, and one has to compute the partial differentials in order to get an expression with the film contribution separated from all other contributions.

The computation was done by Dash[5] and will not be repeated here in detail. Instead, it is felt it is more interesting to start from a relation, suggested by Steele[65] and derived by following simple arguments.

As it was mentioned in section 2.1, the heat capacity C is usually determined experimentally by measuring the temperature change ΔT due to some energy Δq given into the system. Part of this energy Δq is spent to warm up (by ΔT) the solid adsorbent, the gas phase and the film. The rest of the energy Δq is absorbed by some adatoms, which are now energetic enough to return to the gas phase. However, since the number of atoms in the gas phase is increased, the pressure is increased (isothermally), and some energy $V.\Delta P$ is given in the system. Therefore, if the work done by the film as it expands (fewer adsorbed atoms on the same surface), can be neglected, this holds:

$$\Delta q = C_s.\Delta T + C_g.\Delta T + C_a.\Delta T + q_{st}.\Delta N_g - V.\Delta P$$

Using the fact that the gas is perfect, i.e: $V.\Delta P = Tk.\Delta N_g$ the last equation yields:

$$C - C_s = C_g + C_a + q_{st}[\frac{dN_g}{dT}]_{N,V,\Sigma} - kT[\frac{dN_g}{dT}]_{N,V,\Sigma}$$

where C_g is the heat capacity of the gas phase under constant volume, or in our notation:

$$C_g = T(\frac{\partial S_g}{\partial T})_{N_g,V}$$

C_a was written down for the film contribution although the coverage, i.e; N_a, does not remain strictly constant, because the change of the N_a compared to N_a is very small:

For our system, at 4.2 K the equilibrium pressure of Helium at monolayer coverage, was estimated to be less than 0.070 mmHg, and the number of atoms in the gas phase (in the volume V_c, section 2.7, figure 8) about 8×10^{18} compared to 8.4×10^{21} adatoms. Even if it is assumed that all the atoms are adsorbed at 0.5 K, the change in coverage from 0.5 to 4.2 K was 0.1%.

The derivative dN_g/dT is not hard to calculate along the film-gas conversion curve, and following Dash[5] we write down the final equation for the desorption term:

$$C_{des} = \frac{PV}{T}\left(\frac{q_{st}}{kT} - 1 \right)^2 \left[1 + \frac{PV}{kT}\left(\frac{\partial \ln P}{\partial N_a}\right)_{T,\Sigma} \right]^{-1}$$

$$C - C_s = C_g + C_a + C_{des}$$

To proceed one now needs a specific form of an adsorption isotherm. We do not have an isotherm for our particular system, so some approximations will be suggested. Due to its simplicity and partial success for submonolayer

coverages, it was decided to use the Langmuir isotherm equation to substitute for the pressure, in the C_{des} term. (For a discussion of the Langmuir isotherm, see Appendix C). The adsorption isotherms of Helium on Argon coated Grafoil[66],[67] (see also section 4.2) indicate a small value for dP/dN_a, at submonolayer coverages. In fact, this derivative would be exactly zero if there were two film phases in equilibrium. It is, therefore, felt that the term with the partial derivative is very small compared to 1, and can be neglected.

With $x=N_a/N_m$, where N_m is the number of adatoms in the monolayer, E the binding energy, one gets:

$$\frac{C_{des}}{N_a k} = aT^{3/2} e^{-E/kT} \frac{x}{1-x} \left(\frac{q_{st}}{kT} - 1 \right)^2 \frac{V}{N_a k}$$

where

$$a = (2\pi m)^{3/2} k^{5/2} h^{-3}$$

and m is the mass of the adatoms, h Planck's constant. Following Daunt and Lerner[60] we assume

$$q_{st} = E + 5kT/2$$

in accord with the adsorption isotherm used, and finally

$$\frac{C_{des}}{N_a k} = aT^{-1/2} e^{-E/kT} \frac{1}{1-x} \cdot \frac{V}{N_m k} \left(E/k + 3T/2 \right)^2$$

which is almost identical to the desorption contribution calculated by Daunt[10]. The difference being the gas phase contribution, which is included in Daunt's C_{des}

derivation[68]. In any case, C_g was negligible for our system. For the amount N_g estimated in V_c the specific heat was never more than 0.1 mJ/K.

The complete desorption contribution can be written down as:

$$C'_{des} = C_{des}/[\ 1 - (C_{des}/N_a k)(q_{st}/kT - 1)^{-2}\ ]$$

which clearly shows that the approximation suggested above is valid for

$$(q_{st}/kT - 1)^2 \gg 1$$

Indeed, (for our system) the smallest value of q_{st}/kT was about 7.5 (see figure 23, section 4.4 and 4.8) and, therefore, our approximation is good within 2% or better, for the temperature range covered.

Note that the C_{des} decreases rapidly with temperature. At sufficiently low temperatures the film heat capacity is simply given by

$$C_a = C - C_s$$

and this is the quantity calculated from the raw data in sections 4.6 and 4.8. In section 4.8, some of our results are also compared with C_{des}.

3.7. Film Phases

The discussion of the isosteric heat, in section 3.5, emphasized the dependence of the adsorbent-adsorbate potential, as a function of z, the distance of the adatom from the surface. In the case of a solid adsorbent, however, this potential also depends on the lateral position, due to the crystal structure of the adsorbent, i.e: the surface of a solid is not uniform. The shape of the solid-gas potential, as a function of z, does not change across the surface, but the minimum E_m of the potential varies drastically, as shown schematically in figure 19, following the periodicity of the lattice of the adsorbent.

Depending on the kinetic energy, the total energy E can be such that an adatom will be either localized, i.e: trapped in a well ($E_1 > E \gtrsim E_2$), or tunnel from site to site ($E_1 \gtrsim E > E_2$), or translate freely across the surface ($0 > E > E_1$), or even desorb if $E > 0$. The mobility of the adatoms is certainly different for all these situations. In other words, if only because of substrate effects, the adatoms can be characterized by different phases. Like in bulk systems, however, the phase of the film will be governed by the adatom-adatom

interaction as well.

Work with the Helium-Grafoil system[14] showed that the experimental results could be understood in terms of the Helium-Helium interaction only[14],[69]. The effect of the structure of the surface, showed up only for a narrow range of the coverage, where a lattice-gas phase was formed[14], in registry with the substrate. That is, the Grafoil could be assumed as a uniform substrate providing simply the surface to confine the Helium in two dimensions. Coating with a monolayer of Argon was consideredto produce a more uniform substrate. The symmetry of the Grafoil would be screened, as indicated in figure 21, section 4.1. Furthermore, numerical models[17] showed that even the zero point energy was larger than the highest minimum of the Helium-substrate potential. Although preliminary calculations by Novaco and Campbell[70] suggest that the effect of the coating with a rare gas is rather complicated, for our purposes, it will suffice to describe the phases of the film when the substrate can be ignored.

The number of the indepedent thermodynamic variables necessary to describe an adsorption system, can tell us the number of the phases the system can have. Neglecting the solid substrate (being always separable) there

FIGURE 19

Minimum of Solid-Gas Potential vs Lateral Translation

The distance z is assumed constant.

E_1 :adatom above an atom of the solid

E_2 :adatom above an interstitial position

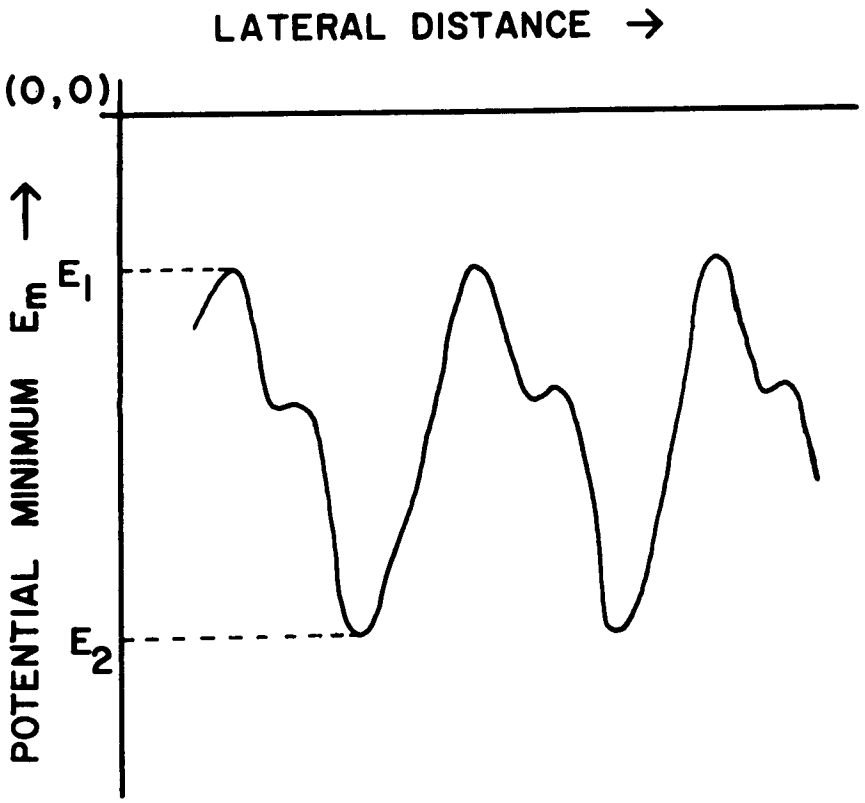
LATERAL DISTANCE →
(0,0)
POTENTIAL MINIMUM E_m →
E_1
E_2

are four variables required. For example: temperature, pressure, number of atoms, surface area. There are, therefore, four phases which, as a matter of fact, can coexist. With the gas phase being one, there remain three phases for the film. One refers to them as 2D gases, 2D liquids and 2D solids, in analogy with the bulk systems.

3.8. 2D Perfect Gases

If the adatom-adatom interaction can be neglected, the adatoms will behave as atoms of a perfect gas with their motion restricted in two dimensions.

At temperatures and areal densities D ($D=N_a/\Sigma$) where the thermal wavelength λ ($\lambda=h/\sqrt{2\pi mkT}$) of the adatoms is much smaller than the average adatom-adatom distance, or equivalently $\lambda^2 D \ll 1$, one expects the Boltzmann statistics to be valid and the equipartition law to hold. Under these conditions, the film is called a classical 2D perfect gas, and the heat capacity C_a is given by

$$C_a = N_a k$$

which is usually written down in reduced form: $C_a/N_a k=1$.

At the temperature and density range where $\lambda^2 D \geq 1$ the quantum effects become important, and Fermi or Bose statistics will be obeyed instead. Despite the great difference in their distribution functions, May[71] showed that non-interacting 2D Fermions and Bosons have the same heat capacity. Following Landau and Lifshitz[72] we shall calculate the heat capacity of 2D Fermions, with spin s.

The volume element in the 4-dimensional phase space is

$$\frac{1}{h^2} dp_x dp_y dx dy$$

with p_x, p_y the components of the momentum along the x,y axis of the surface. The energy ε of a single adatom is

$$\varepsilon = (p_x^2 + p_y^2)/2m = p^2/2m$$

if the substrate effects are ignored. With μ the chemical potential and $g=2s+1$, one can find the Fermi temperature T_F from the expression giving the number of adatoms N_a at T=0

$$N_a = \frac{g}{h^2} \int \frac{dp_x dp_y dx dy}{1+\exp[(\varepsilon - \mu)/kT]} = \frac{g}{h^2} \int_0^{p_F} 2\pi \Sigma p dp$$

$$N_a = g \frac{2\pi m k T_F}{h^2} \Sigma$$

where the Fermi level quantities are related as known:

$$\varepsilon_F = p_F^2/2m = kT_F$$

Solving for T_F we finally get

$$T_F = TD\lambda^2/g$$

Now, the energy of the film E_a, at a temperature $T>0$, is

$$E_a = \frac{2\pi mg\Sigma}{h^2}\int_0^\infty \frac{\varepsilon\, d\varepsilon}{1+\exp[(\varepsilon-\mu)/kT]}$$

which for $T<<T_F$ (or equivalently $D\lambda^2>>1$) yields[72]

$$E_a = \frac{2\pi mg\Sigma}{h^2}\left[\frac{1}{2}(kT_F)^2 + \frac{\pi^2}{6}(kT)^2 + \ldots\right]$$

and a specific heat C_a:

$$\frac{C_a}{N_a k} = \frac{\pi^2}{2}\cdot\frac{T}{T_F}$$

3.9. 2D Interacting Gases. 2D Liquids

The effect of the adatom-adatom interaction can be included in the description of the film properties with a variety of methods, all known from their application to 3D systems.

Particularly succesful, for low densities[69], was shown to be the virial expansion of the thermodynamic functions, where one gets reasonable agreement with the experiment by keeping terms up to the second coefficient only. According to the statistics more appropriate for

the system, Siddon and Schick[69] show how the calculation proceeds. Here we merely state a result of interest to us, i.e: the expression of the specific heat

$$\frac{C_a}{N_a k} = 1 - \beta^2 \frac{d^2}{d\beta^2} \sum_{j=1}^{\infty} B_{1+j} \frac{D^j}{j}$$

where $\beta = 1/kT$ and B_j the jth virial coefficient. This equation is very useful, for it indicates a method to determine how many coefficients are necessary to explain certain data, without computing the coefficients themselves. To see this we rewrite the above equation as follows:

$$\left[\frac{C_a}{N_a k} - 1 \right] / D = -\beta^2 \frac{d^2 B_2}{d\beta^2} - \frac{D}{2} \beta^2 \frac{d^2 B_3}{d\beta^2} - \cdots$$

If the second coefficient (B_2) suffices, plotting the data in the form of the left-hand side vs temperature, should yield one curve for all densities. On the other hand, if the contributions of the third coefficient (B_3) are appreciable, plotting the data in the same form vs density (at a certain temperature), will result in a straight line. Siddon and Schick[69] calculated B_2 quantum-mechanically for the Helium-Helium interaction. They used Lenard-Jones and Beck potentials. Comparison of their results with our data is shown in figures 36 (section 4.7) and 45 (section 4.9).

Very useful, in connecting the regimes of low and high densities, is the description of the film as a Van der Waals fluid[5]. It is, perhaps, the earliest method used[73], which attempts a realistic description, and leads to analytical relations of the thermodynamic quantities[5][74]. Knowledge of the attractive part of the adatom-adatom interaction (as a function of their distance) is necessary for one to derive relations between the critical parameters (temperature $T_c^{(2D)}$ and density $D_c^{(2D)}$) of the film with those of the bulk system ($T_c^{(3D)}$ and $D_c^{(3D)}$ respectively). Nevertheless, all reasonable potentials, for pair interactions, yield similar results. De Boer[75] finds for the familiar inverse sixth power law, that

$$T_c^{(2D)} = T_c^{(3D)}/2$$

and Dash[5] carries this a bit further to show that

$$D_c^{(2D)} = [\ 1.06 \times D_c^{(3D)}\ ]^{2/3}$$

For example, a mobile ^{4}He film should have a critical temperature of 2.6 K and a density of 0.05 $\mathring{A}^{-2}$.

All recent theoretical work on the 2D liquid phase, consists of numerical solutions to the equations of Quantum-Mechanics. For the 2D Helium, several approximations (ref. 70,76,77,78 and references therin) show that

a binding energy of about 0.62 K per atom should be expected at a density of about 0.035 $\mathring{A}^{-2}$. However, these models also indicate how sensitive the results are on small variations of the adatom-adatom potential[76] or, on the modulation of this potential due to substrate effects[70].

3.10. 2D Solids

At the density range where adatom-adatom distances become comparable to their diameter, the adatoms are forced to oscillate around an equilibrium position rather than translate freely. If they all oscillate independently of each other with the same frequency f, the film is described as a 2D Einstein solid, and its specific heat is given by[79]

$$C_a/N_a k = \frac{2z^2 e^z}{(e^z-1)^2} \qquad z=hf/kT$$

the difference from the 3D expression being just the factor 2, i.e: 2 degrees of freedom for every oscillator.

If the adatoms interact with each other, one expects a 2D Debye solid, i.e: collective, phonon-like excitations. Following a standard textbook[79], we write down for the 2D density of states W(f) per unit frequency range:

$$W(f) = (\Sigma/v^2)f$$

where v is the velocity of sound, assumed constant. The expression of the number of adatoms N_a defines the cut-off (Debye) frequency f_D:

$$N_a = \int_0^{f_D} W(f)df = (\Sigma/v^2)(f_D^2/2)$$

which yields $f_D = v\sqrt{2D}$ and a Debye temperature Θ:

$$\Theta = hf_D/k = hv\sqrt{2D}/k$$

The energy E_a is given by

$$E_a = 2\int_0^{f_D} W(f)hf[e^z-1]^{-1}df = 4N_a k\frac{T^3}{\Theta^2}\int_0^{\Theta/T} \frac{z^2dz}{e^z-1}$$

which, for low temperatures ($\Theta/T>>1$), can be easily evaluated by replacing the upper limit of the integral with ∞, i.e:

$$\int_0^{\infty} \frac{z^2dz}{e^z-1} = \int_0^{\infty} \frac{z^2e^{-z}dz}{1-e^{-z}} = \int_0^{\infty} z^2e^{-z}(1+e^{-z}-...)dz = 2 + 1/4 -...$$

Therefore, the reduced specific heat is

$$\frac{C_a}{N_a k} = 27(\frac{T}{\Theta})^2$$

Note that Dash[5] finds the numerical coefficient to be 28.85 instead.

Eventually, at high enough temperatures the 2D solid will 'melt'. Elgin and Goodstein[80] showed that

this melting can simply be promotion to the next layer, which causes the specific heat to develop a sharp peak. Besides this effect, Kosterlitz and Thouless[81] showed that melting of a 2D solid will occur, at any rate, at temperatures where dislocations are able to move under the influence of arbitrarily small stresses, and so produce viscous flow. They predicted a phase transition and derived an expression for the melting temperature T_M. Elgin and Goodstein[82] reviewed the melting theories of 2D solids, and rewrote the expression giving T_M, so that its relation to the Debye temperature becomes clear:

$$T_M = mkD\Theta^2/8h^2$$

CHAPTER 4: RESULTS

4.1. Argon Adsorption Isotherm

The surface area of our substrate was determined by measurement of an Argon adsorption isotherm at 77.3 K according to the procedure outlined in section 3.3. The isotherm is shown in figure 20, where the amount adsorbed expressed in cm^3(STP) is plotted against the pressure of the gas, in mmHg.

The point 'B' method, for which the straight line was drawn, showed a monolayer of 290.3 cm^3(STP), indicated by the arrow in the figure. When preparing the Argon coating for a heat capacity measurement of a Helium film, an amount 3-4% higher than this was allowed to be adsorbed by the Grafoil at 77.3 K, before cooling down to 4.2 K. This was done to assure complete coverage of the available surface, as promotion to the second layer is known[4] to occur before the first is completed, and some amount of the Argon could not be accounted. This was the amount of Argon in the gas phase at monolayer coverage and 77.3 K. At the adsorption temperature the pressure of the Argon monolayer is 22 mmHg, whereas at 4.2 K the Argon partial

pressure is negligible. It is not known where this amount of Argon was adsorbed. Using the equation of state of Argon, with parameters given by Daunt and Rosen[49], it was estimated that 5.60 cm^3(STP) of Argon was in the calorimeter void volume (V_c) and the fill tube (up to the valve TV5 in figure 8). This is less than 2% of the monolayer and constituted our error in the Argon coating.

The surface area Σ was (section 3.3):

$$\Sigma = 0.296 V_M \sigma_{AR} = 988.0 \ m^2$$

and hence the specific area of our sample of 17.09 m^2/g. Values of the Grafoil specific area, reported in the literature vary from 30 m^2/g[27] to 15 m^2/g[66]. This should not be considered a disagreement but rather an indication of how much area is left available for adsorption when the substrate is finally placed in the calorimeter. We have found[83] that the treatment and handling (cutting, pressing, epoxying etc) of Grafoil samples was responsible for blocking considerable area, resulting in specific areas varying a factor of 3.

The Argon isotherm was taken twice, at the begining of this work (all our subsequent reduced data are based on this monolayer), and after all the heat capacity data was taken,

FIGURE 20

Argon Isotherm at 77.3K

\+ Measurements made on March 1975

. Measurements made on September 1976

Two desorption points, March 1975

Desorption points, September 1976

The arrow indicates the monolayer suggested by the point 'B', i.e: the point where the isotherm deviates from the straight line. Equilibrium pressure at monolayer: 22 mmHg. Notice the peculiar behaviour from 1 to 10 mmHg.

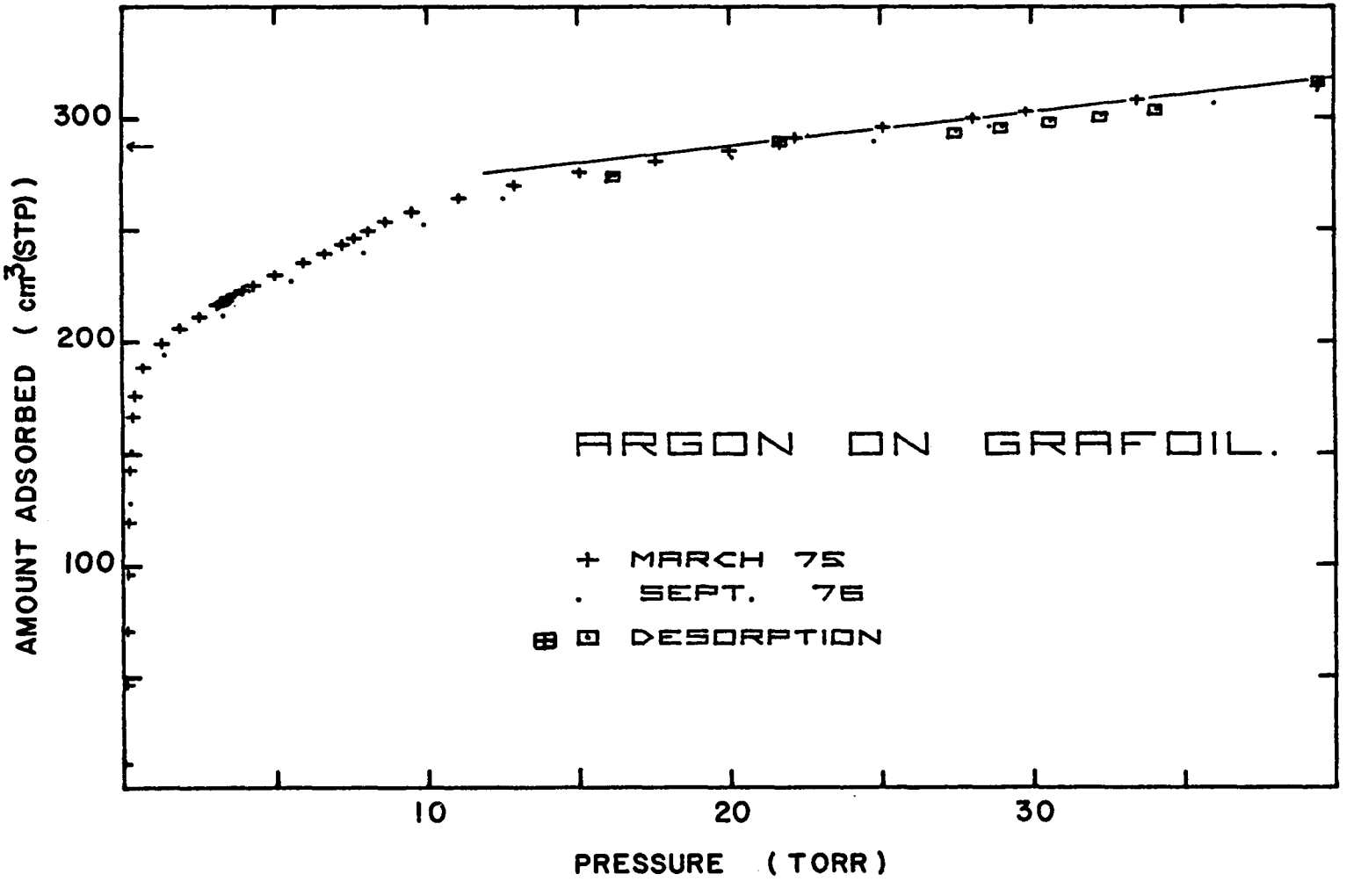
AMOUNT ADSORBED (cm³(STP))
300
200
100
10
20
30
PRESSURE (TORR)
ARGON ON GRAFOIL.
+ MARCH 75
. SEPT. 76
⊞ ⊡ DESORPTION

to check possible contamination of the surface. The values of the second run, marked September 1976, fell about 1% below those of March 1975, but since the error of the isotherm was 1%, as explained in section 2.7, the two runs were considered in excellent agreement. In any case, contaminants tend to introduce heterogeneities and, hence, increase the monolayer.

Figure 21 shows the relative position of the Argon and Carbon atoms at monolayer coverage. The incompatibility of the two structures is obvious. Argon is shown as hard discs with diameter d equal to the nearest-neighbour distance of 3.84 $\mathring{A}$ (that is, at an areal density 0.079 $\mathring{A}^{-2}$). The Carbon atoms are assumed to be at the corners of the (small) hexagons with side equal to 1.42 $\mathring{A}$ [84]. The monolayer forms an ordered triangular lattice, but not in registry with the substrate. If the registry observed for all the other rare gases (Helium[14], Xenon[11], Neon[85], Krypton[86]), i.e: one adatom every three hexagons, should happen for Argon as well, it should occur at areal density equal to 0.0636 $\mathring{A}^{-2}$ (x = 0.81). The area of three graphite hexagons, with side h=1.42 $\mathring{A}$, is

$$\sigma_3 = \frac{3\sqrt{3}}{2}h^2 = 15.716\ \mathring{A}^2$$

and hence the density $1/\sigma_3$. The fractional coverage is now calculated as the ratio of this density and that of the monolayer, as determined from the size of the adatoms.

No registry for Argon on Grafoil has been reported so far. Unfortunately, the work of the Brookhaven group[88] on the study of neutron scattering from adsorbed Argon on Grafoil was done only at monolayer coverages.

It should be pointed out that the anomalous (i.e: deviation from a typical BET isotherm) structure of the Argon isotherm from 1 to 10 mmHg was seen by others[83],[89]. The origin of this anomaly is not clear. However, measurements of the specific heat of Argon adsorbed by Graphon[90] and by graphitized carbon black[91] clearly indicated some transition at submonolayer coverages.

4.2. Helium-4 Adsorption Isotherms

Figure 22 shows the 4.2K isotherms of ^4He adsorbed on Grafoil and on Grafoil coated with a monolayer of Argon, as described in section 2.7. The amount adsorbed is now expressed in $cm^3(STP)/m^2$, since the surface area is presumed to be known. The monolayer coverages are indicated by the arrows. The straight lines were drawn in search of the point 'B' which actually coincided with the point 'A'. This did not come as a surprise, as it is well established that adsorbed Helium forms a monolayer at very small pressures[92],[93].

FIGURE 21

Grafoil and Argon monolayer on Grafoil

Argon is represented by the circles (of diameter 3.84 Å) and the Grafoil by the net of hexagons with side 1.42 Å. The Carbon atoms are at the corners of the hexagons. This arrangement of the adatoms was called 'incommensurate' by Ying (ref. 87).

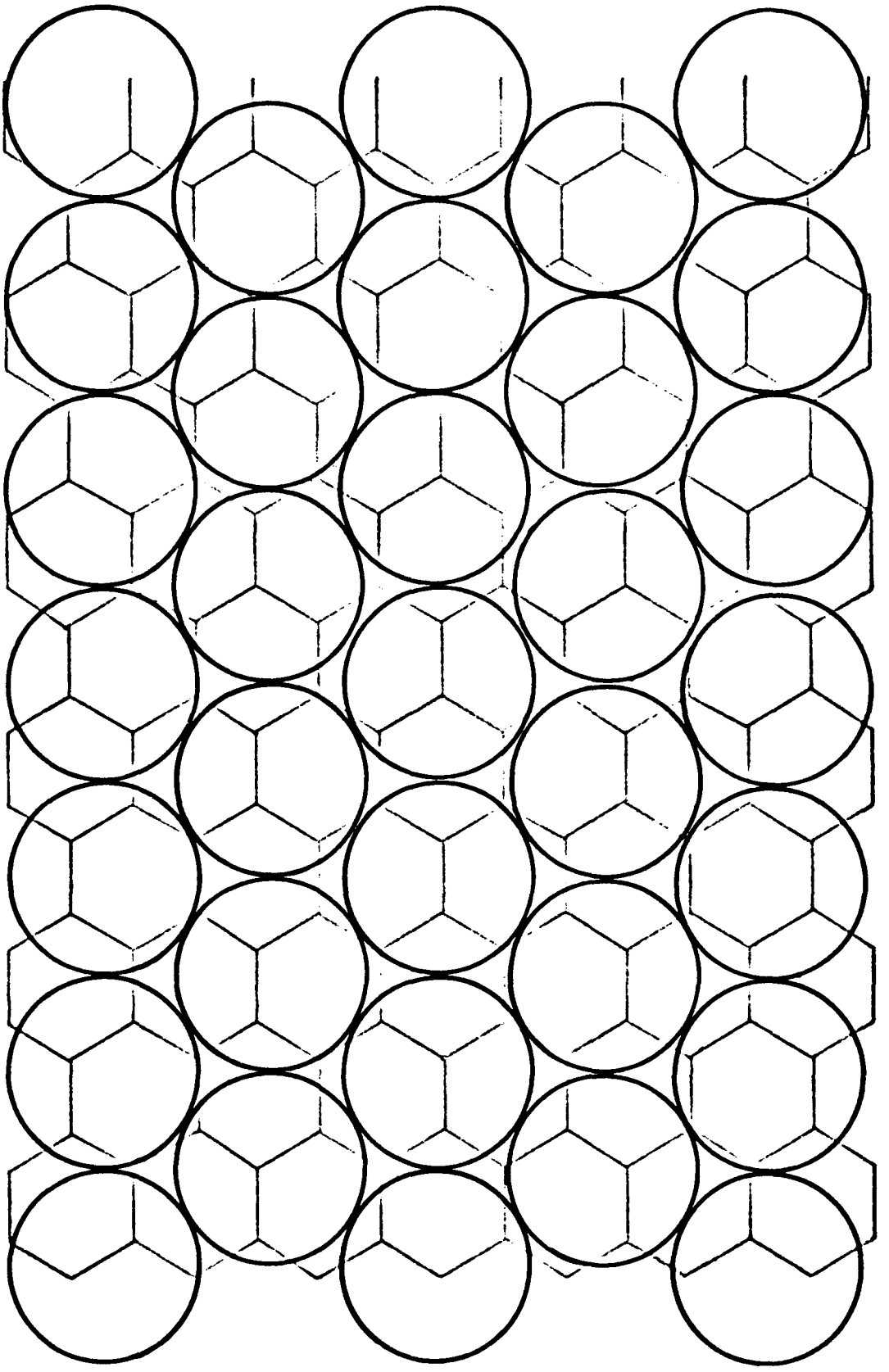

FIGURE 22

Helium Isotherms at 4.2K

\+ On Argon coated Grafoil

. On (bare) Grafoil

Straight lines were drawn in search of the point 'B' (see fig. 14). Arrows indicate the monolayers. Notice the units of the adsorbed amount: $cm^3(STP)/m^2$. The surface area calculated from the Argon monolayer was used.

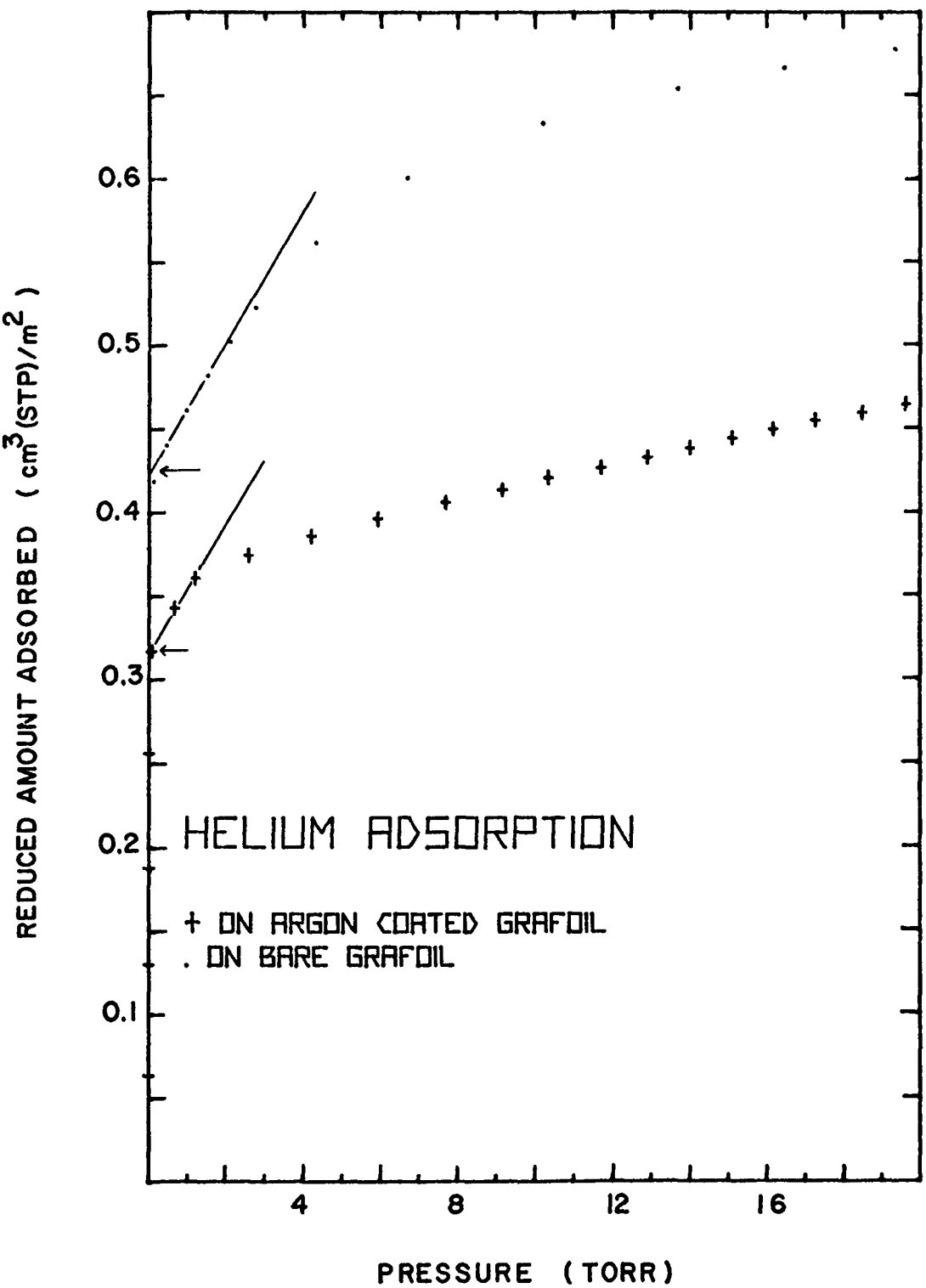
HELIUM ADSORPTION
+ ON ARGON COATED GRAFOIL
. ON BARE GRAFOIL
REDUCED AMOUNT ADSORBED (cm3(STP)/m2)
PRESSURE (TORR)
0.6
0.5
0.4
0.3
0.2
0.1
4
8
12
16

The monolayer of ^{4}He on (bare) Grafoil was found to be 0.432 $cm^3(STP)/m^2$. This implies a nearest-neighbour distance of 3.16 Å and a density of 0.116 $Å^{-2}$, in excellent agreement with other adsorption work[66], theoretical calculations[94], study of the specific heat[14] and study of neutron scattering[96]. Table C shows a comparison of the monolayers, as determined by various methods.

The monolayer of ^{4}He on Argon coated Grafoil was estimated at 0.316 $cm^3(STP)/m^2$, considerably less than that on (bare) Grafoil. This yields a nearest-neighbour distance of 3.69 Å and a density of 0.085 $Å^{-2}$, in excellent agreement with other adsorption work[67] and fair agreement with Milford and Novaco's model[62], which requires one Helium atom for every Argon atom, i.e: a density of 0.079 $Å^{-2}$.

4.3. Helium-3 Adsorption Isotherms

No ^{3}He isotherm was taken. If the monolayer of ^{3}He on Argon coated Grafoil is needed, we shall use the one found by Goellner et al[66], of 0.325 $cm^3(STP)/m^2$ (D_m=0.0873 $Å^{-2}$).

4.4. Isosteric Heat of Helium

As evidence of the improved uniformity of the Grafoil when coated with Argon, it was felt that isosteric heat

TABLE C

Monolayer Densities of ^{4}He Adsorbed on (bare) Grafoil

Monolayer $cm^3(STP)/m^2$	Density $\AA^{-2}$	Method	Reference
0.432	0.1161	Adsorption isotherm	This work
0.426	0.1145	Adsorption isotherm	66
0.428	0.1150	Sp. heat ordering peak	14
0.421	0.113	Neutron scattering	96
0.431	0.116	Theoretical model	62,94,95

measurements should be included here. The Helium isotherms were measured only at 4.2K in order to determine the monolayer and did not suffice for calculating the isosteric heat This was done, however, by Lerner and Daunt[67] for ^{4}He and Goellner et al[66] for ^{3}He.

Figure 23 is reproduced from reference 67. It shows the isosteric heat of ^{4}He on (bare) Grafoil and Grafoil coated with Argon as a function of coverage. In the case of the Argon coated Grafoil the isosteric heat seems to be indepedent of coverage up to about a monolayer and less than that on the (bare) Grafoil, i.e: the attraction from the substrate is weaker. In this figure data for ^{3}He are also included (from reference 66). The results are similar except for the magnitude of the isosteric heat, which is smaller for ^{3}He. Notice that isosteric heat increases below 0.2 layers for both isotopes. A fact usually attributed to inhomogeneities of the substrate existing even after coating with a monolayer of Argon.

4.5. Data Collection. Method of Analysis

The heat capacity was usually measured with the sample warming up. We found it was easier to control the refrigerator this way. As soon as the sample was isolated

from the refrigerator heat pulsing was started and the temperature drift followed, as described in section 2.1. The refrigerator was adjusted so that these drifts were always less than 0.4 mK/sec.

The reading of the magnetic tape, calculations and plotting of the results were done by executing a FORTRAN program on a DEC-PDP10 computer. Figure 24 is a typical plotter output showing the drift values, heat pulse, straight line fit of the drifts and the temperature change. All these plots were visually checked and if the drift was found unacceptable (due to refrigerator instabilities) the point was rejected. The accepted points were tabulated according to their temperature and kept in the memory of the computer for further calculations.

Figure 25 is a plot of the heat capacity against temperature for the calorimeter without Helium and the calorimeter with 0.1 layers of ^{4}He. This figure is shown for comparison and visual evaluation of the errors. Our estimates indicated that the error was never more than 3%.

The long thermal equilibrium times, seen in figures 2 and 24, were responsible for the error. A small error in the slope of the afterdrift would result in a relatively

FIGURE 23

Isosteric Heat of Helium onGrafoil

o ^{4}He on bare Grafoil (ref. 67)

x ^{4}He on Argon coated Grafoil " "

--- ^{3}He on Argon coated Grafoil (ref. 66)

N_m ^{4}He monolayer on Argon coated Grafoil

N'_m ^{4}He monolayer on bare Grafoil

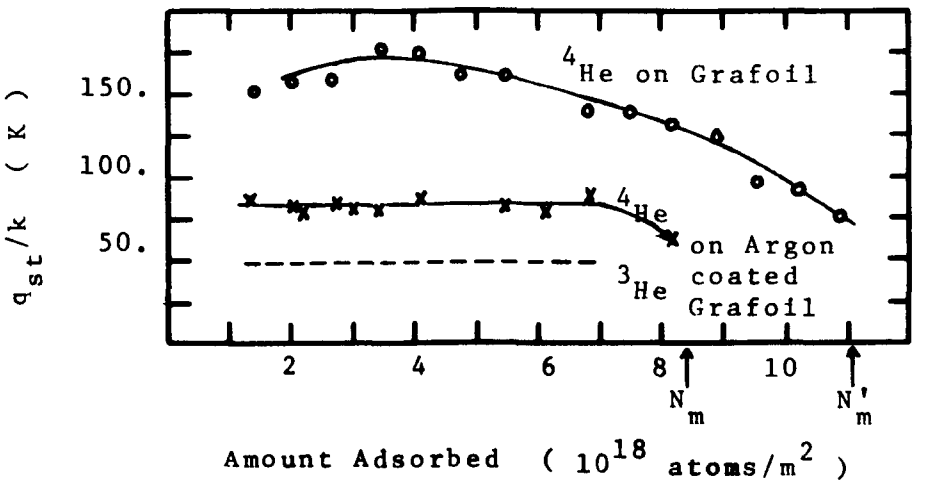
q_{st}/k (K)
150.
100.
50.
^{4}He on Grafoil
^{4}He on Argon coated Grafoil
^{3}He
2
4
6
8
10
N_m
N'_m
Amount Adsorbed (10^{18} atoms/m^2)

FIGURE 24

Computer Output of a Heat Capacity Run

The points show the temperature as read every 7 sec. The 12 last points of the drift were used to calculate the straight lines, which were then assumed to be the drifts thermal equilibrium time were zero. The vertical line indicates the calculated ΔT. The assumed heat pulse and the temperature of the point are also shown. For this run rejected points were #1,#2 because of anomalous drift and #8,#9 because the foredrifts have different slopes from the afterdrifts (due to adjusting the mixing chamber heater).

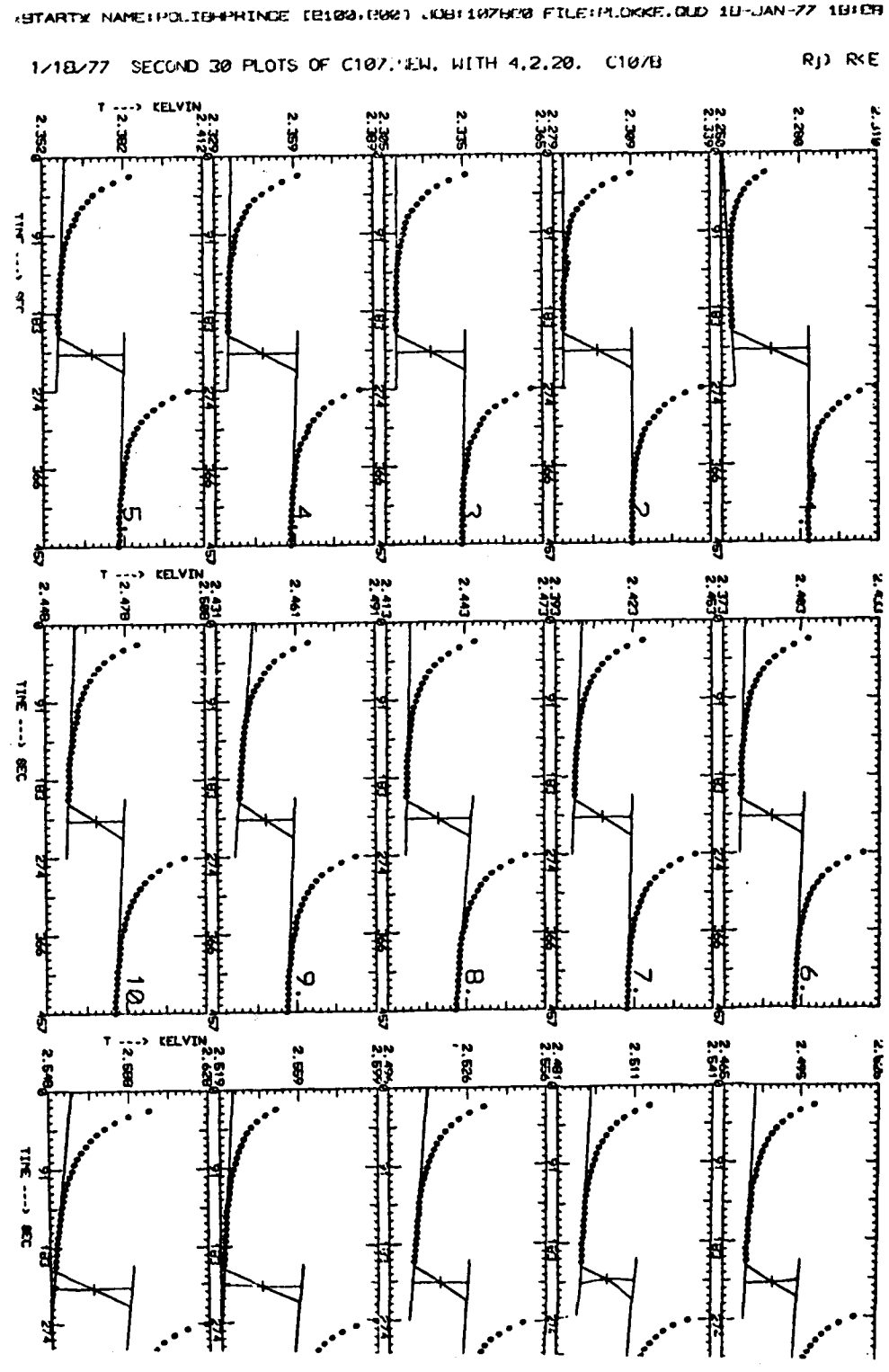
(START)(NAME:POLIB4PRINCE [2100,2002] JOB:107800 FILE:PLOKKE.OUD 10-JAN-77 10:08
1/18/77 SECOND 30 PLOTS OF C107.NEW. WITH 4.2.20. C10/B
RJ) R<E
T ---> KELVIN
TIME ---> SEC
5.
4.
3.
2.
1.
10.
9.
8.
7.
6.

FIGURE 25

Total Heat Capacity vs Temperature

+ 0.1 layers ^{4}He plus the calorimeter

. No Helium

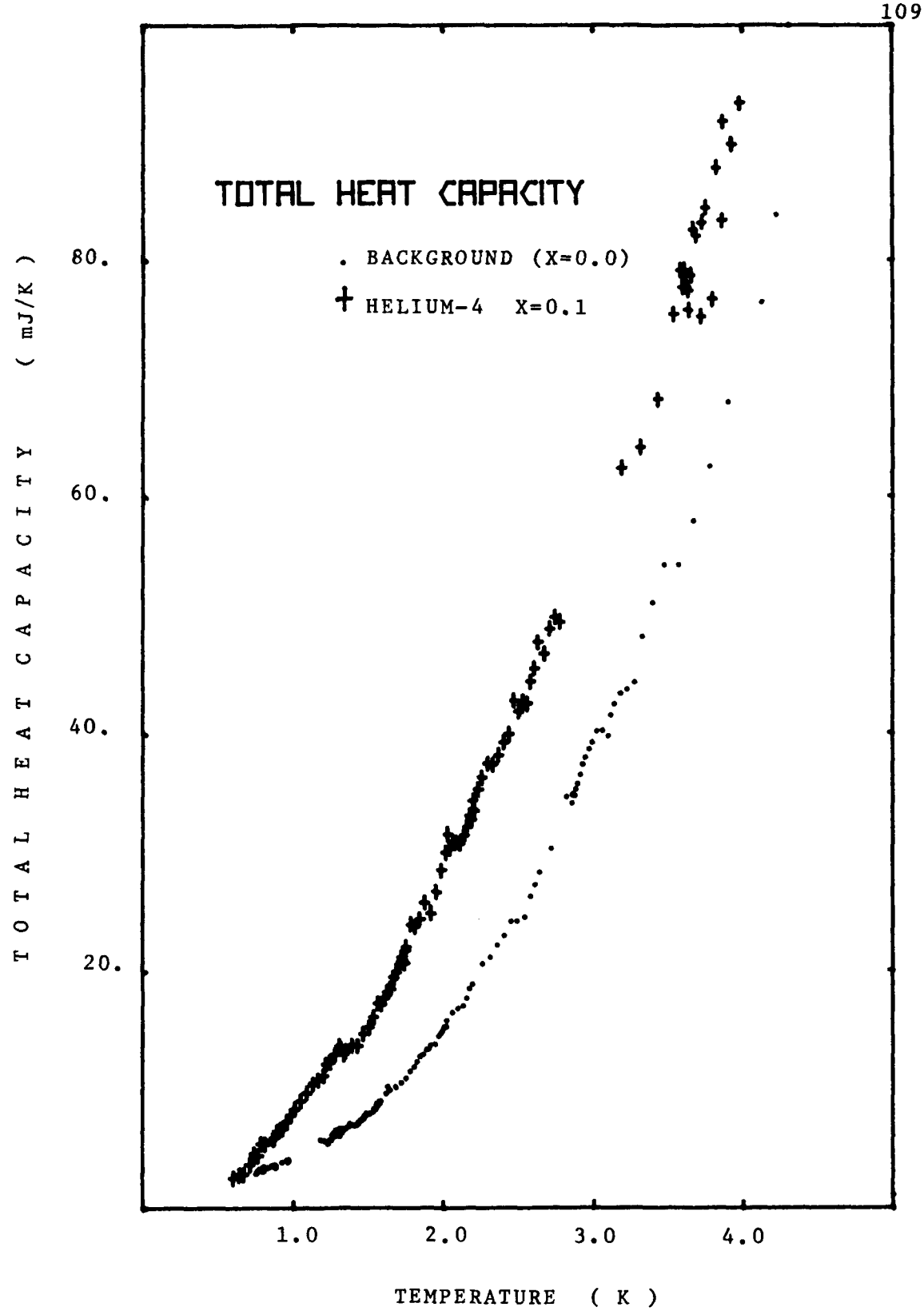
TOTAL HEAT CAPACITY
. BACKGROUND (X=0.0)
+ HELIUM-4 X=0.1
TOTAL HEAT CAPACITY (mJ/K)
80.
60.
40.
20.
1.0
2.0
3.0
4.0
TEMPERATURE (K)

large error in ΔT when extrapolated 140 sec back. Poor heat sinking of the sample most likely caused the long equilibrium times. The distance of the Copper wires (see section 2.3) was calculated so that equilibrium times of a few seconds were expected. The Grafoil thermal conductivity was taken from reference 16. We suspect, however, that the silver epoxy did not adhere to Grafoil as strongly as originally thought.

The heat capacity of a Helium film was calculated from the total heat capacity of the calorimeter by subtracting the proper value of the background heat capacity, found by linear interpolation. The background was the heat capacity of the calorimeter with no Helium adsorbed.

Let us say $C_b(T_i)$, $C_b(T_{i+1})$ were two succesive values of the background heat capacity at temperatures $T_i < T_{i+1}$ and $C_t(T)$ the total heat capacity of the calorimeter with adsorbed Helium, where

$$T_i < T < T_{i+1}$$

Then the heat capacity of the film is given by:

$$C(T) = C_t(T) - C_b(T_i)\frac{T_{i+1} - T}{T_{i+1} - T_i} - C_b(T_{i+1})\frac{T - T_i}{T_{i+1} - T_i}$$

It has been customary to report the specific heat not in absolute units, but compared to the specific heat of a 2D perfect gas. Thus the final quantity calculated is C(T)/Nk where N is the number of adatoms and k Boltzmann's constant.

4.6. ^{4}He Specific Heat on Argon coated Grafoil

Figures 26 through 32 show the specific heat of ^{4}He submonolayer films vs temperature. The areal densities studied ranged from 0.008 to 0.043 $\mathring{A}^{-2}$ ($0.1 \leq x \leq 0.5$) and the temperature covered was 0.6 to 4.2K. With the exception of the lowest coverage,all curves showed peaks, reaching values of C/Nk from 2.5 to 3.2 at the temperature range of 1.95 to 2.55K.

At temperatures below those of the peaks the specific heat seems to rise proportionally to some power of the temperature and be inversely proportional to coverage. This latter effect can be easily seen from a plot of the total heat capacity vs temperature for different areal densities, as the heat capacity will be the same for all. In figure 33 we show such a plot for two films with densities 0.016 and 0.029 $\mathring{A}^{-2}$.

At temperatures above those of the peaks, the specific

FIGURE 26

^{4}He on Argon Coated Grafoil Reduced Specific Heat

X = 0.093
D = 0.00792 $\mathring{A}^{-2}$
n = 1.300 mmol

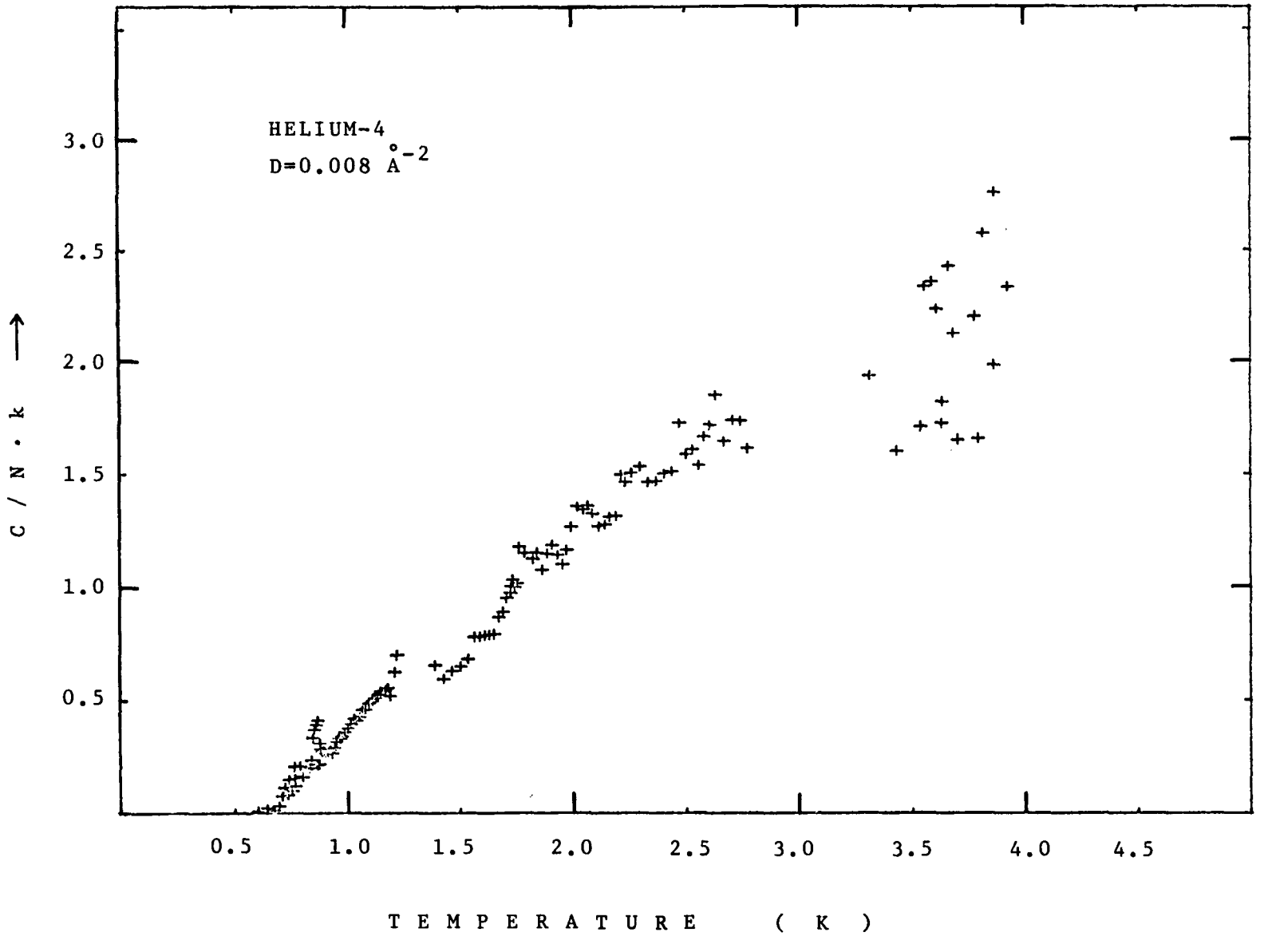
HELIUM-4
D=0.008 Å^{-2}
C / N • k ⟶
3.0
2.5
2.0
1.5
1.0
0.5
0.5
1.0
1.5
2.0
2.5
3.0
3.5
4.0
4.5
T E M P E R A T U R E (K)

FIGURE 27

^{4}He on Argon Coated Grafoil Reduced Specific Heat

X = 0.176
D = 0.01492 $\mathring{A}^{-2}$
n = 2.447 mmol

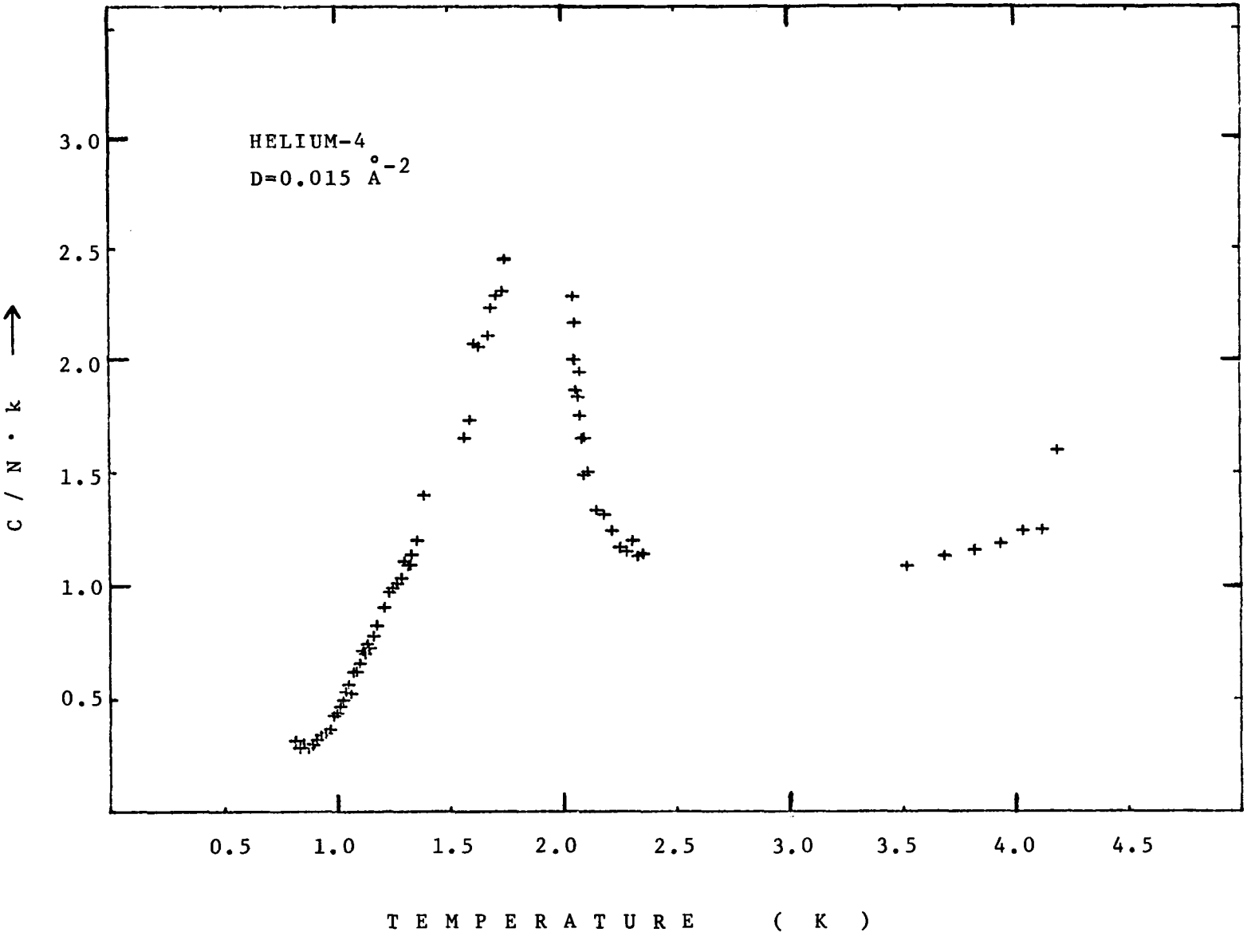
HELIUM-4
D=0.015 Å^{-2}
C / N · k
3.0
2.5
2.0
1.5
1.0
0.5
0.5
1.0
1.5
2.0
2.5
3.0
3.5
4.0
4.5
TEMPERATURE (K)

FIGURE 28

^{4}He on Argon Coated Grafoil Reduced Specific Heat

X = 0.257 $\circ^{-2}$
D = 0.02187 A
n = 3.588 mmol

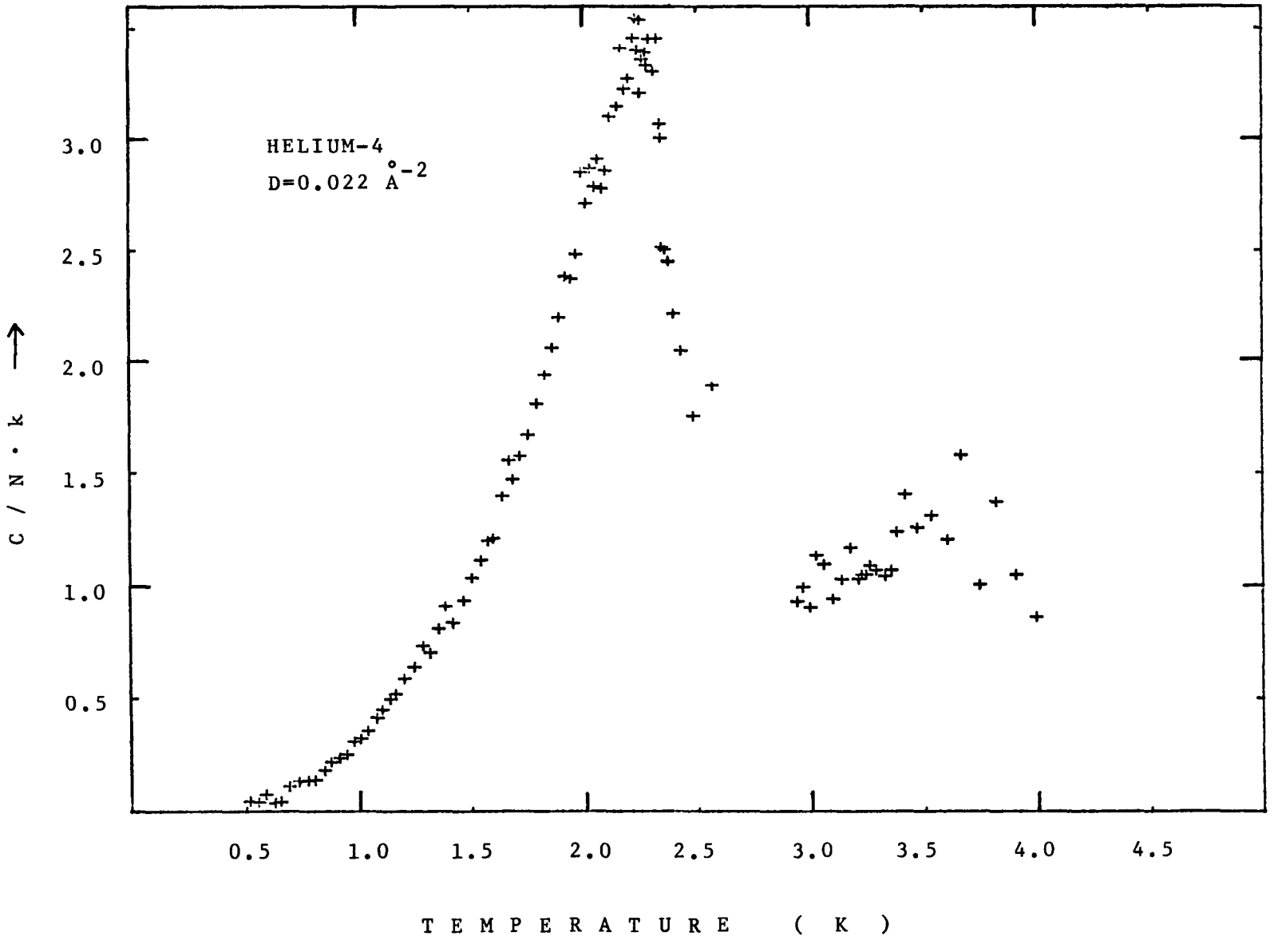
HELIUM-4
D=0.022 Å-2
C / N · k
3.0
2.5
2.0
1.5
1.0
0.5
0.5
1.0
1.5
2.0
2.5
3.0
3.5
4.0
4.5
TEMPERATURE (K)

FIGURE 29

^{4}He on Argon Coated Grafoil Reduced Specific Heat

X = 0.340
D = 0.02891 $\mathring{A}^{-2}$
n = 4.742 mmol

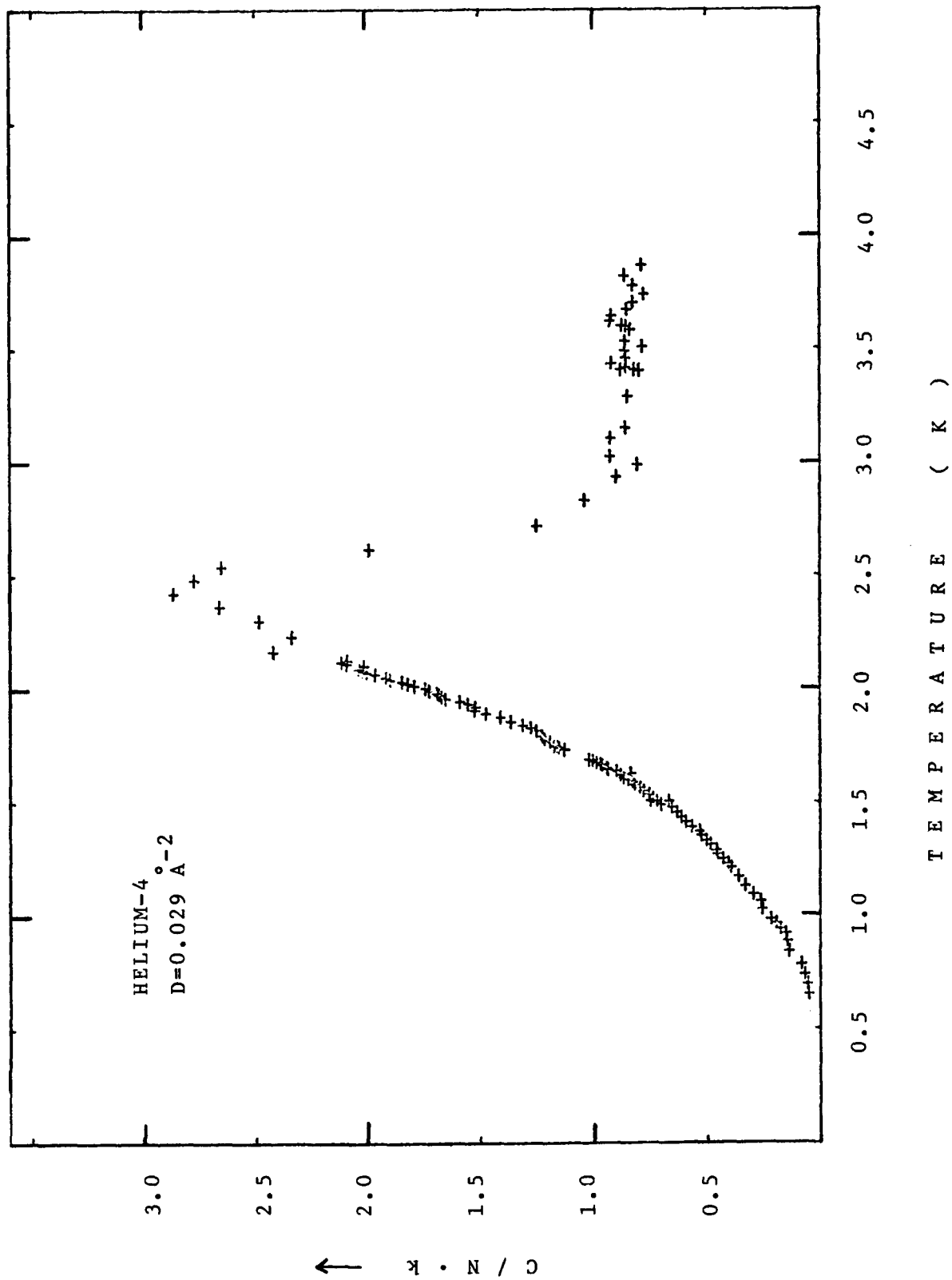
HELIUM-4
D=0.029 Å^-2
C / N • K ←
TEMPERATURE (K)
0.5
1.0
1.5
2.0
2.5
3.0
3.5
4.0
4.5

FIGURE 30

^{4}He on Argon Coated Grafoil Reduced Specific Heat

X = 0.408		for T>1.7K	X = 0.425		for T<1.6K
D = 0.03466	$\mathring{A}^{-2}$	"	D = 0.03607	$\mathring{A}^{-2}$	"
n = 5.685	mmol	"	n = 5.917	mmol	"

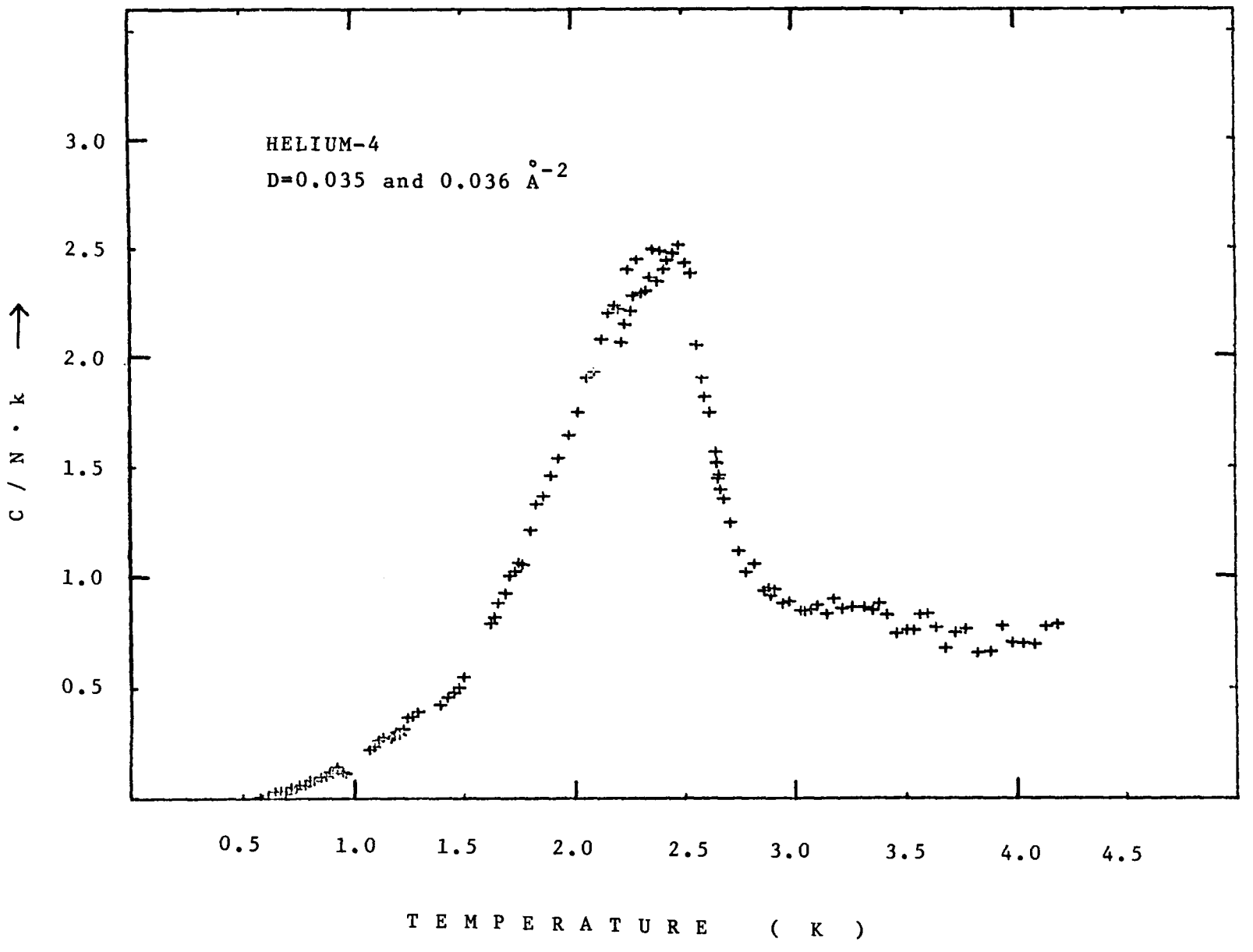
HELIUM-4
D=0.035 and 0.036 Å^{-2}
C / N · k
3.0
2.5
2.0
1.5
1.0
0.5
0.5
1.0
1.5
2.0
2.5
3.0
3.5
4.0
4.5
TEMPERATURE (K)

FIGURE 31

^{4}He on Argon Coated Grafoil Reduced Specific Heat

X = 0.468

D = 0.03978 $\mathring{A}^{-2}$

n = 6.525 mmol

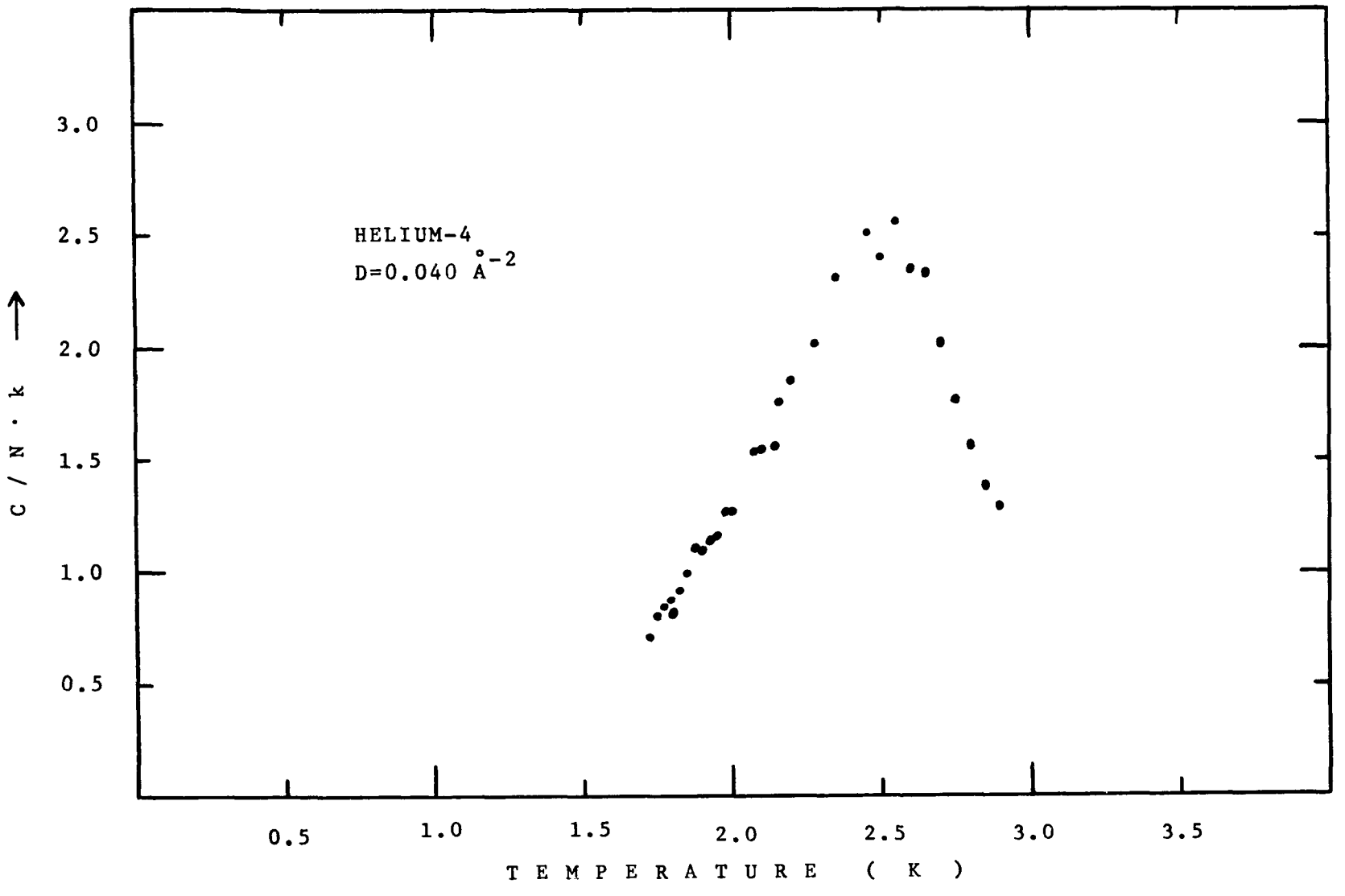
HELIUM-4
D=0.040 Å^{-2}
C / N · k
3.0
2.5
2.0
1.5
1.0
0.5
0.5
1.0
1.5
2.0
2.5
3.0
3.5
T E M P E R A T U R E (K)

FIGURE 32

^{4}He on Argon Coated Grafoil Reduced Specific Heat

X = 0.506
D = 0.04301 $\mathring{A}^{-2}$
n = 7.055 mmol

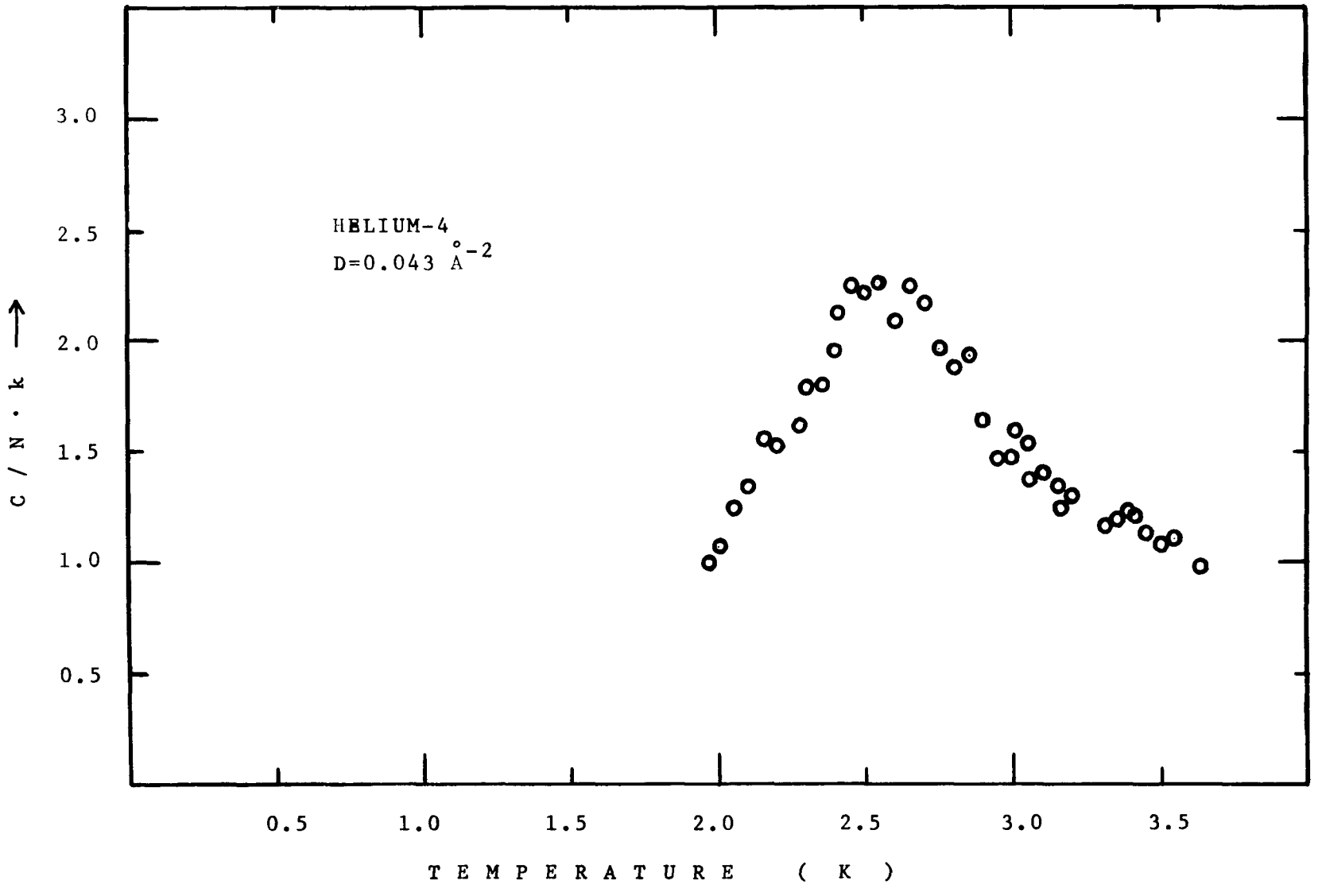
HELIUM-4
D=0.043 Å^{-2}
C / N · k ⟶
3.0
2.5
2.0
1.5
1.0
0.5
0.5
1.0
1.5
2.0
2.5
3.0
3.5
T E M P E R A T U R E (K)

FIGURE 33

Total Heat Capacity vs Temperature

X=0.176 D=0.015 $\mathring{A}^{-2}$

X=0.340 D=0.029 $\mathring{A}^{-2}$

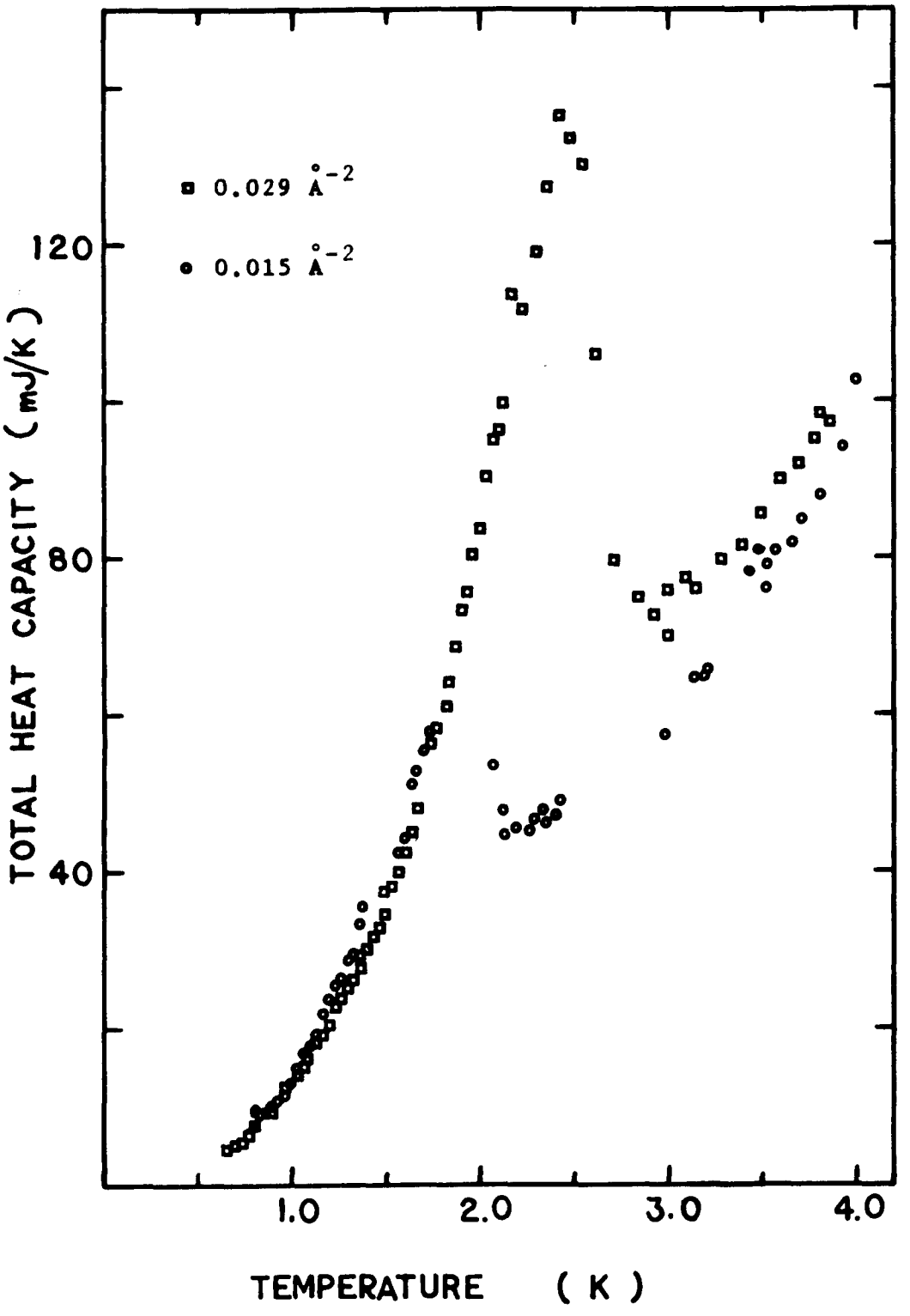
0.029 Å^{-2}
0.015 Å^{-2}
120
80
40
TOTAL HEAT CAPACITY (mJ/K)
1.0
2.0
3.0
4.0
TEMPERATURE (K)

heat drops quickly to values of C/Nk slightly less than 1.

To the best of our knowledge no other substrate causes the ^{4}He to have such a specific heat, i.e: to undergo a transition at these areal densities and temperatures. To show this better figure 34 was made. There, we plot the areal densities vs temperature of the peaks. It is of interest to compare our phase diagram with the one obtained by Bretz et al[14] for the same densities of ^{4}He on (bare) Grafoil. Figure 34 shows the comparison. It can be seen that for ^{4}He on Argon coated Grafoil, the value of the temperature of the peak, for a given areal density, is much higher than that for ^{4}He on (bare) Grafoil. Incidentally, the absolute magnitude of the specific heat peaks on Argon coated Grafoil are twice as large as those on (bare) Grafoil.

4.7. ^{4}He Specific Heat Analysis

To find out the dependence of the specific heat at temperatures below the peaks, logarithmic plots of our data were made. Figure 35 shows the results. Within the error of the measurements, the data fell on straight lines. The slope of these lines varied around the value 3. The exact values of the slopes for each density

together with the temperature of the peaks, are given in table D. For temperatures below the transition, we can, therefore, write down for the specific heat

$$C/Nk = aT^3$$

provided this formulation is regarded as an interpolation formula only. Further interpretation must await detailed measurements of the specific heat below 0.7 K.

For the data above the transition temperatures, the generally accepted[69] interpretation for (these) low densities, is that one is observing a 2D gas, which due to adatom-adatom interactions shows a specific heat (per atom) deviating somewhat from the ideal 2D gas value of 1 (see section 3.9). Siddon and Schick[69] calculated the deviation for Helium as adatoms. Figure 36 shows the plot of (C/Nk-1)/D vs T for our data, the broken line being the calculated values[69]. We do not seem to find a universal curve, but we feel a fair test should include data for temperatures 2 - 3 times above that of the transition.

4.8. ^{3}He Specific Heat on Argon coated Grafoil

Figures 37 - 44 show the C/Nk vs T of ^{3}He submonolayer films. The densities studied ranged from 0.012 to 0.073 $\mathring{A}^{-2}$ ($0.14 \leq x \leq 0.84$) and the temperature covered was 0.8 to 6.0 K.

FIGURE 34

^{4}He Low Density Phase Diagram

◘ Bretz et al[14] : ^{4}He on (bare) Grafoil

O This work : ^{4}He on Argon coated Grafoil

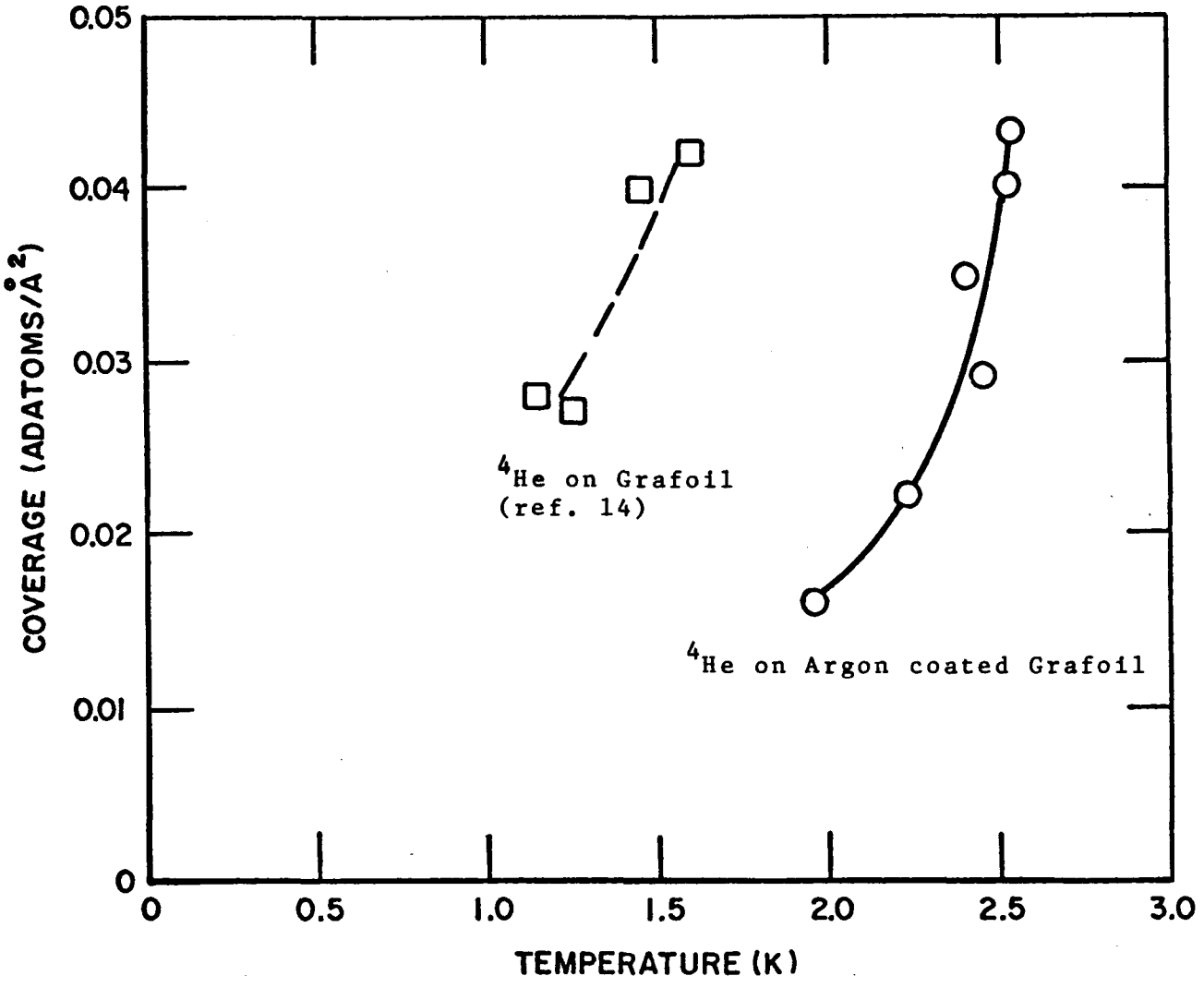
0.05
0.04
0.03
0.02
0.01
0
COVERAGE (ADATOMS/Å²)
0
0.5
1.0
1.5
2.0
2.5
3.0
TEMPERATURE (K)
⁴He on Grafoil
(ref. 14)
⁴He on Argon coated Grafoil

FIGURE 35

^{4}He Reduced Specific Heat. Log-Log Plot

▽ X=0.176 D=0.015 $\mathring{A}^{-2}$

\+ X=0.257 D=0.022 "

□ X=0.340 D=0.029 "

◇ X=0.425 D=0.036 "

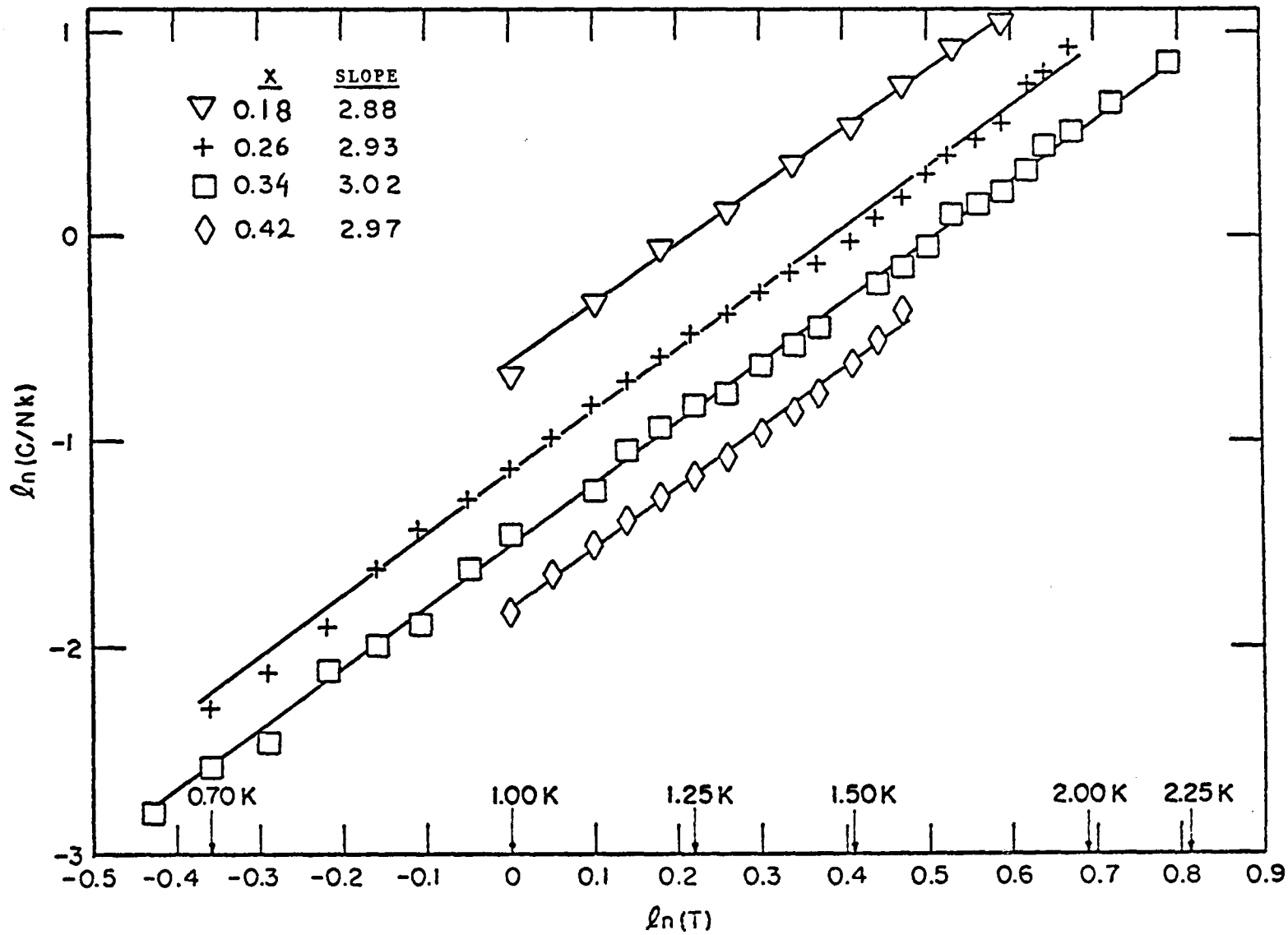
X SLOPE
0.18 2.88
0.26 2.93
0.34 3.02
0.42 2.97
0.70 K
1.00 K
1.25 K
1.50 K
2.00 K
2.25 K
ℓn (C/Nk)
ℓn (T)
1
0
-1
-2
-3
-0.5 -0.4 -0.3 -0.2 -0.1 0 0.1 0.2 0.3 0.4 0.5 0.6 0.7 0.8 0.9

FIGURE 36

^{4}He [C/Nk-1]/D vs T

▽ X=0.176 D=0.015 Å^{-2}

+ X=0.257 D=0.022 "

□ X=0.340 D=0.029 "

◇ X=0.408 D=0.035 "

The broken line is Siddon and SchicK[69] calculation. The heavy continuous line was drawn as a guide to the eye.

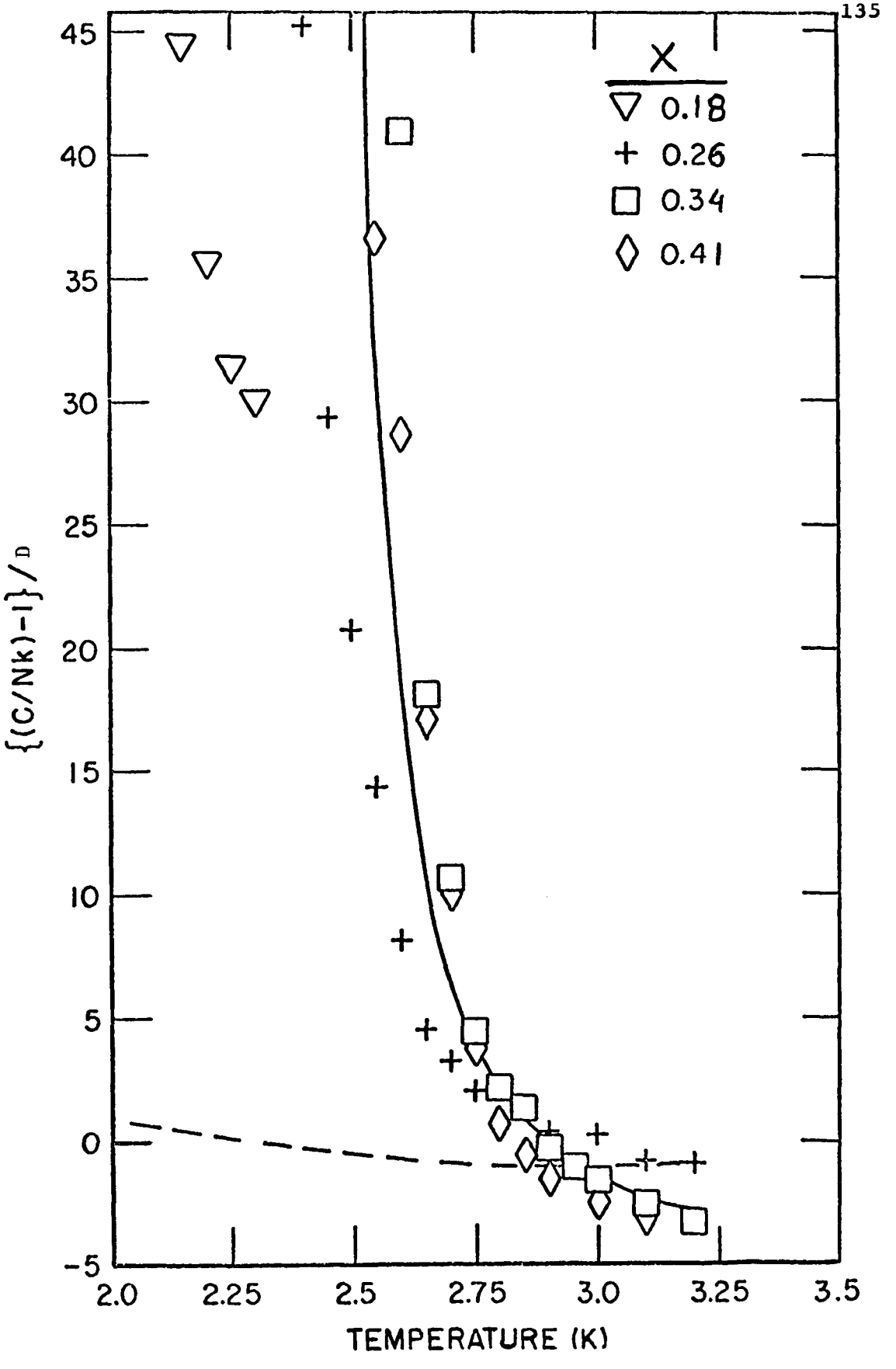
X
0.18
0.26
0.34
0.41
45
40
35
30
25
20
15
10
5
0
-5
{(C/Nk)-1}/D
2.0
2.25
2.5
2.75
3.0
3.25
3.5
TEMPERATURE (K)

TABLE D

^{4}He on Argon Coated Grafoil Phase Diagram Data

Coverage mmol	Fractional coverage x	Areal density $\AA^{-2}$	Peak temperature K	Slope
1.300	0.093	0.00792	-	
2.447	0.176	0.01492	1.95	2.88
3.588	0.257	0.02187	2.22	2.93
4.742	0.340	0.02891	2.45	3.02
5.685	0.408	0.03466	2.40	-
5.917	0.425	0.03607	-	2.97
6.525	0.468	0.03978	2.52	
7.055	0.506	0.04301	2.54	3.37

These measurements were done on two different amounts of Argon coating. The purpose was to check how sensitive the Helium film is on small changes of the amount of the underlying Argon. Figures 37 to 41 show data for ^{3}He on 288.0 cm^3(STP) Argon (adsorbed on Grafoil), i.e: 0.8% less than a monolayer. From here on, data taken on this substrate will be referred to as data from the Argon under-coated Grafoil. Figures 42 to 44 show data for ^{3}He on 304.0 cm^3(STP) Argon, i.e: 4.8% more than the monolayer. This substrate shall be referred to as (usually) Argon coated Grafoil. For comparison we note that the ^{4}He data was taken on Argon coating about 3% more than the monolayer (see section 4.1). To facilitate identification of the ^{3}He films studied in this work, table E is included with relevant information.

The ^{3}He data was taken using thermometers calibrated by others (see section 2.2), who supplied us with tables of the (true) resistance vs temperature. Our method, therefore, of reversing the thermometer current to compensate for thermal EMF's at the various junctions along the evanohm wiring, could not be used due to the systematic error introduced, as explained in Appendix A. The current reversing program was therefore omitted then. Instead the voltage across the thermometers with zero current was recorded every 1-2 hours, and the value subtracted from the thermo-

FIGURE 37

^{3}He on Argon Coated Grafoil Reduced Specific Heat

X(AR) = 0.99

X = 0.14

D = 0.012 $\mathring{A}^{-2}$

n = 2.061 mmol

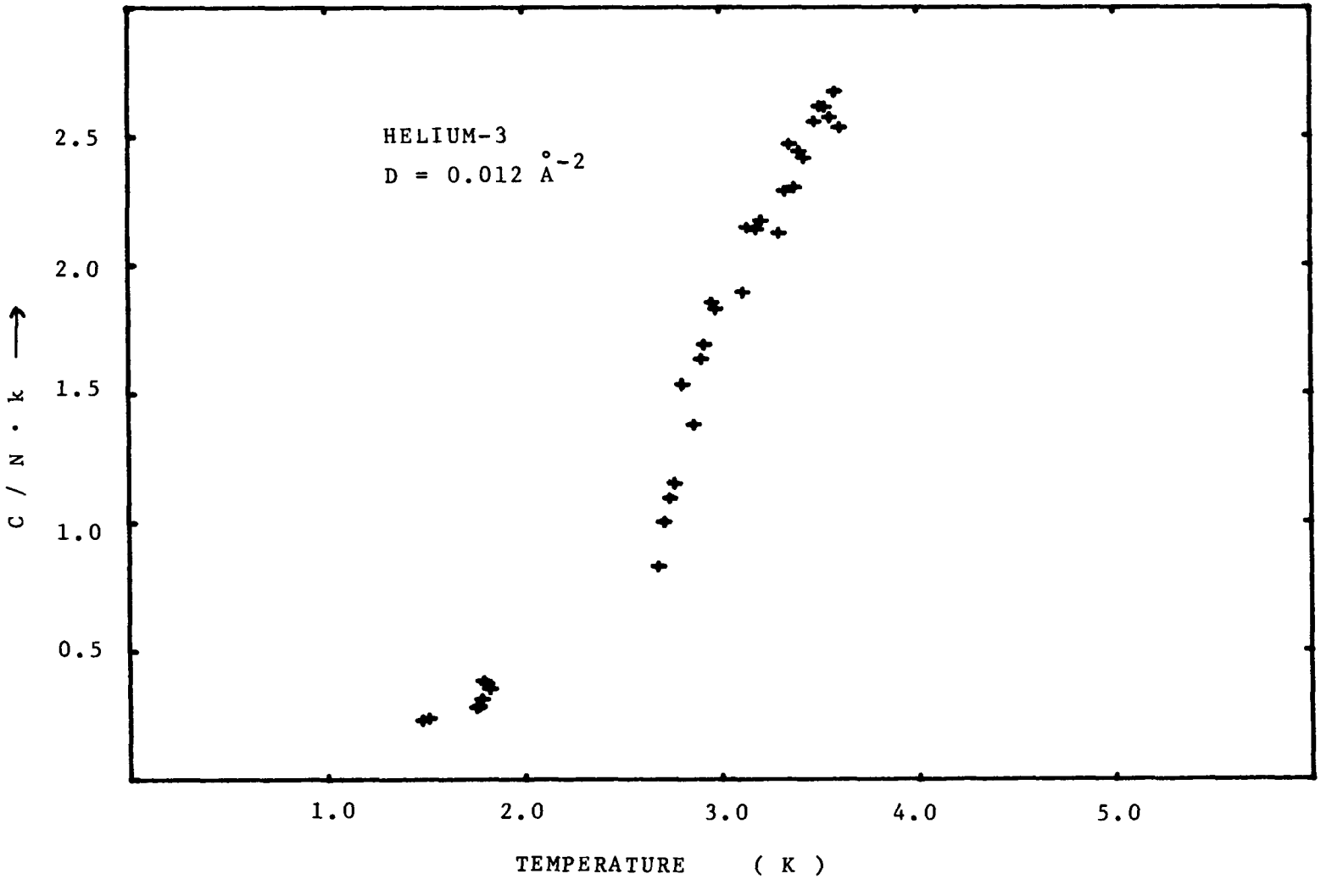
HELIUM-3
D = 0.012 Å^{-2}
C / N · k ⟶
2.5
2.0
1.5
1.0
0.5
1.0
2.0
3.0
4.0
5.0
TEMPERATURE (K)

FIGURE 38

^{3}He on Argon Coated Grafoil Reduced Specific Heat

X(AR) = 0.99
X = 0.27
D = 0.024 $\mathring{A}^{-2}$
n = 3.876 mmol

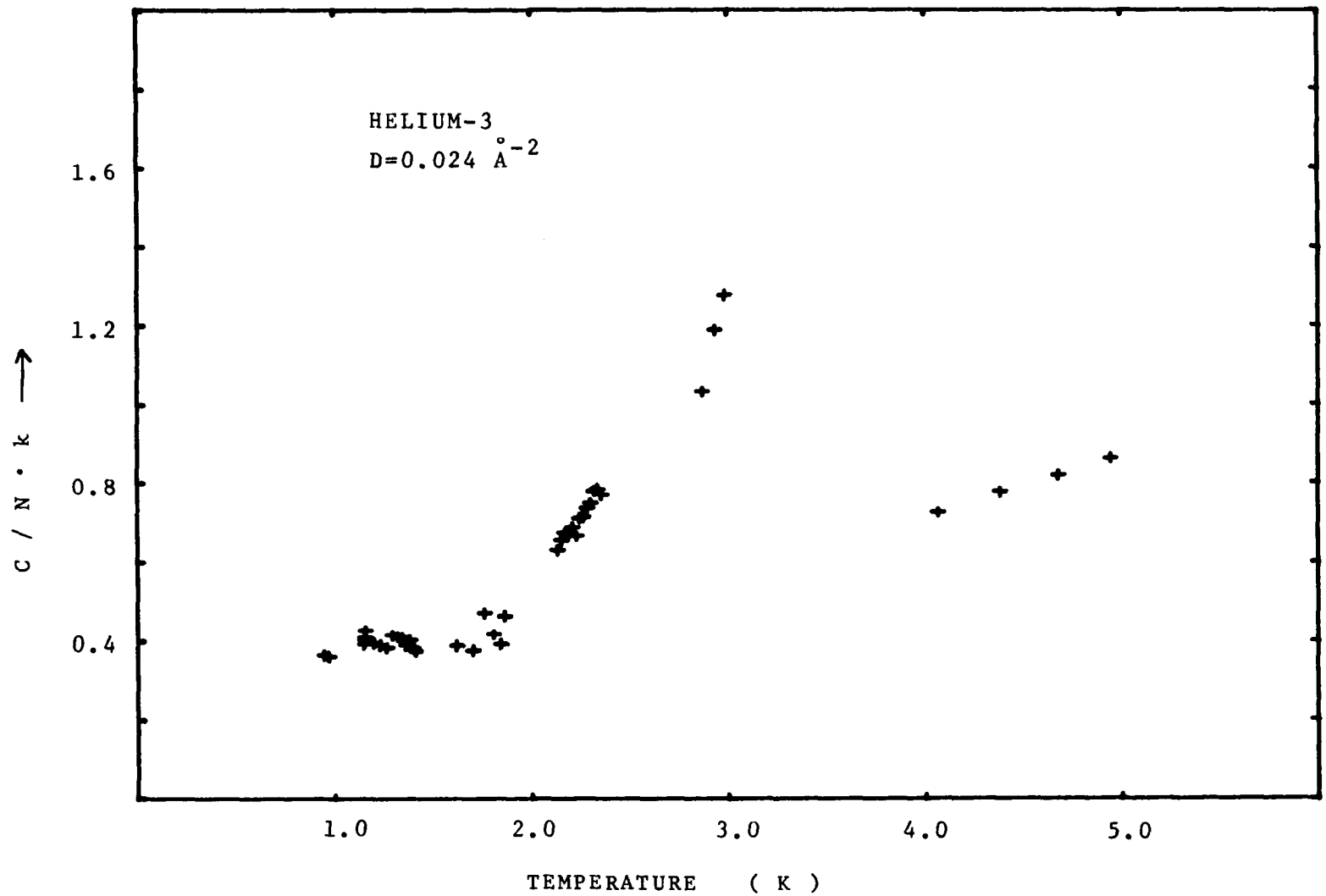
HELIUM-3
D=0.024 Å^{-2}
1.6
1.2
0.8
0.4
C / N · k ⟶
1.0
2.0
3.0
4.0
5.0
TEMPERATURE (K)

FIGURE 39

^{3}He on Argon Coated Grafoil Reduced Specific Heat

X(AR) = 0.99

X = 0.40

D = 0.035 $\mathring{A}^{-2}$

n = 5.688 mmol

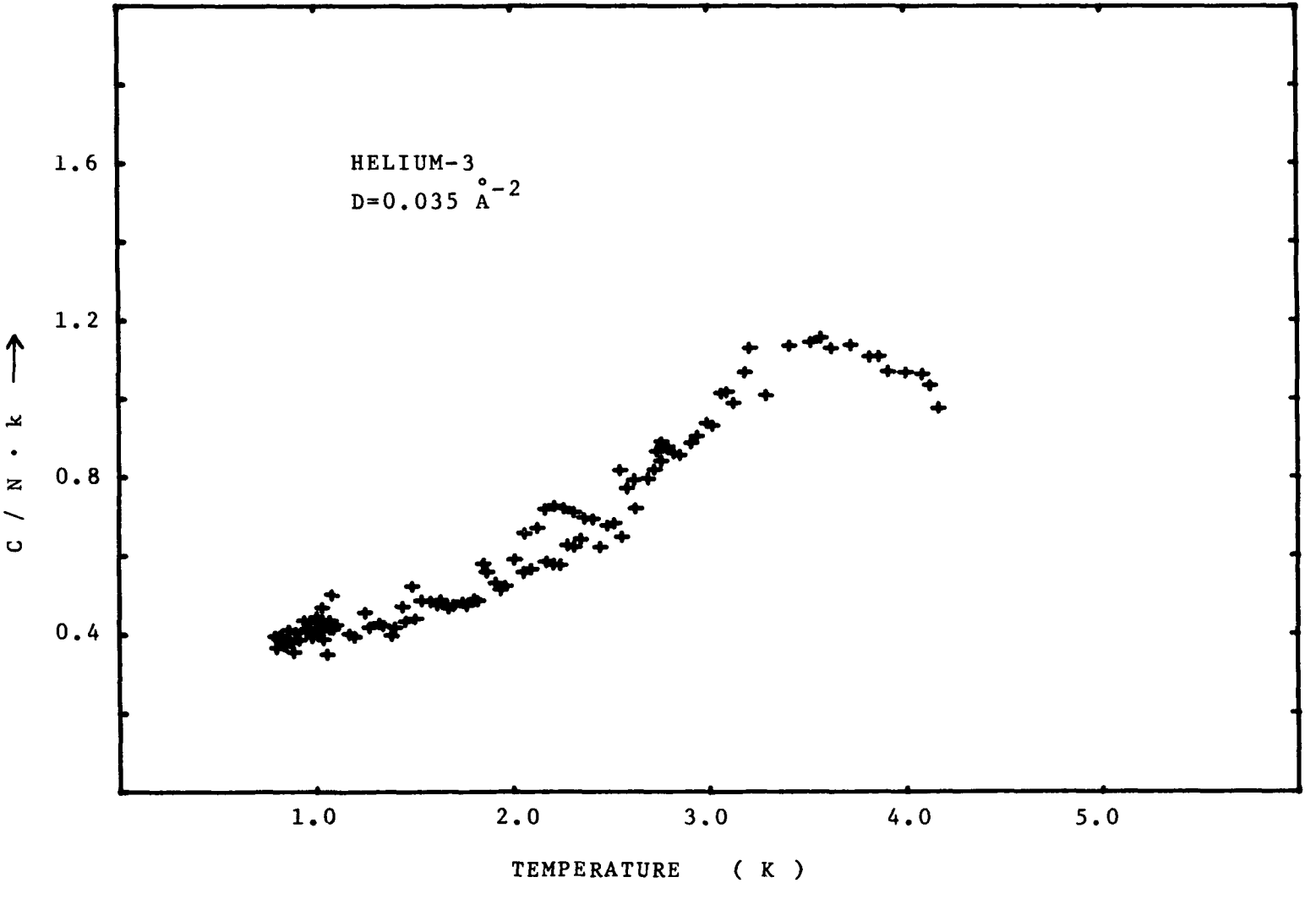
HELIUM-3
D=0.035 Å^{-2}
1.6
1.2
0.8
0.4
C / N · k
1.0
2.0
3.0
4.0
5.0
TEMPERATURE (K)

FIGURE 40

^{3}He on Argon Coated Grafoil Reduced Specific Heat

X(AR) = 0.99

X = 0.52

D = 0.045 $\mathring{A}^{-2}$

n = 7.439 mmol

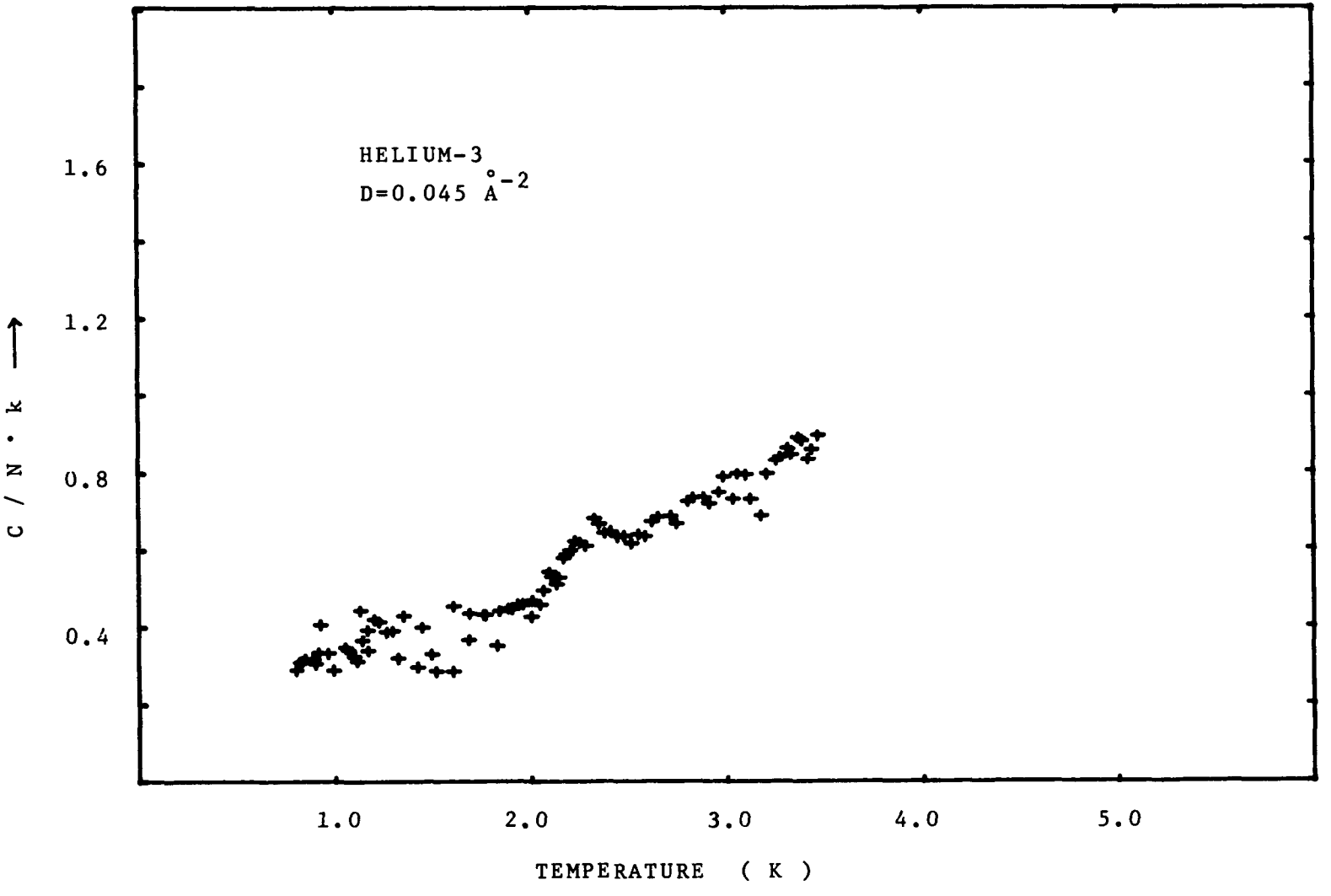
HELIUM-3
D=0.045 Å^{-2}
1.6
1.2
0.8
0.4
C / N • k
1.0
2.0
3.0
4.0
5.0
TEMPERATURE (K)

FIGURE 41

^{3}He on Argon Coated Grafoil Reduced Specific Heat

X(AR) = 0.99

X = 0.64

D = 0.056 $\mathring{A}^{-2}$

n = 9.176 mmol

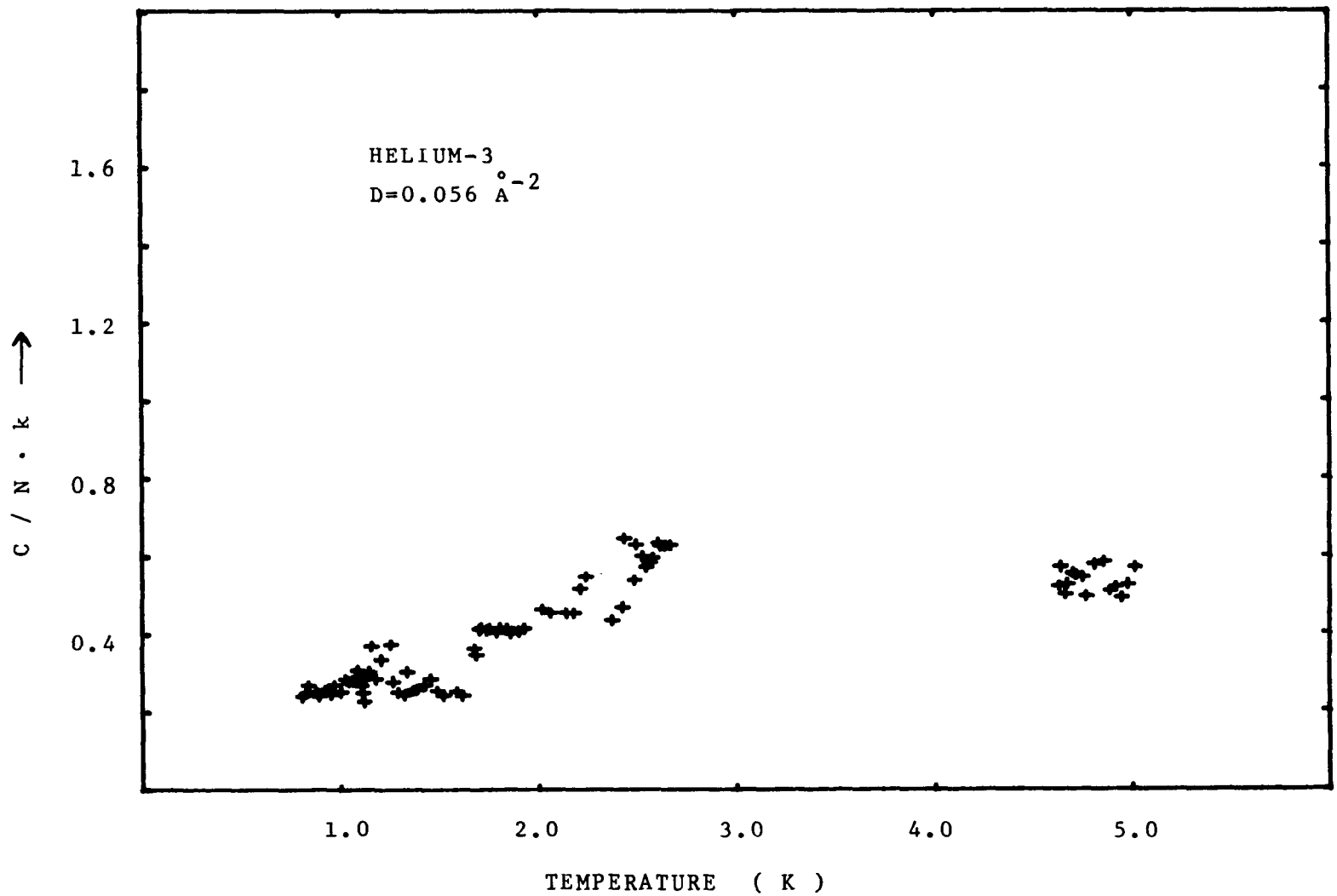
HELIUM-3
D=0.056 Å^{-2}
1.6
1.2
0.8
0.4
C / N · k
1.0
2.0
3.0
4.0
5.0
TEMPERATURE (K)

FIGURE 42

^{3}He on Argon Coated Grafoil Reduced Specific Heat

X(AR) = 1.05

+ { X = 0.26 for T>3K
  { D = 0.023 Å^{-2}
  { n = 3.737 mmol

. { X = 0.27 for T<3K
  { D = 0.023 Å^{-2}
  { n = 3.837 mmol

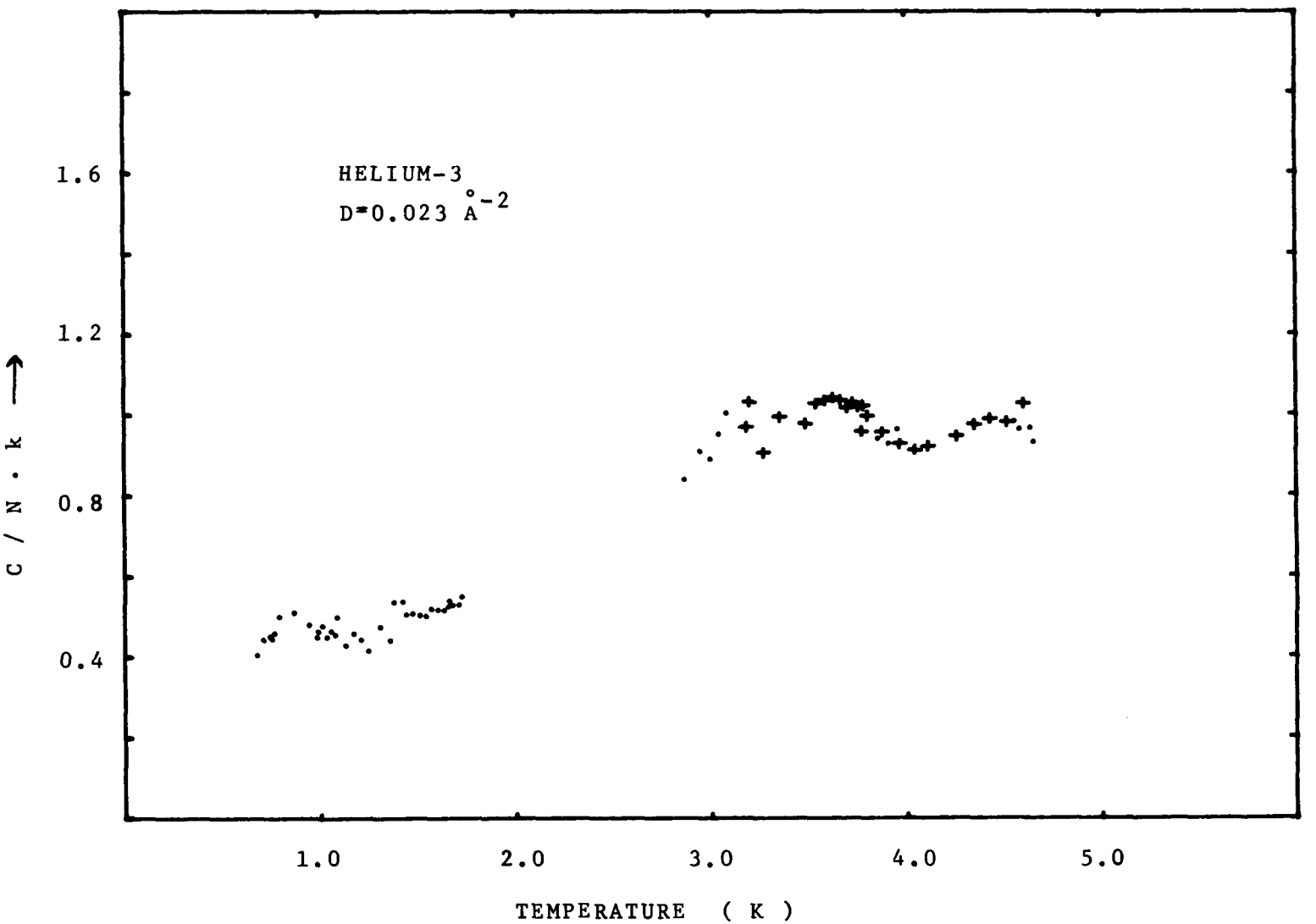
HELIUM-3
D=0.023 Å^{-2}
1.6
1.2
0.8
0.4
C / N · k
1.0
2.0
3.0
4.0
5.0
TEMPERATURE (K)

FIGURE 43

^{3}He on Argon Coated Grafoil Reduced Specific Heat

X(AR) = 1.05

X = 0.52

D = 0.045 $\mathring{A}^{-2}$

n = 7.441 mmol

The continuous line is the calculated desorption contribution (section 3.6), with E=61 K, plus a constant term equal to 0.6

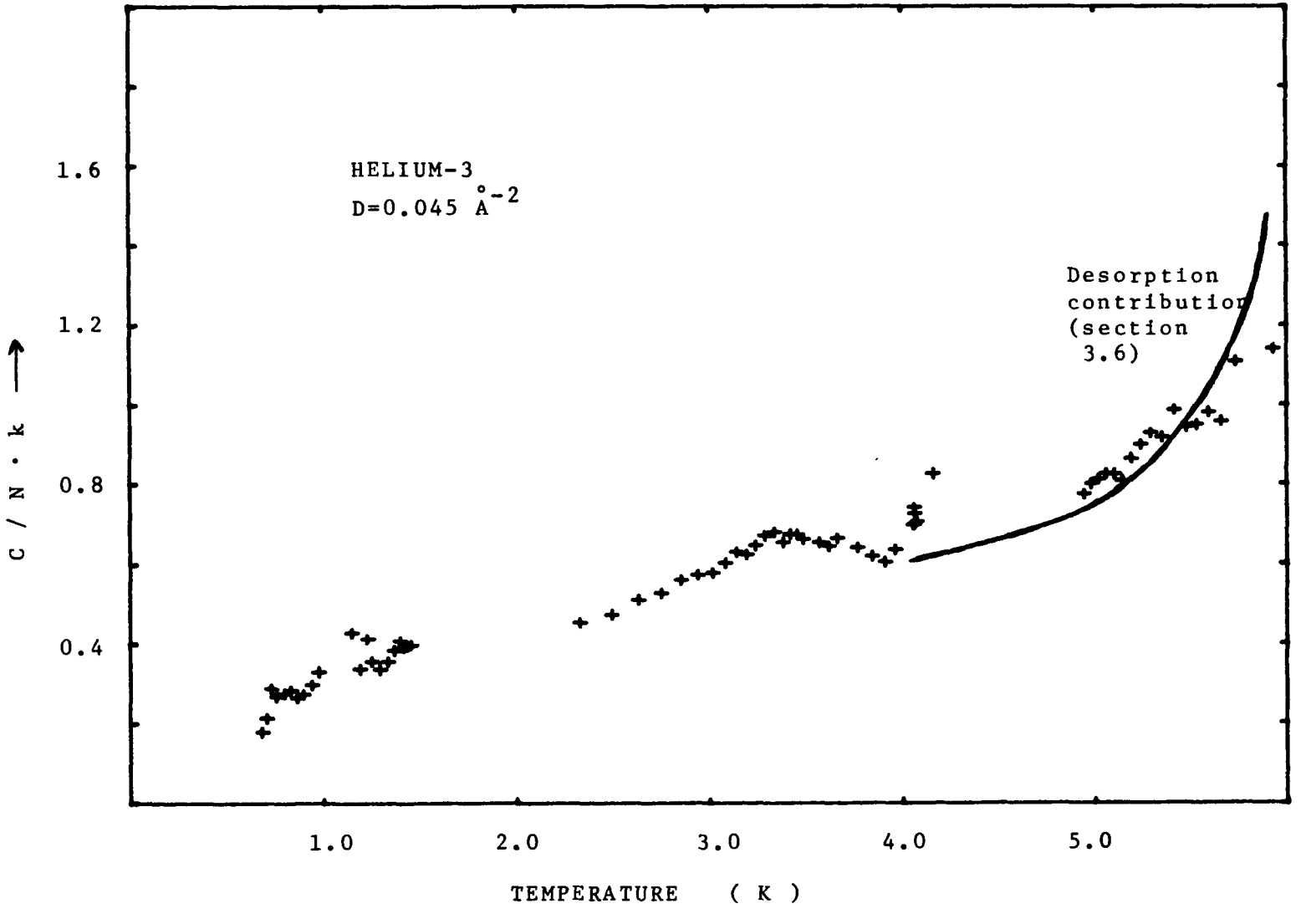
HELIUM-3
D=0.045 Å-2
Desorption
contribution
(section
3.6)
1.6
1.2
0.8
0.4
C / N · k
1.0
2.0
3.0
4.0
5.0
TEMPERATURE (K)

FIGURE 44

^{3}He on Argon Coated Grafoil Reduced Specific Heat

X(AR) = 1.05

X = 0.84

D = 0.073 $\mathring{A}^{-2}$

n = 12.03 mmol

The continuous line is the calculated desorption contribution (sectiom 3.6),with E=61 K, plus a constant term equal to 0.4

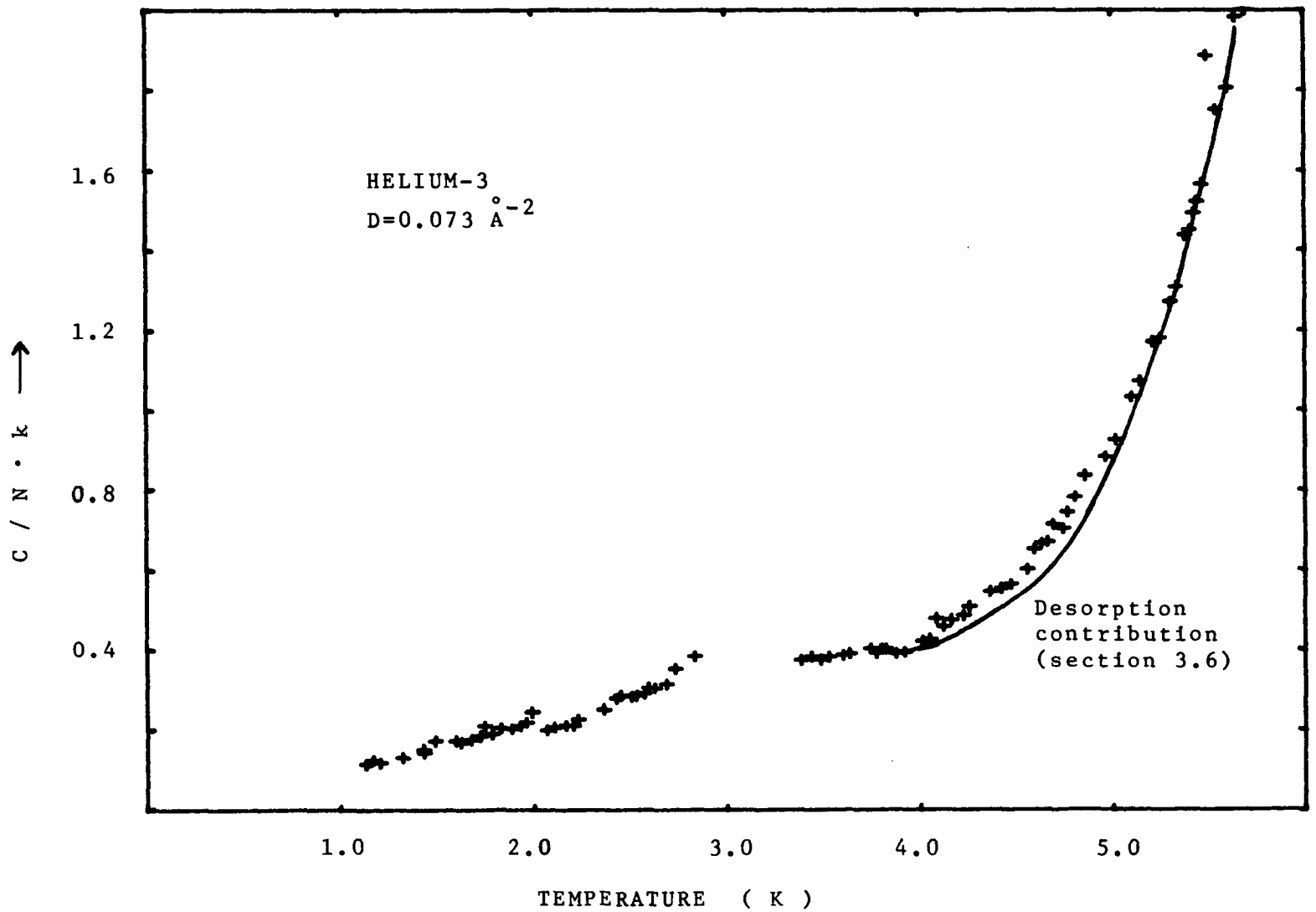
HELIUM-3
D=0.073 Å^{-2}
1.6
1.2
0.8
0.4
C / N · k
1.0
2.0
3.0
4.0
5.0
TEMPERATURE (K)
Desorption
contribution
(section 3.6)

TABLE E

Data ^{3}He on Argon Coated Grafoil

Coverage mmol	Fractional coverage x	Areal density $\mathring{A}^{-2}$	Argon coating cm^3(STP)	Argon fractional coverage
3.737	0.26	0.02278	304.0	1.05
3.837	0.27	0.02339	304.0	1.05
7.441	0.52	0.04536	304.0	1.05
12.027	0.84	0.07332	304.0	1.05
2.061	0.14	0.01256	288.0	0.99
3.876	0.27	0.02363	288.0	0.99
5.688	0.40	0.03467	288.0	0.99
7.439	0.52	0.04535	288.0	0.99
9.176	0.64	0.05594	288.0	0.99

meter readings with current on. This was considered sufficient because we assumed the cause of the EMF drift was the change of the liquid Helium level in the main bath, which would result in a monotonic drift of the EMF value. Nevertheless, oscillations of the EMF value were often observed. The result was an increased random error, as evidenced from figures 37-44.

The low density curves of ^{3}He ($D<0.035$ $\mathring{A}^{-2}$) showed maxima at about 3.5K with a maximum value of C/Nk 2.6 for the lowest density (0.012 $\mathring{A}^{-2}$). The maximum was just over 1 for the 0.035 $\mathring{A}^{-2}$ film. The maxima seemed to be more pronounced for the ^{3}He on the Argon under-coated Grafoil. In fact, comparison of the C/Nk for two common densities indicated the ^{3}He on Argon under-coated Grafoil values to be always larger than those of the ^{3}He on Argon coated Grafoil.

The higher density (0.045 and 0.073 $\mathring{A}^{-2}$) data for ^{3}He on Argon coated Grafoil showed a rapid increase of C/Nk with temperature above 4.5 K, whereas in the case of the Argon under-coated Grafoil C/Nk reached a certain value where it remained (unfortunately the data for the 0.045 $\mathring{A}^{-2}$ film did not go beyond 3.5 K).

No curves, except the one for the highest density,

seemed to extrapolate back to the (0,0) point of the graphs.

4.9. ^{3}He Specific Heat Analysis

To find out if ^{3}He on Argon coated Grafoil behaves like a 2D virial gas, we plotted the (C/Nk-1)/D against temperature for the three densities studied together with Siddon and Schick's[69] calculated values for $-\beta^2(d^2B/d\beta^2)$. The plot is shown in figure 45.

For temperatures larger than 3.75K the data for the lowest density (0.024 $\mathring{A}^{-2}$) agree with the calculated values. They are not even close to the points from the other two densities. On the contrary, these higher densities (0.045 and 0.073 $\mathring{A}^{-2}$) do not agree with the calculated values at all, but seem to fall on one curve above 1.5K. The sudden change above 5.0K is most likely due to desorption effects.

Figure 45 does not include data from the Argon under-coated Grafoil for reasons of clarity. The resulting curves do not exactly fall on the curves from the Argon coated Grafoil, but follow the same trend, i.e: results from low density films look drastically different from the results

of the more dense ^{3}He films. All curves cross each other at about 2.75 K.

4.10. Interpretations. Comparisons

Following the suggestion given by Bretz et al[14] and Elgin and Goodstein[80] we interpret the specific heat data of small areal densities (0.01 $\mathring{A}^{-2}$ and less) for both isotopes as indicating localization of the adatoms on sites with unusually high binding energy. Surface heterogeneities can cause this behaviour. The adatoms are strongly bound to these adsorption sites, which exist on all real surfaces, as discussed in sections 4.4 and 3.5, and this does not allow lateral mobility. it was felt that by reducing the amount of the Argon coating the inhomogeneities of the Grafoil were not smoothed out as much and, therefore, this localization persisted at higher densities, at least up to 0.035 $\mathring{A}^{-2}$. In any case, this localization seemed to be unimportant at about 3.7 K according to the ^{3}He data, the ^{4}He measurements being inconclusive (see fig. 26).

At higher temperatures the ^{3}He data suggests the formation of a 2D interacting gas.

As the density of the films increased, the behaviour

FIGURE 45

^{3}He [C/Nk-1]/D vs T

+ X=0.26 D=0.023 $\mathring{A}^{-2}$ X(AR)=1.05

□ X=0.52 D=0.045 " " "

○ X=0.84 D=0.073 " " "

. Siddon and Schick[69] calculation

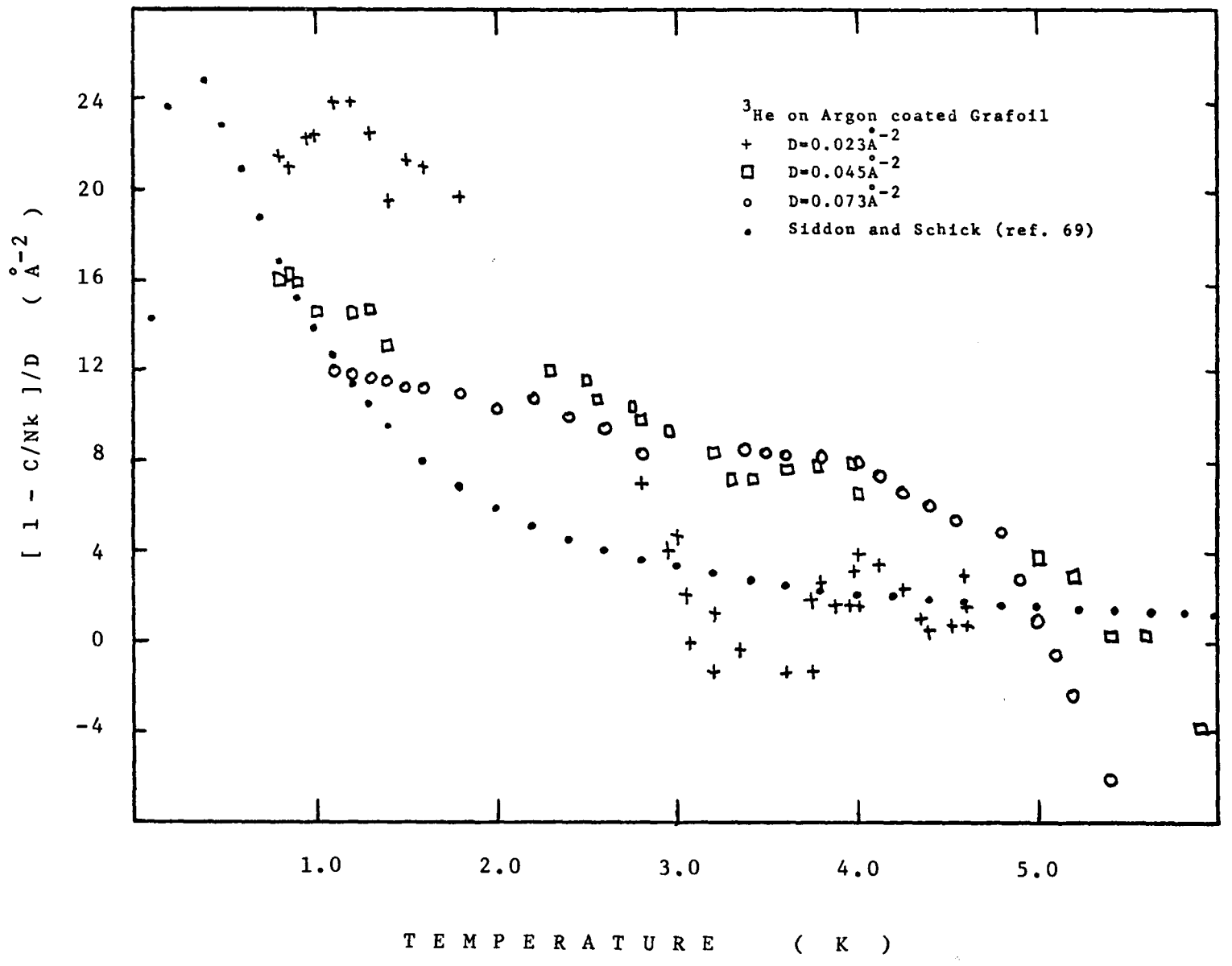
^{3}He on Argon coated Grafoil
+ D=0.023Å^{-2}
□ D=0.045Å^{-2}
o D=0.073Å^{-2}
• Siddon and Schick (ref. 69)
[1 - C/Nk]/D (Å^{-2})
24
20
16
12
8
4
0
-4
1.0
2.0
3.0
4.0
5.0
T E M P E R A T U R E (K)

of the two isotopes became quite different. At low temperatures the ^{4}He seemed to form a 2D liquid. By this we mean a phase, which did not yield C/Nk values proportional to the square of the temperature, nor as expected for a 2D interacting gas. At high temperatures a transition to another phase was seen, most likely a 2D gas, but with specific heat not accounted for by the Siddon and Schick[69] model. The transition temperature increased with density reaching a maximum value of 2.55 K at 0.040 $\mathring{A}^{-2}$, as far as our data can suggest. The ^{3}He did not show such a transition at all.

The possibility of the difference in behaviour due to the mass difference of the two isotopes has been discussed by Novaco[97]. He argued that the higher kinetic energy of the lighter ^{3}He adatom could be enough to overcome the 2D liquid weak binding. Using the results of theoretical[77,78] calculations for the properties of the ground state of the adsorbed Helium (with the substrate effects ignored), Novaco[97] calculated the specific heat of adsorbed ^{3}He at x=0.5, including the effect of small surface heterogeneity. His calculated C/Nk values as a function of the temperature have the same dependence as our results, but the transition temperature is much less, about 0.8 K. This is so because the predicted stable phase was a 2D liquid with lateral binding

energy per atom about 0.61K and an areal density of 0.037 $\mathring{A}^{-2}$ (see reference 77 for example). Our results do not disagree with the density, but suggest a binding energy at least three times as large.

It should be pointed out though, that the arguments just presented are by no means a complete and exhaustive comparison with the available literature of the properties of the 2D Helium. In fact, they are speculations rather than interpretations, as we know of no model calculations for Helium adsorbed on Grafoil coated with a monolayer of Argon.

Hegde and Daunt[89][98] studied the magnetic susceptibility of ^{3}He films on Argon coated Grafoil by measuring the nuclear magnetic resonance linewidth. His results for coverages below x=0.40 indicated a 2D gas with the measured susceptibility in fair agreement with the one calculated from Siddon and Schick model[69], although a small but systematic deviation was observed at low temperatures. The linewidths for x=0.60 and 0.80 were found to be indepedent of temperature suggesting either a liquid or a solid.

Crary and Vilches[99] measured the specific heat of Helium on Argon coated Grafoil. Their results are in good agreement with ours. The position of the specific heat peaks

in the density vs temperature diagram is in excellent agreement with our diagram. They calculated an exponent of 3.3 for the specific heat power law dependence for temperatures below those of the peaks. However, the least dense film they studied, with an areal density of 0.009 $\mathring{A}^{-2}$, also showed a peak at 1.92K with C/Nk reaching a maximum value of 2.7 (compared to our smallest density film, 0.008 $\mathring{A}^{-2}$, which did not show any peaks). They only studied two ^{3}He films with small densities and seemed to find a small peak at about 0.75K with C/Nk values reaching about 1.

CHAPTER 5: SUGGESTIONS FOR FURTHER WORK

In view of the ^{4}He data it is felt it should be of interest to extend the specific heat measurements at lower temperatures as well as higher densities. Measurements at low temperatures will greatly help in deciding if the specific heat obeys a power or an exponential law, while measurements at higher densities will help to complete the phase diagram.

In view of the ^{3}He data it is also considered of interest to extend the specific heat measurements. At low temperatures the question of the possibility of a peak may give a more definitive answer. At even lower temperatures (below 0.3K) the spin ordering may be seen.

In view of the difference of the specific heat of Helium on (bare) Grafoil and on Argon coated Grafoil it is considered of interest to investigate the effect of the Argon coating in greater detail,i.e: study the properties of the Helium as a function of the amount of the Argon coating in search of an even more uniform substrate.

In fact, detailed study of the Argon film per se should

promote our understanding of the adsorption of the rare gases by Grafoil. Search for an Argon registered phase, the so called lattice gas phase, should be very rewarding.

APPENDIX A

Figure 46 is the equivalent circuit diagram of the system measuring the resistance of the Germanium thermometers. The measured current I_M was found by measuring the voltage V_s across the known resistor R_s, with the Digital Voltmeter (DVM):

$$I_M = E/\left[\frac{R_s R_H}{R_s+R_H} + 2R + R_L + \frac{R_x(2R+R_K)}{R_x+2R+R_K} \right]$$

$$V_s = I_M \cdot R_s R_H/(R_s+R_H)$$

Substituting the values of the resistances used (see figure 46), one can see that the expression giving I_M can be simplified, i.e:

a) 2R is negligible compared to the other terms,
$2R/R_K \simeq 2\times10^{-6}$, $2R/R_L \simeq 5\times10^{-5} - 10^{-6}$

b) $R_x R_K/(R_x+R_K) = R_x/(1 + R_x/R_K) = R_x\cdot(1 - R_x/R_K + \ldots)$
This correction to R_x is less than 10^{-4} correction to the whole denominator, and therefore, negligible.

c) $R_s R_H/(R_s+R_H) = R_s/(1 + R_s/R_H) \simeq R_s/1.01$

The voltage V_s is then given by

$$V_s = \frac{ER_s/1.01}{R_s/1.01 + R_L + R_x}$$

The voltage V_x across the thermometer was also

measured with the DVM, after it was amplified by the D.C. nV amplifier. That is, the DVM was disconnected from R_s and, therefore, the thermometer current I was slightly different:

$$I = E/[\ R_s + 2R + R_L + \frac{R_x(2R+R_K)}{R_x+2R+R_K}\ ] \simeq E/(R_L+R_s+R_x)$$

$$V_x = \frac{E}{R_L+R_s+R_x} \cdot \frac{R_x(2R+R_K)}{R_x+2R+R_K} \simeq \frac{E}{R_L+R_x+R_s} \cdot \frac{R_xR_K}{R_x+R_K}$$

The expressions for the voltages V_s and V_x yield the following equation, correct to better than 0.01%

$$\frac{V_s}{V_x} \cdot \frac{R_L + R_s/1.01}{R_L + R_s} \cdot \frac{1.01}{R_s} \cdot \frac{R_xR_K}{R_x+R_K} = 1$$

from which R_x can be calculated. If one writes V_{s+}, V_{s-}, V_{x+}, V_{x-} for the measured voltages as the current alternates, the final equation is

$$R_x^{-1} = \frac{V_{s+} - V_{s-}}{V_{x+} - V_{x-}} \cdot \frac{R_L+R_s/1.01}{R_L + R_s} \cdot \frac{1.01}{R_s} - \frac{1}{R_K}$$

or, within 0.1%

$$R_x = \frac{R_s}{1.01} \cdot \frac{V_{x+} - V_{x-}}{V_{s+} - V_{s-}}$$

The error of the heat capacity was a few per cent (see section 4.5), and the last formula was found adequate.

The measured voltage V_x was not always the voltage across the thermometer. Depending on thermometer, temperature

and thermometer current, it would take as much as 15 sec for the Keithley nV amplifier to read the correct voltage. But, the unit time was set at 7 sec (see section 2.8). The effect of this 'clipping' became very obvious at temperatures below 0.4 K (see figure 4). By varying the unit time from 3 to 40 sec, it was found that the error in temperature due to the 'cliiping' was about 0.1% at 0.5 K and less than 0.01% at 4.2 K. In any case, this was a systematic error and thermometers calibrated with this system were not affected by the clipping at all, as it was reproducible better than 0.01%.

Figure 47 is the equivalent circuit diagram of the system measuring the power dissipated in the sample heater R_x. The heating period was varying from 4 to 8 unit times, i.e: 27 to 56 sec. During the first two unit times, the DVM measured V_x, the voltage across the heater, then it was connected across the standard resistor R_s to measure V_s, the heater 'current':

$$V_x = E\frac{\dfrac{R_x(R_H+2R)}{R_x+R_H+2R}}{R_L+2R+R_s+\dfrac{R_x(R_H+2R)}{R_x+2R+R_H}} \simeq E\frac{R_x(1-r_1)}{R_L+2R+R_s+R_x}$$

where $r_1=R_x/R_H=1.1^{\times}10^{-4}$. The $1-r_1$ factor was not included in the denominator being a negligible correction.

FIGURE 46

Temperature Measurement Circuit

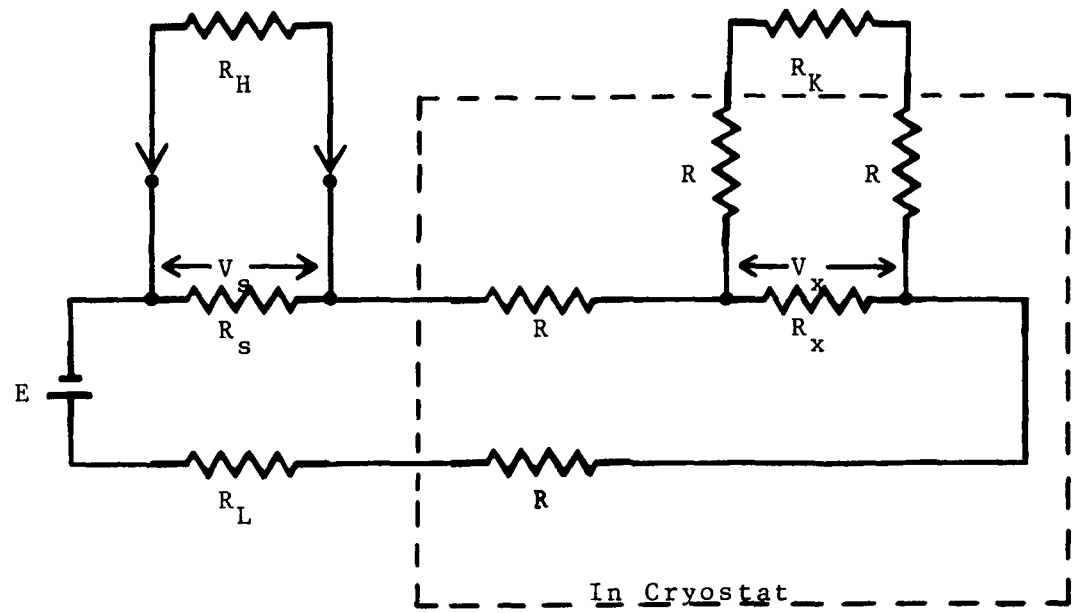

R_H = 10 MΩ, DVM input impedance (figure 9, section 2.8)
R_K = 30 MΩ, D.C. nV amp. input impedance (figure 9)
R_s =0.1 MΩ, standard resistor (R_{st} in figure 13)
R_L = 1.5 - 50 MΩ, current limiter (RT1-RT9 in figure 13)
E = 12.6 V (E1 in figure 13)
R_x = 0.10 - 5.0 KΩ, thermometer resistance (fig. 4 and 5)
R ≃ 25 Ω, evanohm wiring resistance

FIGURE 47

Sample Heater Power Measurement Circuit

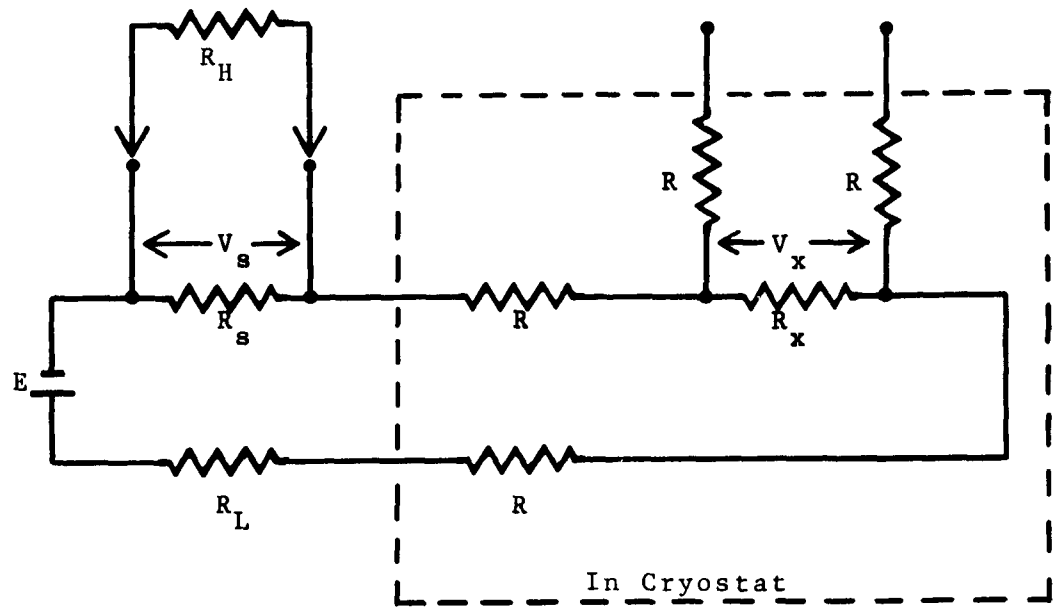

R_H = 10 MΩ, DVM input impedance (figure 9, section 2.8)
R_s = 10 KΩ, standard resistor (RSH in figure 13)
R_L = 10 - 300 KΩ, current limiter (RH1 - RH8 in figure 13)
E = 12.6 V (E2 in figure 13)
R = 25 Ω, evanohm wiring resistance
R_x = 1100 Ω, heater resistance (evanohm)

$$V_s = E\frac{\dfrac{R_s R_H}{R_s+R_H}}{R_L+2R+R_x+\dfrac{R_s R_H}{R_s+R_H}} \simeq E\frac{R_s(1-r_2)}{R_L+2R+R_s(1-r_2)+R_x}$$

where $r_2=R_s/R_H=10^{-3}$.

During measurement of the V_x the power dissipated in the heater was V_x^2/R_x, while during measurements of the V_s the power was $V_s^2 R_x/[R_s(1-r_2)]^2$. The energy, therefore, given into the sample was

$$Q' = t_1 V_x^2/R_x + t_2 V_s^2 R_x/[R_s(1-r_2)]^2$$

with t_1, t_2 the time the DVM was connected across the heater and the standard resistor, respectively. However, the calculated energy was:

$$Q = (t_1+t_2)V_s V_x/[\ R_s(1-r_2)\ ]$$

The difference of Q' and Q was estimated to be about 0.05% for the maximum heater current (R_L=10 KΩ), and the formula used was, therefore, considered adequate.

APPENDIX B

To calibrate the thermometers, a platform was mounted at the Mixing Chamber instead of the calorimeter. It was made of Oxygen Free High Conductivity Copper. It consisted of three parts. The platform body, where three thermometer holders and a 0.2 cm^3 vapour pressure bulb were silver soldered. An OFHC Copper cylinder, where the thermometer leads were thermally anchored (the same way they were anchored on the calorimeter body, section 2.3). And a magnetic thermometer, as described by Harley et al[100].

In the temperature range of 2.3 to 4.2 K, the thermometers were calibrated against the vapour pressure of ^4He[101]. In the range of 0.7 to 3.0 K, against the vapour pressure of ^3He[102]. To verify the presence of liquid in the pressure bulb at high pressures, some amount of the test gas was occasionally pumped. The pressure was measured with a Ruska[47] pressure counter, model XR-38, and corrected for thermomolecular effects according to the Weber-Schmidt equation[50]. The combined (random) errors of the pressure and resistance measurements, were estimated to result in a temperature error of ±0.2% at the limits of the calibration range, and less than 0.1%

in the range 1.0 - 1.5 K.

Cerium Magnesium Nitrate (CMN) has been extensively used as the material for magnetic thermometers designed to be sensitive in the temperature range of 0.1 to 1.0 K. It is a paramagnetic salt obeying Curie's law down to the mK region. Betts et al[103] showed that if the inductance of a tuned circuit encloses a paramagnetic salt, the change of the susceptibility due to a temperature change, will cause a frequency shift:

$$\frac{f_o - f}{f_o} = \frac{a}{T}$$

where f_o is the high temperature ($T \to \infty$) frequency and a is a constant. Thus, one converts a temperature measurement to frequency measurement. Oscillations can be set up and maintained by a properly biased tunnel diode. The theory of such an oscillator has been given by Boghosian et al[104].

The magnetic thermometer used was designed to be similar to the one described in a paper by Harley et al[100] except that the oscillator section was mounted in the 4.2 K bath, instead the 1.0 K pot. The operating frequency was 1.0 MHz. The signal was amplified by a Hewlett-Packard 461A amplifier and the frequency measured by a Hewlett-Packard 50 MHz Universal Counter, model 5302A. The constant

a was 0.55 mK. This means a sensitivity of 0.5 Hz/mK at 1.0 K, and 5 Hz/mK at 0.1 K. Given that the frequency stability was about 2-3 Hz the error in $\Delta f = f_o - f$ was about 0.1%. The temperature error in the range of 0.3 to 0.7 K was estimated to be about 0.2%.

APPENDIX C

I. Langmuir[4] derived an adsorption isotherm for the solid-gas system using arguments of the kinetic theory of gases, i.e: treating the adsorption as a dynamic process. The solid was assumed to provide identical sites able to accomodate only one adatom, and the adatoms were assumed localized with their energies independent of the occupancy of the neighbouring sites. The form of the isotherm is the following:

$$P = b \cdot \frac{N_a}{N_m - N_a} = b \cdot \frac{x}{1 - x}$$

where P is the pressure of the gas phase, N_a the number of the adsorbed atoms, N_m the number of the available sites, $x = N_a/N_m$ and b a constant, function of the temperature only:

$$b = \left[\frac{2\pi mkT}{h^2} \right]^{3/2} \cdot kT \cdot \frac{f_g(T)}{f_a(T)} \cdot \exp(-q/kT)$$

with m the mass of the adatoms, k Boltzmann's constant, h Planck's constant, T the temperature, f_g, f_a the internal partition functions of the atoms in the gas and adsorbed phase respectively, and q the energy difference of the ground states of the gas and adsorbed phases (i.e: q_{st}).

The value of b was found when statistical mechanics

was used to derive the Langmuir equation. Furthemore, these derivations made clear that the condition for the Langmuir equation to be obeyed, is b to be a constant[105] (independent of coverage), and the original assumptions of surface uniformity and absence of adatom-adatom interaction were very restrictive. For b to be constant, which implies q constant, on a real surface, all one needs is compensating effects (see section 3.5).

The assumption of a single layer adsorption remains unrealistic for physisorbed systems, which tend to form multilayer films. However, at low pressures, i.e: at submonolayer coverages, the Langmuir equation is considered a good approximation [105]. Plots of our adsorption data according to this equation (i.e: P/N_a vs P), did not yield straight lines, but the limit of the slope, at low pressures, indicated monolayers in fair agreement (within 15%) with the values found by using the point 'B' method (see section 3.2).

The BET equation[59] is essentially an extension of the Langmuir equation, allowing for multilayer adsorption. With the assumption that adatoms are adsorbed at the top of other adatoms, and that the isosteric heat of the second layer and above, is equal to the heat of lique-

faction (or solidification), one can derive the following form for the isotherm:

$$N_a = \frac{CN_m P}{(P_o - P)[\ 1 - (C-1)P/P_o\ ]}$$

with P_o the condensation pressure of the gas phase at the temperature of the isotherm, and C a constant that is given by[105]:

$$C = \exp[\ -\frac{F_o - F_L}{kT}\ ]$$

where F_o the free energy of the first layer (per adatom), and F_L the energy of condensation.

The assumptions of the BET model are many and unrealistic, and much criticism has been raised[106]. The BET theory, however, has very succesfully explained almost all isotherms of physisorption, and yielded reasonable values for the physical quantities involved, specially the monolayer coverage. It's success lies in the fact that all original assumptions are not necessary. As in the case of the Langmuir equation, The BET equation should be obeyed if C is independent of coverage, i.e: the effect of surface non-uniformity is compensated for by adatom-adatom interaction. So, it will fail for adsorption on a uniform surface (unless the adatom interaction is negligible). Furthermore, it can not

explain isotherms with breaks corresponding to 2D phase changes[105].

REFERENCES

1. R.Peierls, Proc. Cambridge Phil. Soc. 32,477 (1936)
See also R.B.Griffiths, Phys. Rev. 136,A437 (1964)
2. M.F.M.Osborne, Phys. Rev. 76,396 (1949)
3. J.Daunt, K.Mendelssohn, Proc. Roy. Soc. A170,439 (1939)
4. D.M.Young, A.D.Crowell, 'Physical Adsorption of Gases', Butterworths 1962
5. J.G.Dash, 'Films on Solid Surfaces', Academic Press 1975
6. H.P.R.Frederikse, Physica 15,860 (1949)
7. D.F.Brewer, A.Evenson, A.L.Thompson, J. Low Temp. Phys. 3,603 (1970)
8. J.G.Daunt, P.Mahadev, Physica 69,555 (1973)
D.C.Hickernell, E.O.McLean, O.E.Vilches, J. Low Temp. Phys. 13,241 (1973)
9. J.G.Daunt, P.Mahadev, Physica 69,562 (1973)
G.A.Stewart, J.G.Dash, Phys. Rev. A2,918 (1970) and J. Low Temp. Phys. 5,1 (1971)
10. Anomalous terms were often constructed in order to unify experimental results. See for example J.G.Daunt, Physics Letters 41A,223 (1972)
11. J.J.Lander, J.Morrison, Sur. Sci. 6,1 (1967)
12. A.Thomy, X.Duval, J. Chim. Phys. 67,1101 (1970)
13. Grafoil is the trademark of a product manufactured by

Union Carbide Corp., Carbon Products Div., New York, N. Y. Manufacturing details are in U.S.Patent 3,404,061

14. M.Bretz, J.G.Dash, D.C.Hickernell, E.O.McLean, O.E.Vilches, Phys. Rev. A8,1589 (1973) and A9,2814 (1974)
15. J.G.Dash, Sci. Amer. May 1973, p. 30. This is actually a short review of reference 14.
16. J.G.Daunt, S.G.Hegde, E.Lerner, 'Monolayer and Submonolayer Helium Films',ed. J.G.Daunt and E.Lerner, Plenum Press 1973
17. A.D.Novaco, F.J.Milford, Phys. Rev. A 5,783 and 6,526 (1972)
18. D.H.Parkinson, Repts. Progr. Physics 21,226 (1958)
19. Cryo-Cal Inc., Minneapolis, Minnessota
20. We thank Professor F.W.Smith, Physics Dept., C. C. N. Y., New York, N. Y., for kindly allowing us to use his calibrated thermometer.
21. F.W.Smith, Phys. Rev. B9,942 (1974)
22. We thank Cryo-Cal Inc. (ref. 19) for sending us one of their standards to use in our experiment
23. E-Solder 3021, Epoxy Products Co., New Haven, Connecticut
24. Evanohm is an alloy manufactured by Wilbur B. Driver Co., Newark, New Jersey, containing 75% Ni, 20% Cr, 2.5% Al, 2.5% Cu. Its resistivity changes about 1% from room temperature to 0.5 K.
25. General Electric 7031, Schenectady, New York
26. Cry-Con grease, Air Products and Chemicals Inc.,

Allentown, Pennsylvania

27. J.K.Kjems, L.Passell, H.Taub, J.G.Dash, A.D.Novaco, Phys. Rev. B 13,1446 (1976)
28. Private communication. We thank Dr. L. Passell for making available to us results of the BNL group before publication.
29. The heat treatment of the Grafoil was performed at RCA Research Laboratories, Princeton, New Jersey.
30. We thank Dr J. Dooley, Physics Dept., Brooklyn College, N. Y., for allowing us to use his furnace.
31. 99.9% purity, manufactured by A.D.Mackey Inc., New York, N. Y. We used a wire 0.015" dia. and 1.1" long
32. Perfect Wire Solder, a low melting temperature soft solder. Manufactured by Torrey S. Crane Co., Plantsville, Connecticut
    A heating gun was used to melt the solder. Surfaces were cleaned with a mild acid: diluted Stay Clean Flux, manufactured by J.W.Harris Co., Cincinnati, Ohio
33. For Lead C = 30 K^2. See C.V.Heer, C.B.Barnes, J.G.Daunt Rev. Sci. Instr. 25,1088 (1954)
34. For a compilation of the literature on thermal conductivities see NBS Monograph 131
35. 75% Nb, 25% Zr manufactured by Supercon Div., National Research Corp., Natick, Massachussetts. Our wire was 0.012" dia. including 0.001" copper cladding and 0.001"

formvar insulation.

36. Kepco Inc., Flushing, New York
37. Pennsalt Chemical Corp., Philadelphia, Pennsylvania
38. Designed by R.J.Roberts and constructed by J.Sangeorge, Cryogenics Center, Stevens Institute of Technology, Hoboken, New Jersey.
39. A.C.Anderson, Rev. Sci. Instr. 41,1446 (1970)
40. J.G.Wheatley, R.E.Rapp, R.T.Johnson, J. Low Temp. Phys. 4,1 (1971)

    J.G.Wheatley, O.E.Vilches, W.R.Abel, Physics 4,1 (1968)
41. National Research Corp., Equipment Div., Newton 61, Massachussetts. The fluid used was DC702 manufactured by Dow Corning Corp., Midland, Michigan
42. Pennwalt Corp., Wallace and Tiernan Div., Belleville, New Jersey
43. Edwards High Vacuum Ltd., Crawley, England.
44. Fisher Scientific Co., Failawn, New Jersey
45. Hastings-Raydist, Hampton, Virginia
46. Veeco Instr. Inc., Plainview, New York
47. Ruska Instruments Corp., Houston, Texas
48. Sargent-Welch Scientific Co., Skokie, Illinois
49. J.G.Daunt, C.Z.Rosen, J. Low Temp. Phys. 3,89 (1970)
50. T.R.Roberts, S.G.Sydoriac, Phys. Rev. 102,304 (1956)
51. Dymec, a division of Hewlett -Packard Co., Palo Alto, California

52. Kennedy Co., Pasadena, California

53. FX Systems Corp., Digitem Div.,Sangerties, New York

54. Teletype is the tradename of a slow printer manufactured by Teletype Corp., Skokie, Illinois

55. We thank Mr. P. Lynch, Physics Dept., C.C.N.Y., New York, for the help in constructing the power supply, programmer and controller.

56. Nixie is a trademark of Burroughs Corp., Warren Township, New Jersey

57. Electro Scientific Industries, Portland, Oregon

58. S.Brunauer, P.H.Emmett, J. Amer. Chem. Soc. 57,1754 (1935) S.Brunauer, 'The Adsorption of Gases and Vapours', Clarenton Press 1945

59. S.Brunauer, P.H.Emmett, E.Teller, J. Amer. Chem. Soc. 60,309 (1938)

60. J.G.Daunt, E.Lerner, J. Low Temp. Phys. 8,79 (1972)

61. C.Kittel, 'Introduction to Solid State Physics', John Wiley & Sons 1968, 3rd ed., p. 29

62. F.J.Milford, A.D.Novaco, Phys. Rev. A 4,1136 (1971)

63. Reference 61, p. 81

64. A.C.Hollis-Hallett, 'Argon, Helium, and the Rare Gases', ed. G.A.Cook, Interscience 1961

65. W.A.Steele, J. Low Temp. Phys. 3,257 (1970)

66. G.J.Goellner, J.G.Daunt, E.Lerner, J. Low Temp. Phys. 21,347 (1975)

67. E.Lerner, J.G.Daunt, J. Low Temp. Phys. 10,299 (1973)

68. Note that a temperature exponent (-1/2) was misprinted in reference 10.

69. R.L.Siddon, M.Schick, Phys. Rev. A 9,907 and 1753 (1974)

70. A.D.Novaco, C.E.Campbell, Phys. Rev. B 11,2525 (1975)

71. R.M.May, Phys. Rev. 135,A1515 (1964)

72. L.D.Landau, E.M.Lifshitz, 'Statistical Physics', 2nd ed., Addison-Wesley Publishing Co., 1969, p. 148-157

73. R.Fowler, E.A.Guggenheim, 'Statistical Thermodynamics', Cambridge Univ. Press, 1949

74. W.A.Steele, 'The Solid Gas Interphase', ed. E.A.Flood, Marcel Dekker Inc., 1967, vol. #1

75. J.H.De Boer, 'The Dynamical Character of Adsorption', Clarenton Press 1953

76. R.H.Anderson, T.C.Foster, Phys. Rev. 151,190 (1966)

77. C.E.Campbell, M.Schick, Phys. Rev. A 3,691 (1971)

78. M.D.Miller, C-W.Woo, C.E.Campbell, Phys. Rev. A 6,1942 (1972)

79. reference 61, p. 168-180

80. R.L.Elgin, D.L.Goodstein, Phys. Rev. A 9,2657 (1974)

81. J.M.Kosterlitz, D.J.Thouless, J. Phys. C: Solid State 6,1181 (1973)

82. R.L.Elgin, D.L.Goodstein, in reference 16, p. 35

83. D.L.Husa, private communication

84. R.W.G.Wyckoff, 'Crystal Structures', Interscience 1963,

2nd ed., vol #1, p. 27

85. C.B.Huff, J.G.Dash, J. Low Temp. Phys. 24,155 (1976)

86. F.A.Putnam, T.Fort Jr., J. Phys. Chem. 79,459 (1975)

87. S.C.Ying, Phys. Rev. B 3,4160 (1970)

88. H.Taub, L.Passell, J.K.Kjems, K.Carneiro, J.P.McTague, J.G.Dash, Phys. Rev. Lett. 11,654 (1975)

89. S.G.Hegde, Ph.D. Thesis, Stevens Inst. of Techn. 1977, unpublished. The Argon isotherm was reproduced in reference 66.

90. R.J.Bobka, R.E.Dininny, A.R.Siebert, E.L.Pace, J. Phys. Chem. 61,1646 (1957)

91. W.A.Steele, R.Karl, J. Colloid and Interface Sci. 28,397 (1968)

92. F.D.Manchester, Rev. Mod. Phys. 39,383 (1967)

93. W.A.Steele, J. Chem. Phys. 25,819 (1956)

94. A.D.Novaco, Phys. Rev. A 7,678 (1973)

95. A.D.Novaco, J. Low Temp. Phys. 21,359 (1975)

96. K.Carneiro, W.D.Ellenson, L.Passell, J.P.McTague, H.Taub, Phys. Rev. Lett. 37,1695 (1976)

97. A.D.Novaco, J. Low Temp. Phys. 9,457 (1972)

98. S.G.Hegde, J.G.Daunt, Brookhaven Conference on Physical Adsorption, Dec. 1976, unpublished

99. S.B.Grary, O.E.Vilches, in reference 98

100. R.T.Harley, J.C.Gustafson, C.T.Walker, Cryogenics p.511, December 1970

101. The 1958 ^{4}He temperature scale

102. The 1962 ^{3}He temperature scale

103. D.S.Betts, D.T.Edmonds, B.E.Keen, P.W.Matthews, Rev. Sci. Instrum., 41,515 (1964)

104. C.Boghosian, H.Meyer, J.E.Rives, Phys. Rev. 146,110 (1966)

105. S.Brunauer, L.E.Copeland, D.L.Kantro, in reference 74

106. G.D.Halsey Jr., in reference 74 and J. Chem. Phys., 16,931 (1948)

AUTOBIOGRAPHICAL STATEMENT

Born in Athens, Greece, on August 17, 1943. Attended primary and high school in Athens as well as university. Graduated from the Physics Department, Physico-Mathematical School, University of Athens in June 1967. While student, was granted state subsidy for research work at the Nuclear Research Center 'Democritus', Athens, Greece, where remained untill June 1968 working as an assistant in the fast chopper group, and taking courses at the graduate level.

Entered the U.S.A. in June 1968 as an exchange student for research work at the Brookhaven National Laboratory, Upton, New York, where joined the triple axis neutron spectrometer group. In September 1968, enrolled in the Physics Department of the City College of the City University of New York. Granted the Master's Degree in February 1970. Fulfilled all the requirements for the Ph. D. Degree in October 1977.

While student, got married to Georgia Dimitrakopoulos in January 1968. Blessed with two sons, Nikolaos, born in February 1970, and Demosthenes, born in July 1972.